2014

Estimating the Amount of Information Conveyed by a Population of Neurons

Marshall Crumiller

Estimating the Amount of Information Conveyed by a Population of Neurons

Marshall Crumiller

A dissertation submitted to the Graduate Faculty of the Graduate School of Neuroscience Doctoral Program, in partial fulfillment of the requirements for the degree of Doctor of Philosophy, Icahn School of Medicine at Mount Sinai.

2014

Abstract

Recent advances in electrophysiological recording technology have allowed for the collection of data from large populations of neurons simultaneously. Yet despite these advances, methods for the estimation of the amount of information conveyed by multiple neurons have been stymied by the "curse of dimensionality"–as the number of included neurons increases, so too does the dimensionality of the data necessary for such measurements, leading to an exponential and, therefore, intractible increase in the amounts of data required for valid measurements. Here we put forth a novel method for the estimation of the amount of information transmitted by the discharge of a large population of neurons, a method which exploits the little-known fact that (under certain constraints) the Fourier coefficients of variables such as neural spike trains follow a Gaussian distribution. This fact enables an accurate measure of information even with limited data. The method, which we call the *Fourier Method*, is presented in detail, tested for robustness, and its application is demonstrated with both simulated and real spike trains.

Foreward

The field of neuroscience comprises several disciplines. Some of these disciplines are heavily grounded in the biological substrate of the brain, and pursue knowledge governing the physical material which forms the basis of all neural activity— neurons, synapses, and the swath of complex machinery that enables our brains to function. Others seek to shed light on the biological underpinnings of the more macroscopic, *emergent* properties of the brain: how our genetic makeup influences brain structure, and how this structure correlates with disease, behavior, and perception.

This dissertation focuses on yet another area: how neurons in the brain work together to process and encode *information*. This filed is grounded in experimental data and theory generated from electrophysiological recordings— recordings that measure the spiking activity of individual neurons, often in response to an external, driving stimulus. Such experiments allow us to learn the functional properties of neurons, how their activity is influenced by the outside world, how neurons influence each other and, in turn, addresses a critical question: *how does the brain encode information*?

This thesis focuses on the measurement of information in the brain, using the visual system as a convenient model. The findings presented in this dissertation fill a gaping hole in the field of neuroscience: how to measure the amount of information in populations of simultanenously recorded neurons. Previous efforts of such measurement have been consistently thwarted by the combinatorial explosion of possible spike patterns found even in small populations of neurons; it presents an new method that elegantly bypasses this obstacle, and provides a computationally efficient solution to the problem of measuring multi-neuronal information.

Contents

1 Introduction

1.1 Neural Coding

The establishment of the ways by which neurons receive, encode, and transmit information is a primary goal in neuroscience. The common metaphor of the brain as a computer describes the brain primarily as an *information processor* (Pinker, 1999; von Neumann, 2000): our behavior and actions, both conscious and subconscious, are governed by the brain, and result from the coordinated effort of many neurons intercepting signals from the external world, storing these signals, and applying computation– the rearrangement of patterns of neural activity– to generate predictions and behavior that influence our survival. Defining how these patterns of activity represent information is prerequisite to understanding brain function, and is referred to as the *coding problem*.

Deciphering the transformation from stimulus, which encompasses not only the range of modalities forming our senses, but also of the output from other neurons, into a neural pattern of activity is a problem shrouded in complexity attributable to many biophysical, evolutionary, and circuit-level phenomena in the brain. The high metabolic demand of the brain, approaching 25% of the body's entire metabolism in humans (Mink et al., 1981), places immense evolutionary constraints on the brain's design (Niven and Laughlin, 2008), requiring a minimization of energy consumption while maximizing the ability to respond to a wide variety of stimuli. This necessity for an economical approach to coding favors compression schemes that further obscure the transformation of the original signal into the resulting patterns of neural activity. Furthermore, the fundamental unit of computation– the neuron (according to the Neuron Doctrine)– is itself stochastic: the timing of individual spikes often follow probabilistic, rather than deterministic, rules of activity. Whether this variability itself is critical to the encoding process (Eyherabide and Samengo, 2013; Levine et al., 2002; Averbeck and Lee, 2003, 2006; Masuda and Aihara, 2002) or it is the inevitable result of simple neurobiomechanics (Softky and Koch, 1993) remains a matter of debate. Furthermore, the fact that computation is carried out at the level of the synapse in both the retina (Sivyer and Williams, 2013) and cortex (Smith SL and M, 2013) continues to obscure the level of precision at which information is stored and processed.

1.1.1 Computational Methods

The field of computational neuroscience began perhaps with the introduction of the integrate-and-fire model neuron of Lapicque in 1907 (Abbott, 1999), with critical contributions by K. Hartline and Hogkin & Huxley paving the way for the application of mathematical descriptors to biological phenomena. In 1943, Warren McCulloch and Walter Pitts introduced concept of the mathematically manipulable artificial neuron. The notion that thought and behavior are modified through the reorganization and alteration of synapses was inspired by *The Organization of Behavior* of Hebb (1949), bringing about a circuit-level view of memory and learning through activity-dependent plasticity in the brain (see Markram et al. (2011) for a thorough review of its impact). Neurons relay information through the timing of their action potentials, which is a point-process of discrete events (Daley and Vere-Jones, 2007). The goal of computational neuroscience is to describe the coding strategy that maps external events to series of discrete spiking patterns found in the brain. Such maps undoubtedly come in many forms, dependent on the evolutionary pressures that guided their development, and on the nature of the computation to be performed. Our various sensory modalities each involve machinery designed to compute specific tasks; sensory organs that feed input into specialized subpopulations of cells that process the information in some manner presumed to be useful for the modality. Even within sensory modalities, for example within the visual system, we find a diversity of coding schemes, a major example being the progressive decrease in the precision of topographic mapping that accompanies the progression through higher visual areas. Understanding how a particular population of cells in the brain encodes information requires specialized analyses, which means that assumptions concerning the nature of the code must be made.

1.1.2 Rate coding *versus* Timing coding?

Given the stochastic nature of neurons, much debate has ensued regarding the nature of information transmission: does a neuron convey information through its firing rate, or through the precise timings of its spikes? This question was defined rigorously by Theunissen and Miller (1995), who distinguished temporal coding, based on precise spike times, from those based on windowed-average measures. Studies showing that neurons can integrate and react to stimuli with millisecond (deCharms and Merzenich, 1996) and even sub-millisecond (Carr, 1993; Softky, 1994; Bullock, 1970; Vardi et al., 2013) precision indicate that the machinery is available for specifically timed spikes, and the sparsity and high precision of spiking events in the retina, for example as shown by Berry et al. (1997), demonstrates that some areas of the brain may benefit more greatly from using codes in which the timing of a spike is more important than its probability of occurring (Van Rullen and Thorpe, 2001; Gawne, 2000). However, the higher variability of neural responses in the cortex to identical stimuli (Richmond and Optican, 1987; Victor and Purpura, 1996; Tolhurst et al., 1983) precludes such reliance on precise timing, with *in vivo* evidence suggesting that rate coding takes precedence in higher cortical areas (London et al., 2010; Shadlen and Newsome, 1998; Georgopoulos et al., 1992, 1986, 1988). The apparent use of both coding schemes in the rat barrel cortex (Ahissar et al., 2000; Panzeri and Schultz, 2001) suggests that coding schemes may be chosen appropriately, according to the encoding task at hand. Finally, the increasing evidence for the importance of neuronal oscillations and cross-frequency interactions in the temporal coordination of neuronal firing in learning and memory (Buzsáki and Draguhn, 2004; Shirvalkar et al., 2010; Trimper et al., 2013; Vaidya and Johnston, 2013), and the implication that the deterioration of such mechanisms contribute to diseased states of mind such as schizophrenia (Tan et al., 2013; Uhlhaas and Singer, 2013), imply that the dynamic configuration of large-scale functional coding networks may rely on the integration of multiple coding methods across and within brain regions.

1.2 Population codes

1.2.1 Neurons work together

Our discussion above of the somewhat abstract questions surrounding possible coding methods leads to a critically important point in our discussion: that no single neuron performs its action alone, but rather always works in concert with populations of others cells (Pouget et al., 2000). Examples of population coding are numerous: pyramidal cells in the rat hippocampus generate a geographic mental map of the local environment, where the firing rates of individual neurons are tightly correlated with a specific location, and firing oscillation frequency is correlated with the animal's velocity. Some interesting features of these "place cells" highlight the importance of understanding a neuron's function in the context of its population. Populations of place cells generate a local theta rhythm, on the order of $6 - 10\,\mathrm{Hz}$. Individual place cells oscillate slightly faster than the population rhythm; the geographic separation between the place fields represented by the neurons, and the motion of the rat through those fields, creates a temporal disparity between the individual neurons' oscillations. This slight delay in activation of sequential neurons as the rat progresses through overlapping place fields creates a sequence of delayed oscillations which, taken together, produce slightly slower population oscillations(O'Keefe and Recce, 1993; Dragoi and Buzsáki, 2006). One of the interesting consequences of these *time compressed sequences* is the resulting phase precession (O'Keefe and Recce, 1993) that occurs, whereby the position of the rat within the place field can be inferred based on the relation (phase) between the field neuron's spike timing and the population theta rhythm.

Similar examples of population coding can be found elsewhere in the brain: Georgopoulos and colleagues (1986) found broadly-tuned neurons in the primate motor cortex, each with a preferred axis of arm movement. These neurons fire with an intensity dependent on the similarity of the arm movement direction to the preferred direction. Prediction of the actual direction of arm movement from the joint output of a population of these cells is performed by a weighted summation of each individual neuron's movement vector contribution. In this particular study, a selection of 224 neurons provided, in general, 95% confidence in the accuracy of the prediction.

A follow-up study by Tanaka (1994), using simulations, estimated that accuracy of 1 degree root mean square error requires on the order of 10,000 neurons. Yet, despite the assertion that neurons in the brain operate exclusively in large numbers, the conceptual and mathematical tools for the analysis of neurophysiological data have lagged behind the rapidly improving technology of recording or imaging large neuronal populations. Popular methods, for example the Gravity Method of Gerstein et al. (1989), deal with neurons in an exclusively pairwise fashion, and fail to properly provide insight into neural coding at the population level.

1.2.2 Electrophysiology and the advent of multi-neuronal recordings

Despite the necessity for methodologies that deal with population codes as outlined above, technological constraints have by and large limited neuroscience until recently to the study of individual neurons and their biophysical and electrophysiological response properties, despite a general awareness for the need for methods dealing with multiple neurons (Krüger, 1983). The technological requirements for measuring the output of neurons, given their high temporal precision and small physical size, did not exist until the last few years, and depends heavily on electrode fabrication and data acquisition methods. As hardware and software technologies have progressed, however, multi-channel electrophysiological recording is rapidly becoming the norm, and scientists shift to experiments involving neural ensemble recordings of diverse nature, including massive multi-neuronal recordings of the retina (Doi et al., 2012; Vidne et al., 2011; Field et al., 2010), *two-photon calcium imaging of thousands of neurons simultaneously (Bock et al., 2011; Andermann et al., 2010; Ch'ng and Reid, 2010; Ziv et al., 2013; Deisseroth and Schnitzer, 2013; Marshall and Schnitzer, 2013; Sinha et al., 2013),* chronic non-human primate, and even human, awake recordings (Nicolelis and Ribeiro, 2002).

1.2.3 The Need for multi-neuronal mathematical tools

The theoretical and mathematical tools designed to deal with multineuronal data sets have necessarily followed the prerequisite technologies for acquiring such data. Some of the recent developments in multineuronal coding indicate a promising future in neuroscience, including the ability to directly encode visual images into retinal ganglion cells (Nirenberg and Pandarinath, 2012). However, these methods rely on a limited knowledge of the interactions between neurons on a population level: how do the neurons work together to produce an outgoing retinal code? The importance of interactions between neurons and the extent to which knowledge of correlations and interactions between cells influence the brain's coding system is still a matter of debate (Nirenberg et al., 2001; Levine et al., 2002; Golledge et al., 2003), a debate that depends in large part on our ability to measure such interactions. As is shown in the following section, this ability has been obstructed by our *inability* to adequately measure the extent of overlap in the amounts of information conveyed by a population of neurons. This thesis provides such a measure, and thus fills a much-needed hole in the arsenal of multineuronal analysis methods.

1.3 Information

A thriving area of mathematics directly applicable to neural processing in the brain is *Information theory*, which quantifies the degree of *novelty* transmitted in a particular message. While the idea of novelty associated with a message may be difficult to intuit or describe colloquially, Shannon and Weaver (1949) provided an explicit method of mathematically defining this measure in their seminal paper on information theory. Information theory is an important foundation for the study of neural systems because it establishes limits on the processing capabilities of these systems, describes their behavior, and allows the scientist to gauge the efficiency of the system in processing its input and conveying its output. As an example, consider the mammalian visual system. After light enters the eye and is absorbed by photoreceptors in the retina, neural mechanisms encode a view of the outside world into a sequence of action potentials that are transmitted, via retinal ganglion cells, to the lateral geniculate nucleus (LGN). The encoding varies from cell to cell and, through a combination of different inputs, encoding schemes, and transmission rates, provides the LGN with a signal that appears remarkably different

from the initial electromagnetic stimulus. How, then, does one meaningfully quantify the rate of information transmission of a given input? We note that neural action potentials, being "all-or-none" events, lend themselves to the view of a binary code, in which a spike may be considered a "1," and the absence of a spike a "0." As a result, the application of digital information theory is a natural next step.

1.3.1 Definition

We wish to understand how the outside world is represented by the neural code of neuronal ensembles, and more generally, how neuronal groups process and transmit information in the brain. Shannon's Information Theory (Shannon and Weaver, 1949) provides a quantitative approach to this problem. By noting that any given input signal comes from a distribution of all possible input signals, we can derive a measure of likelihood for the output signal. The net likelihood of all possible signals— which depends on the system's ability to produce different signals given the input— is commonly referred to as the *entropy*: the amount of available information in a given information channel. If the input probability distribution is, say, a delta function— i.e. it can only receive one specific input— no information can be transmitted, since the input can be trivially inferred. Similarly, if an output is limited to only one pattern, then inference of the input is impossible, as all inputs produce identical outputs. Information is thus a measure of *uncertainty* of a random variable x, with various constraints, such as additivity of independent variables, that can be expressed as a continuous function of its probability distribution $P(x)$:

$$S = -\int dx P(x) log(P(x))$$

Intuitively, therefore, the entropy is the number of questions required to determine the value of a variable; it is the logarithm of the number of possible values for x. Several methods exist for calculating the entropy of a *single* spike train from a given neuron: the entropy is derived from both the variability of the neuron's spike patterns and the set of possible outputs. In a sense, if we were given one particular encoded input, the information is the number of bits required to accurately point to the address in our index of possible inputs. A major current hurdle in the field of information neuroscience, however, has been the inability to calculate the amount of information delivered by *multiple neurons* simultaneously, and with the recent advent of simultaneous multi-neuronal recordings, information neuroscience acutely needs such a method. We have recently devised and published such an approach for calculating the information conveyed by a population of cells; this thesis will apply this method to the visual system to gain further insights into the networking processing and function dynamics of its constituent cells.

The application of information theory to neural systems has been mostly focused on the visual system, with rather few exceptions (DiCaprio, 2004; Belitski et al., 2010; Marsat and Pollack, 2010). The visual system is accessible: it has controllable inputs (i.e. stimulus presented to the eye), and its outputs are readable from several points along the visual pathway, from the retina to the LGN to the visual cortex and extrastriate areas. The ability to control the stimulus is appealing, and a range of visually-driven areas have been studied for information, including: the fly visual H1 cells (Brenner et al., 2000), the salamander retina (Puchalla et al., 2005; Pillow and Latham, 2008), the cat LGN (Reinagel and Reid, 2000; Sincich et al., 2009), and areas V1, IT and MT in the macaque (Optican and Richmond, 1987; Gawne and Richmond, 1993; Brown et al., 2004).

1.3.2 Redundancy and Synergy

Given that a cell is capable of transmitting information about particular aspects of a stimulus, what can we say about a *group* of cells working together? It is likely that different cells might transmit some of the same information, for a variety of reasons: to ensure fidelity in the face of injury, to emphasize certain aspects of the stimulus deemed more important by the system; to allow for increased multiplexing in later visual areas (Victor and Purpura, 1996). This *redundancy*— duplicated information— can be measured only if some measure of total group information is available, and is compared to the information provided by each cell individually. Conversely, if the information conveyed by all cells together exceeds the sum of the individual cells' information, we have

synergy— information that is *only* conveyed when the outputs of all cells are taken into account. Redundancy can be mathematically expressed:

$$R = 1 - \frac{I(G)}{I(C)}$$

Crumiller et al. (2013), where $I(G)$ is the total group information, taking correlations into account, and $I(C)$ is the sum of the individual information contributions of the constituent cell when correlations are ignored. The largest potential source of redundancy for a group of cells is the input that each cell receives; presumably, cells with identical properties and inputs should exhibit high redundancy. The number of studies of redundancy among visual neurons is limited. Puchalla et al. (2005) found that approximately 40% of retinal ganglion cells located within $500\,\mu\mathrm{m}$ of each other showed redundancy values greater than 0.05, and of those, the average redundancy for nearby cells was ~0.14, in close agreement with our surrogate simulations (Yu et al., 2010). Reich et al. (2001) found redundancy in the macaque primary visual cortex ranging up to 0.5. Until now, however, measures of redundancy have been limited to pairwise measurements and, as demonstrated in the simulated results of Crumiller et al. (2013), the application of such pairwise measurements of redundancy to large populations of neurons may grossly misrepresent the true rate of information processed by the population.

1.3.3 A Brief History of Information Theory

The roots of information theory can be traced back to the introduction by Ludwig Boltzmann in 1872 of the quantity *H*, now better known as entropy, first used to describe the distribution of energy of an ideal gas in thermodynamic equilibrium, and demonstrate the logarithmic relationship between entropy and the number of microstates of the system. The *H*-Theorem describing this quantity was founded in statistical mechanics, and describes the tendency of *H*, determined by the gas's energy distribution function, to decrease with time (Boltzmann, 1872). Working from this notion, and founded on developments by J. Willard Gibbs (1878), James Clerk Maxwell (Leff and Rex, 1990; Maxwell, 2001), Max Planck (1945), Harry Nyquist (1924), Ralph Hartley (1928), and others, Shannon extended the notion of statistical entropy describing the motion of particles to that of the uncertainty in any random variable (Shannon, 1945, 1948).

The application of information theory to the nervous system began with MacKay and McCulloch (1952), in which various aspects of neural coding, including noise and coding method, were considered in generating estimates of the limits of information bandwidths within the nervous system, and thus began the field of inquiry seeking to relate information processing capabilities of a neural system to the outside word. Fred Attneave (1954) provided an initial taste of the application of information theory to the visual system, relating various aspects of the statistics of the natural visual world to the coding requirements of the retina, with special emphasis on the high levels of redundancy found in natural scenes. Horace Barlow (1961), in a celebrated article in *Sensory Communication*, further emphasized the notion that the visual system, in order to maximize information transmission, is designed to deal with, and discard, redundancy in the natural scene, and the emphasis on measuring information in the presence of noise was advanced by Shannon and McCarthy (1956) and Winograd and Cowan (1963). A more detailed view of some of the more modern the applications of information theory in the neurosciences can be found in Dimitrov et al. (2011),Victor (2006),Cover and Thomas (2006), and Dayan and Abbott (2001).

1.3.4 Modern Approaches

The Direct Method (Strong et al., 1998) is perhaps the best-known method of estimating information in neural spike trains, due in large part to its simplicity and rather close adherence to Shannon's definition. In the Direct Method, a set of spike trains are discretized into bins of width Δt, where each bin contains a number indicating the number of spikes contained within the range of the bin. As Δt decreases in length, this sequence of values approaches a binary code, such that at most a single spike occupies each bin. A length *L* is chosen, and all patterns of length *L* are indexed and accounted for; the unique entropy is then directly calculated for the set of patterns, where each p_i in the distribution is the probability of occurrence of a particular pattern. The value of

L is successively increased until the method breaks down due to insufficient data, and an extrapolation is made as $L \to \infty$. The main limitation of this method is the large quantity of data required to generate a reasonable estimate of entropy: the number of possible neural patterns of length L using a binary binning procedure (Δt is generally set to $1\,\mathrm{ms}$) is 2^L; thus, as word length increases, the number of possible patterns, and therefore the data required to generate good estimates of the underlying pattern distribution, increases exponentially. Other methods make use of the discretization procedure, such as the Context Tree Method of London et al. (2002) and Kennel et al. (2005), which is less dependent on a large amount of data, and attempts to use a measure of the complexity of coding to generate estimates of entropy, similar to that found in Compression Methods that use compression algorithms, such as the Lempel-Ziv-Welch algorithm (Ziv and Lempel, 1978; Ziv and A, 1978; Welch, 1984) used in *compress*, the Unix file compression utility, or in the widely-used Graphics Interchange Format, more commonly known as the GIF image format. Other methods attempt to improve on the stringent requirements imposed on the data by the Direct Method. The Metric Space Method (Victor and Purpura, 1997; Victor, 2005; Victor and Purpura, 1996) uses the similarity *between* spike trains to measure entropy, dispensing with the binning procedure which necessarily introduces a free parameter (Δt) that destroys some of the information contained within the spike train and increases the problems associated with the number of possible patterns, and therefore the length of data, required. The Metric Space method relies heavily on the assumption that spike trains carry information in the precise timing of their spikes, and remains limited in the face of longer-duration, rich stimuli (Victor, 2006). Other approaches, such as the Reconstruction Method of Bialek et al. (1991), estimate entropy via a transformation from neural code to stimulus.

2 The Fourier Method

One of the greatest obstacles in the field of information theory has been the exponential relationship between the number of neurons and the amount of data required to accurately measure the information conveyed by those neurons. The most straightforward application of information theory to spike trains, the Direct Method by Strong et al. (1998), directly measures information by the distribution of patterns of spikes from a group of neurons. The relationship in this case is exponential in that each additional neuron doubles the number of possible spike patterns in a population; as a result, populations of even modest size quickly become intractable. In the following three papers, we present a new method of estimating informatino, which we call the Fourier method; for the core of the method relies heavily on the extraction and entropy of the Fourier coefficients of the data.

The first two papers, Yu et al. (2010) and Crumiller et al. (2011), introduce the Fourier method and describe in detail its construction and application to neural spike trains, including the representation of spike trains in the frequency domain, the extraction of Fourier coefficients, the measuring of entropy from both unique and repeated stimuli, and the estimation of information from the subtraction of the two entropies. In addition, it provides a measure of population information, whereby information resulting from neuronal correlations is discarded as redundant information. This critical step allows for the measurement of redundancy in large population of neurons. The third paper, Crumiller et al. (2013), tests the robustness of the Fourier Method in the face of limited and unwieldy data. It provides estimates of a lower bound for the quantity of data required to generate accurate measurements, and further demonstrates the feasibility of using the method on large data sets.

2.1 Estimating the amount of information carried by a neuronal population.

Yu Y, Crumiller M, Knight B, Kaplan E.

Front Comput Neurosci. 2010 Apr 26;4:10.

frontiers in
COMPUTATIONAL NEUROSCIENCE

ORIGINAL RESEARCH ARTICLE
published: 26 April 2010
doi: 10.3389/fncom.2010.00010

Estimating the amount of information carried by a neuronal population

Yunguo Yu[1], Marshall Crumiller[1], Bruce Knight[2] and Ehud Kaplan[1]*

[1] *Neuroscience Department, The Mount Sinai School of Medicine, New York, NY, USA*
[2] *Laboratory of Biophysics, The Rockefeller University, New York, NY, USA*

Edited by:
Jakob H. Macke, MPI for Biological Cybernetics, Germany

Reviewed by:
Simon R. Schultz, Imperial College London, UK
Stefano Panzeri, Italian Institute of Technology, Italy

***Correspondence:**
Ehud Kaplan, Department of Neuroscience, The Mount Sinai School of Medicine, One Gustave Levy Place, Box 1065, New York, NY 10029, USA.
e-mail: ehud.kaplan@mssm.edu

Although all brain functions require coordinated activity of many neurons, it has been difficult to estimate the amount of information carried by a population of spiking neurons. We present here a Fourier-based method for estimating the information delivery rate from a population of neurons, which allows us to measure the redundancy of information within and between functional neuronal classes. We illustrate the use of the method on some artificial spike trains and on simultaneous recordings from a small population of neurons from the lateral geniculate nucleus of an anesthetized macaque monkey.

Keywords: information, neural population, thalamus, redundancy

INTRODUCTION

The brain processes information, and it is therefore natural to estimate the amount of information that a neuron transmits to its targets. In the past, several methods that derive such estimates from the firing pattern (Optican and Richmond, 1987; Richmond and Optican, 1987; Richmond et al., 1987; Bialek et al., 1991; Rieke et al., 1997; Strong et al., 1998; Brenner et al., 2000) or membrane potential (Borst and Theunissen, 1999; DiCaprio, 2004) of individual neurons have been used. The information from spike trains was estimated by calculating the entropy associated with the various temporal patterns of spike discharge, using Shannon's formula (Shannon and Weaver, 1949).

Since all brain functions involve many neurons, it is desirable to provide similar information estimates for a neuronal population (Knight, 1972). To simply add up the information amounts from individual neurons in the population would be valid only if the neurons were all independent of one another, an assumption that usually is incorrect (see, for example, Zohary et al., 1994; Bair et al., 2001; Pillow et al., 2008). Approaches like the *Direct Method* (Strong et al., 1998) are impractical for a population, because the multi-dimensional space occupied by many spike trains can be sampled only sparsely by most neurophysiological experiments. Calculating the information carried by a population of many neurons thus has remained a challenge (Brown et al., 2004; Quiroga and Panzeri, 2009). At the same time, the need for such estimates has become increasingly urgent, since the technology of recording simultaneously from many neurons has become much more affordable and wide-spread, and data from such recordings are becoming common.

We describe here a method that estimates the amount of information carried by a population of spiking neurons, and demonstrate its use, first with simulated data and then with data recorded from the *lateral geniculate nucleus* (LGN) of an anesthetized macaque monkey.

MATERIALS AND METHODS

SURGICAL PREPARATION

The experimental methods were similar to those used in our lab in the past (Uglesich et al., 2009). Housing, surgical and recording procedures were in accordance with the National Institutes of Health guidelines and the Mount Sinai School of Medicine Institutional Animal Care and Use Committee. Adult macaque monkeys were anesthetized initially with an intramuscular injection of xylazine (Rompun, 2 mg/kg) followed by ketamine hydrochloride (Ketaset, 10 mg/kg), and then given propofol (Diprivan) as needed during surgery. Local anesthetic (xylocaine) was used profusely during surgery, and was used to infiltrate the areas around the ears. Anesthesia was maintained with a mixture of propofol (4 mg/kg-hr) and sufentanil (0.05 μg/kg-hr), which was given intravenously (IV) during the experiment. Propofol anesthesia has been shown to cause no changes in blood flow in the occipital cortex (Fiset et al., 1999), and appears to be optimal for brain studies. Cannulae were inserted into the femoral veins, the right femoral artery, the bladder, and the trachea. The animal was mounted in a stereotaxic apparatus. Phenylephrine hydrochloride (10%) and atropine sulfate (1%) were applied to the eyes. The corneas were protected with plastic gas-permeable contact lenses, and a 3-mm diameter artificial pupil was placed in front of each eye. The blood pressure, electrocardiogram, and body temperature were measured and kept within the physiological range. Paralysis was produced by an infusion of pancuronium bromide (Norcuron, 0.25 mg/kg-hr), and the animal was artificially respired. The respiration rate and stroke volume were adjusted to produce an end-expiratory value of 3.5–4% CO_2 at the exit of the tracheal cannula. Penicillin (750,000 units) and gentamicin sulfate (4 mg) were administered IM to provide antibacterial coverage, and dexamethasone was injected IV to prevent cerebral edema. A continuous IV flow (3–5 ml/kg-hr) of lactated Ringer's solution with 5% dextrose was maintained throughout the experiment to keep the animal properly hydrated,

and the urinary catheter monitored the overall fluid balance. Such preparations are usually stable in our laboratory for more than 96 h. The animal's heart rate and blood pressure monitored the depth of anesthesia, and signs of distress, such as salivation or increased heart rate, were watched for. If such signs appeared, additional anesthetics were administered immediately.

VISUAL STIMULATION

The eyes were refracted, and correcting lenses focused the eyes for the usual viewing distance of 57 cm. Stimuli were presented monocularly on a video monitor (luminance: 10–50 cd/m^2) driven by a VSG 2/5 stimulator (CRS, Cambridge, UK). The monitor was calibrated according to Brainard (1989) and Wandell (1995). Gamma corrections were made with the VSG software and photometer (OptiCal). Visual stimuli consisted of homogeneous field modulated in luminance according to a pseudo-random naturalistic sequence (van Hateren, 1997). Eight second segments of the luminance sequences were presented repeatedly 128 times ('repeats'), alternating with 8 s non-repeating ('uniques') segments of the sequence (Reinagel and Reid, 2000). In addition, we used steady (unmodulated) light screens and dark screens, during which spontaneous activity was recorded.

ELECTROPHYSIOLOGICAL RECORDING

A bundle of 16 stainless steel microwires (25 μ) was inserted into a 22 gauge guard tube, which was inserted into the brain to a depth of 5 mm above the LGN. The microwire electrodes were then advanced slowly (in 1 μ steps) into the LGN, until visual responses to a flashing full field screen were detected. The brain over the LGN was then covered with silicone gel, to stabilize the electrode bundle. Based on the electrode depth, dominant eye sequence and cell properties (Kaplan, 2007), we are confident that all the electrodes were within the parvocellular layers of the LGN. The receptive fields of the recorded cells covered a relatively small area (~4° in diameter), which suggests that the electrodes bundle remained relatively compact inside the LGN.

The output of each electrode was amplified, band-pass filtered (0.75–10 kHz), sampled at 40 kHz and stored in a *Plexon* MAP computer for further analysis.

DATA ANALYSIS

Spike sorting

Sorting procedures. The spike trains were first thresholded (SNR ≥5) and sorted using a template-matching algorithm under visual inspection (*Offline Sorter,* Plexon Inc., Dallas, TX, USA). In most cases, spikes from several neurons recorded by a given electrode could be well-separated by this simple procedure. In more difficult cases, additional procedures (peak- or valley-seeking, or multivariate t-distributions) (Shoham et al., 2003) were employed. Once the spikes were sorted, a firing times list was generated for each neuron and used for further data analysis.

Quality assurance. To ensure that all the spikes in a given train were fired by the same neuron, we calculated for each train the interspike interval (ISI) histogram. If we found intervals that were shorter than the refractory period of 2 ms, the spike sorting was repeated to eliminate the misclassified spikes. We ascertained that all the analyzed data came from responsive cells by calculating the coefficients of variation of the peristimulus time histogram bin counts for the responses to the repeated and unique stimuli, and taking the ratio of these two coefficients. Only cells for which that ratio exceeded 1.5 were included in our analysis.

Generation of surrogate data

To test our method we generated synthetic spike trains from a Poisson renewal process, in which the irregularities of neuronal spike times are modeled by a stochastic process whose mathematical properties are well defined. Recent interest and success in modeling a neuron spike-train as an inhomogeneous Poisson process (Pillow et al., 2005, 2008; Pillow and Simoncelli, 2006) led us to that choice.

Firing rates and input. Our modeling necessarily addressed two major features of the laboratory data. The nine real neurons show a range of mean firing rates, from 3.04 impulses per second (ips) to 28.72 ips, which span an order of magnitude. To mimic this, we gave our 12 model cells 12 inputs which consecutively incremented by a factor of $10^{(1/11)}$, to give firing rates spanning an order of magnitude. The second major feature was that our laboratory neurons evidently received inputs processed in several ways following the original retinal stimulus. To make a simple caricature of this, we drove each of our Poisson model neurons with a separate input that was a weighted mean admixture of two van Hateren-type stimuli. The first was that which we used in the laboratory and the second was the time-reversal of that stimulus. Calling these A and B, the stimuli were of the form $S = (1 - x)\cdot A + x\cdot B$, where the admixture variable x took on 12 equally spaced values starting with 0 and ending with 1. As shown in **Table 1**, the pairs (admixture, mean rate) were chosen in a manner that allowed the whole grouping of model cells to be divided into smoothly changing subsets in different ways, and evenly distributed the range of properties across all cells.

Estimation of the information delivered by a subset of neurons

If we have data from numerous parallel spike trains, the familiar *Direct method* (Strong et al., 1998) for computing signal information delivered requires an impractical time span of data. As a

Table 1 | Parameters for stimulating the surrogate neurons. Each surrogate neuron was driven by a mixture of two *van Hateren* inputs, chosen to cover uniformly the range of firing rates and mixture ratios.

Cell #	1	2	3	4	5	6	7	8	9	10	11	12
Firing rate	4.98	6.18	7.58	9.38	11.42	14.13	17.47	21.64	26.79	32.74	40.60	50.09
Admixture	0	0.27	0.55	0.82	0.09	0.36	0.64	0.91	0.18	0.45	0.73	1

practical alternative we advance a straightforward multi-cell generalization of a method of information computation from basis-function coefficients.

Shannon has observed (Shannon and Weaver, 1949, Chapter 4; see also Shannon, 1949) that the probability structure of a stochastic signal over time may be well approximated in many different ways by various equivalent multivariate distribution density functions of high but finite dimension. He further observed that when some specific scheme is used to characterize both the distribution of signal-plus-noise and the distribution of noise alone, the information quantity one obtains for the signal alone, by taking the difference of the information quantities (commonly called 'entropies') evaluated from the two distributions, has a striking invariance property: the value of the signal information is universal, and does not depend on which of numerous possible coordinate systems one has chosen in which to express the multivariate probability density (see extensive bibliography, and discussion, in Rieke et al., 1997, chapter 3). We will follow Shannon (1949), whose choice of orthonormal functions was Fourier normalized sines and cosines, over a fixed, but long, time span T. This choice has the added virtue of lending insight into the frequency structure of the information transfer under study.

Here we outline our approach for obtaining the signal-information rate, or 'mutual information rate', transmitted by the simultaneously recorded spikes of a collection of neurons. The mathematical particulars are further elaborated in the Appendix. Following Shannon (1949), if one has a data record that spans a time T, it is natural to use the classical method of Fourier analysis to resolve that signal into frequency components, each of which speaks of the information carried by frequencies within a frequency bandwidth of $1/T$. If this is repeated for many samples of output, one obtains a distribution of amplitudes within that frequency band. In principle, that probability distribution can be exploited to calculate how many bits would have to be generated per second (the information rate) to describe the information that is being transmitted within that frequency band.

However, part of that information rate represents not useful information but the intrusion of noise. To quantify our overestimate we may repeat the experiment many times without variation of input stimulus, and in principle may employ the same hypothetical means as before to extract the 'information', which now more properly may be called 'noise entropy'. When this number is subtracted from the previous, we obtain the mutual information rate, in bits per second, carried by the spikes recorded from that collection of neurons.

In order to reduce the above idea to practice, we have exploited the following fact (which apparently is not well known nor easily found in the literature): if our response forgets its past history over a correlation time span that is brief compared to the experiment time span, T, then the central limit theorem applies, and our distribution of signal measurements within that narrow bandwidth will follow a Gaussian distribution. If we are making simultaneous recordings from a collection of neurons, their joint probability distribution within that bandwidth will be multivariate Gaussian. A Gaussian with known center of gravity is fully characterized by its variance, and similarly a multivariate Gaussian by its covariance matrix. Such a covariance matrix, which can be estimated directly from the data, carries with it a certain entropy. By calculating the covariance matrices for responses to both unique and repeated stimuli, one can determine the total signal information flowing through each frequency channel for a population of neurons.

To verify that our Gaussian assumption is valid, we have applied to our Fourier-coefficient sample sets two standard statistical tests that correctly identify a sample as Gaussian with 95% accuracy. For our 12 surrogate cells and 9 laboratory LGN cells, the degree of verification across the frequency range for 2560 distribution samples (160 Hz × 8 bins/Hz × 2, with each sine and cosine term sampled 128 times) is shown in **Table 2**. Because of its importance, we return to this issue in the Discussion, where further evidence is provided for the Gaussian nature of the underlying distributions.

RESULTS

ANALYSIS OF SIMULATED SPIKE TRAINS

Entropy vs temporal frequency

In anticipation of analyzing simultaneous laboratory records of actual neurons, we have created 12 Poisson model neurons with firing rates that overlap those of our laboratory neurons and with inputs as discussed above in Section 'Materials and Methods', presented at the same rate (160 Hz) used in the laboratory experiments. **Figure 1** shows, for a single simulated cell, the entropy rate per frequency, for responses to unique and repeat stimuli. The entropy from the responses to the unique stimulus (signal plus noise) exceeds that of the responses to the repeated stimulus (noise alone) at low frequencies, and the two curves converge near the monitor's frame-rate of 160 Hz, beyond which signal-plus-noise is entirely noise. Hence we will terminate the sum in (Eq. A26) at that frequency. The difference between the two curves at any temporal frequency is the mutual information rate at that frequency.

Table 2 | The Fourier coefficients for the surrogate and LGN data follow a Gaussian distribution. We sampled the Fourier coefficients 128 times for each of the 2560 sine and cosine terms that we tested for each cell. Each distribution was tested with two standard tests for normality: the Shapiro–Wilk's test and the Lilliefors test. The percentage of distributions that passed each test at the $p < 0.05$ significance level was calculated for each cell, and the table gives the mean and standard deviation for the test results.

	Repeats (% passed)		Uniques (% passed)	
TEST	**SHAPIRO–WILK**	**LILLIEFORS**	**SHAPIRO–WILK**	**LILLIEFORS**
Surrogate data (12 cells)	95.3 ± 0.31	95.2 ± 0.34	95.3 ± 0.41	95.1 ± 0.3
LGN cells (9 cells)	94.9 ± 1.62	94.6 ± 0.35	93.9 ± 1.31	94.6 ± 0.45

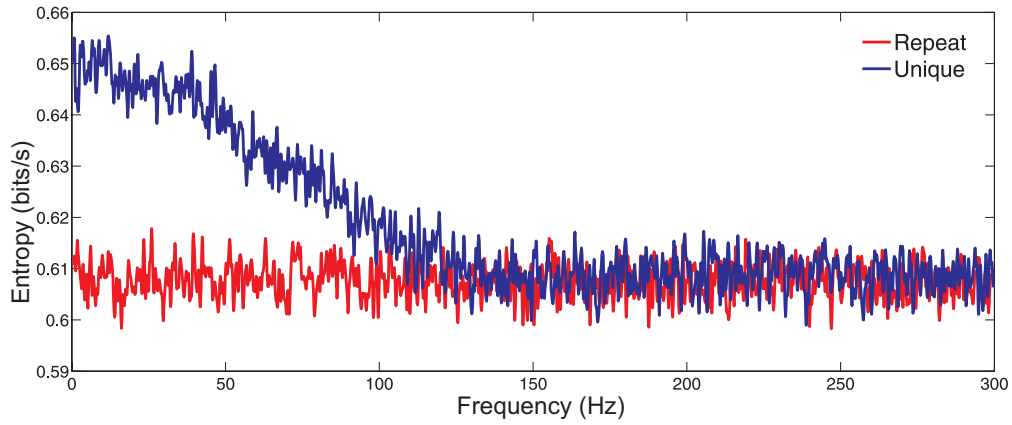

FIGURE 1 | Entropy per frequency conveyed by a single surrogate neuron. The signal-plus-noise entropy (derived from the unique stimuli) is shown in blue, and the noise entropy (from the repeated stimulus) is shown in red. The data shown are typical of data from other cells.

Single cell information

For the 12 model cells, the cumulative sum of information over frequency (Eq. A26) is given in **Figure 2** (left frame). We note that all the curves indeed finish their ascent as they approach 160 Hz. More detailed examination shows a feature that is not obvious: the output information rate of a cell reflects its input information rate, and the input information rate of a mixed, weighted mean input is less than that of a pure, unmixed input. This accounts for the observation that the second-fastest cell (cell 11, with a near even mixture) delivers information at only about half the rate of the fastest (cell 12).

Group information

We turn now to the information rate of a *group* of cells, firing in parallel in response to related stimuli. We proceed similarly to what is above, but use the multi-cell equation (Eq. A25) and its cumulative sum over frequencies. As a first exercise we start with the slowest-firing surrogate cell and then group it with the next-slowest, next the slowest 3 and so on up to the fastest; the set of cumulative curves we obtain from these groupings are shown in the left frame of **Figure 3**. Again we see that the accumulation of information appears to be complete earlier than the frame-rate frequency of 160 Hz.

REDUNDANCY AND SYNERGY AMONG NEURONS IN A POPULATION

Redundancy

The mutual information communicated by a group of cells typically falls below the sum of the mutual information amounts of its constituent members. This leads us to define a measure of information redundancy. The redundancy of a cell with respect to a group of cells can be intuitively described as the proportion of its information already conveyed by other members of the group. For example, if a cell is added to a group of cells and 100% of its information is novel, then it has 0 redundancy. If, on the other hand, the cell brings *no* new information to the group, then it contains only redundant information, and it therefore has redundancy 1. With this in mind, we define the redundancy of a cell C, after being added to a group G, as:

$$r_{c,g} = \left(I(c) - \left(I(g+c) - I(g)\right)\right)/I(c).$$

According to this formula, if all the information of the additional cell appears as added information in the new group, then that cell's redundancy is zero.

The procedure of information redundancy evaluation is general, and can be applied to the addition of any cell to any group of cells. Thus for the cell groups of **Figure 3**, we can evaluate the redundancy of each newly added cell not only upon its addition to the group but also thereafter. This is shown for the 70 resulting redundancies, in **Figure 4** (Left).

Synergy

When the total information conveyed by several neurons exceeds the sum of the individual ones, the neurons are synergistic (Gawne and Richmond, 1993; Schneidman et al., 2003; Montani et al., 2007). When this happens, our formula yields a negative redundancy value.

ANALYSIS OF MONKEY LGN SPIKE TRAINS

We now apply the same techniques to simultaneous laboratory recordings of 9 parvocellular cells from the LGN of a macaque monkey, responding to a common full-field naturalistic stimulus (van Hateren, 1997; Reinagel and Reid, 2000).

Figure 2 (right frame) shows the single cell cumulative information of these neurons as frequency increases. In two obvious ways their behavior differs from that of the Poisson model neurons. First, at low frequency there is a qualitative difference indicative of initially very small increment, which differs from the Poisson model's initial linear rise. Second, the real geniculate neurons show a substantial heterogeneity in the shape of their rise curves. For example, the second most informative cell (cell 8), has obtained half its information from frequencies below 40 Hz, while the most informative cell (cell 9) has obtained only 11% of its information from below that frequency.

The right frame of **Figure 3** shows for LGN cells the accumulating multineuron group information, while the left frame shows it for the surrogate data.

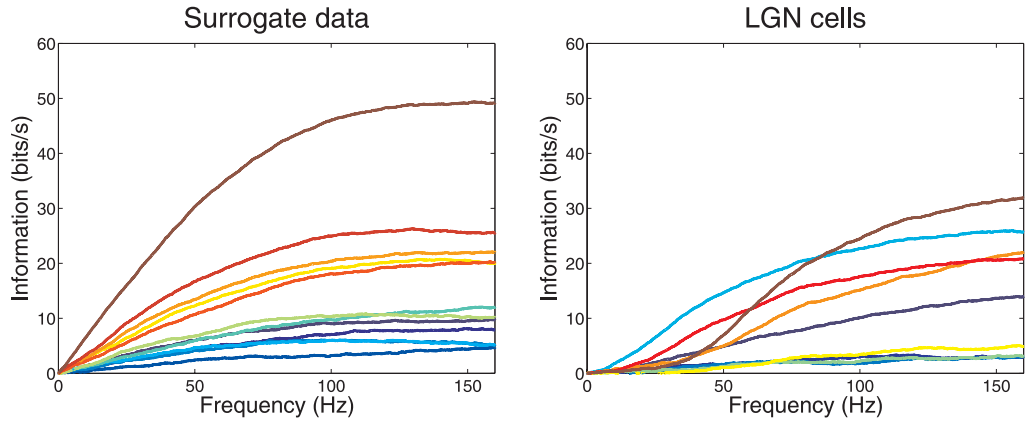

FIGURE 2 | Cumulative information rate vs frequency for 12 surrogate Poisson model neurons and 9 LGN cells. The firing rates of the various neurons in the two groups were similar.

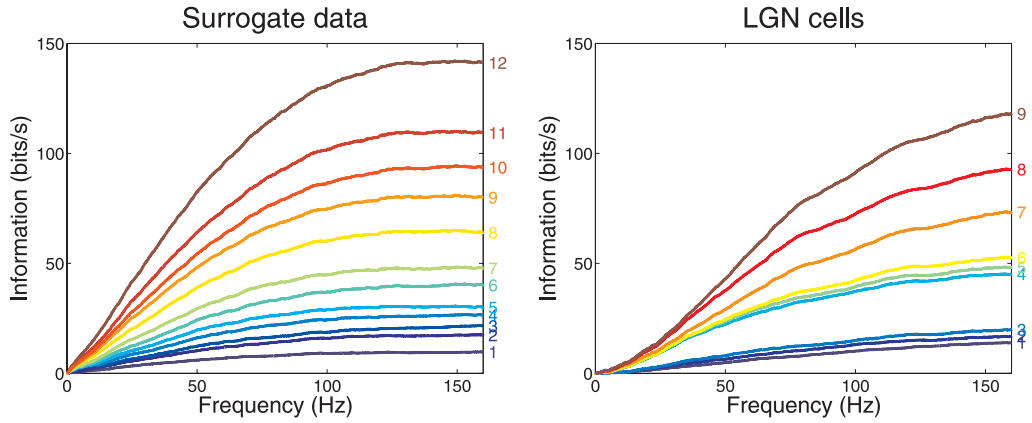

FIGURE 3 | Group information vs frequency for our Poisson model surrogate neurons and 9 LGN cells. The group size is indicated to the right of the cumulative curve for each group. The neurons were ranked according to their firing rate. The first group contained only the slowest firing neuron, and each new group was formed by adding the next ranking cell.

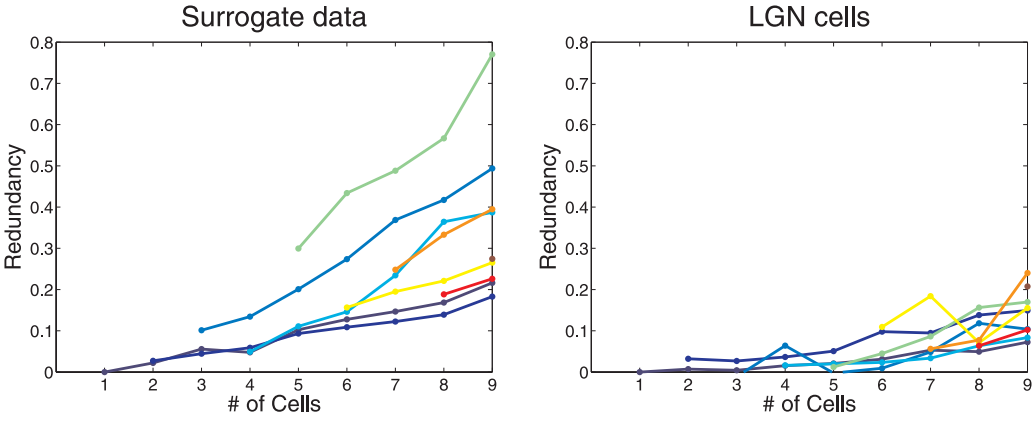

FIGURE 4 | Accumulating redundancy as more cells are added to a population. The cells are added in order of their mean firing rates, starting with the slowest firing cells, with each cell taking its turn as a starting point for a new population.

Redundancy in surrogate and real LGN neurons

Figure 4 (right frame) compares the redundancy over the 9 LGN cells with what was shown for the first 9 Poisson model neurons in **Figure 4** (left frame). The pair of sharp features at cells 4 and 7 might be attributed to difficulties in spike separation. Note that the redundancy of real neurons appears to be quite different from that of their Poisson model counterparts: as cluster size increases, real cells manifest a stronger tendency than our simulated neurons to remain non-redundant. This implies that the different LGN neurons are reporting with differences in emphasis on the various temporal features of their common stimulus.

DISCUSSION

THE VALIDITY OF THE GAUSSIAN ASSUMPTION

Our method exploits the theoretical prediction that the distribution of each stochastic Fourier coefficient of our data should be Gaussian. Our evidence supports this prediction. A standard visual check is to normalize a distribution by a *Z*-score transformation and plot its quantiles against those of a standard Gaussian. If the distribution is likewise Gaussian, the points will fall near a unit-slope straight line through the origin. **Figure 5** shows two typical cases, each with 128 points: surrogate data in the left frame and LGN cell data on the right. Both show good qualitative confirmation of the Gaussian assumption.

We have proceeded to apply to our numerous Fourier coefficient distributions two standard statistical tests for Gaussian distribution: the Shapiro–Wilk test and the Lilliefors test. Both are designed to confirm that a sample was drawn from a true Gaussian distribution in 95% of cases. **Table 2** shows that in almost all cases for both unique and repeat responses of our 12 surrogate and 9 LGN cells our distributions passed both tests at the 95% significance level.

SMALL SAMPLE BIAS

In the extraction of mutual information from spike data, traditional methods suffer from a bias due to the small size of the sample. We checked the Fourier method for such bias by dividing our sets of 128 runs into subsets of 64, 32 and 16 runs. The results for one surrogate cell (number 12) and one LGN cell (number 8) are shown in **Figure 6**. These results are typical, and show no clear small-sample

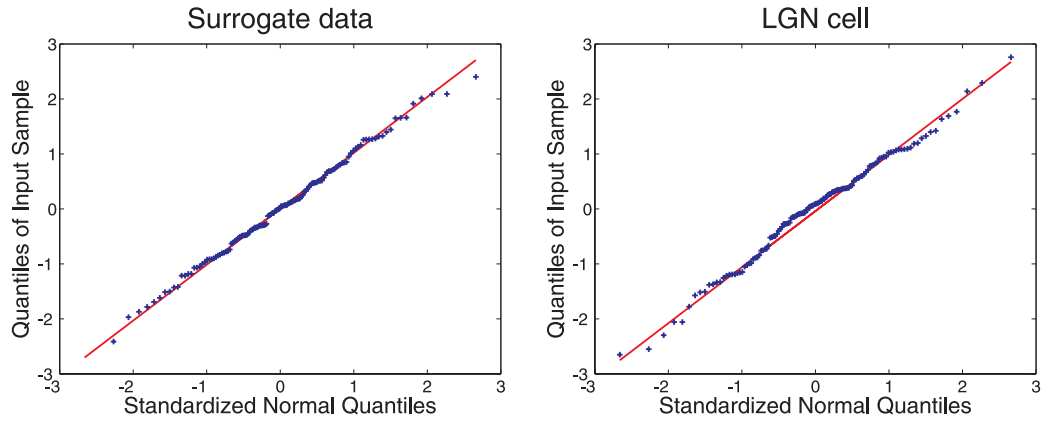

FIGURE 5 | Q–Q plots for the Fourier coefficients of one surrogate cell (#6) and one LGN cell (#4). The data are typical of data from other cells. The fact that the data points hug the $y = x$ line demonstrates the Gaussian nature of the distributions of the Fourier coefficients.

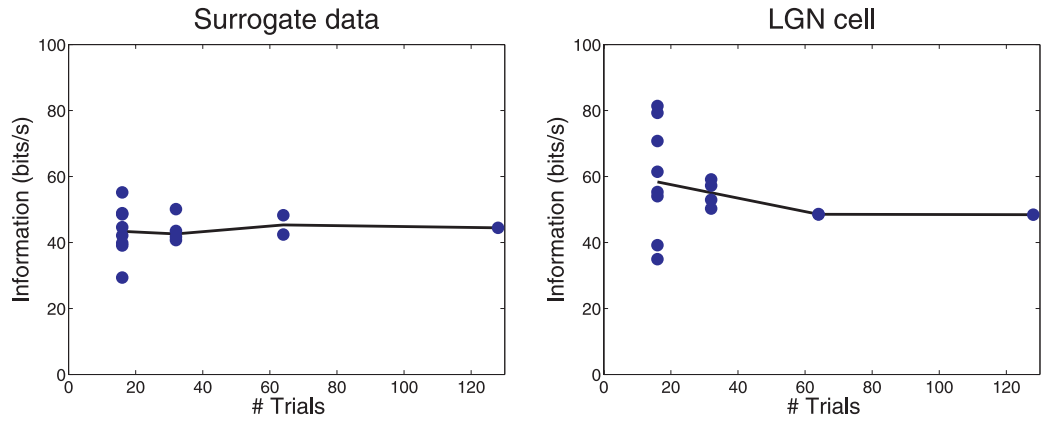

FIGURE 6 | The effect of the number of trials on information calculation. Data are from surrogate cell #12 and LGN cell #8, which were typical of other cells. Solid symbols show the information calculated from individual segments of the record. The solid line connects the medians of the samples. Note the rapid convergence of the information estimates as the number of trials increases.

bias. We also notice that, for these data, a sample of 64 runs gives a mutual information estimate reliable to better than ±10%. A summary of small-sample bias and estimated reliability for several recent techniques for calculating spike-train mutual information is given by Ince et al. (2009) (their Figure 1).

In addition to the number of data segments, the number of spikes used in estimating the mutual information is also an important factor, and we discus it further at the end of the Appendix.

SUMMARY AND CONCLUSIONS

We have presented a new method for calculating the amount of information transmitted by a neuronal population, and have applied it to populations of simulated neurons and of monkey LGN neurons. Since the method can be used also to calculate the information transmitted by individual cells, it provides an estimate of the redundancy of information among the members of the population. In addition, the method reveals the temporal frequency bands at which the communicated information resides.

The new method fills a gap in the toolbox of the modern neurophysiologist, who now has the ability to record simultaneously from many neurons. The methodology presented here might permit insights regarding the mutual interactions of neuronal clusters, an area that has been explored less than the behavior of single neurons or whole organisms.

APPENDIX

Suppose we have a stochastic numerical data-stream that we will call $u(t)$, and which becomes uncorrelated for two values of t that are separated by a time interval greater than a maximum correlation time-interval t^*. That is to say, if $t_2 - t_1 > t^*$, then $u(t_2)$ and $u(t_1)$ are *independent* random variables in the probability sense. Suppose now that in the laboratory, by running the probabilistically identical experiment repeatedly, we gather N realizations (samples) of $u(t)$, the n^{th} of which we will call $u^{(n)}(t)$. Suppose further that we collect each data sample over a time-span T that is large compared to the correlation time interval t^*.

We can represent each sample $u^{(n)}(t)$ to whatever accuracy we desire, as a discrete sequence of numbers in the following way. Over the time interval $t = 0$ to $t = T$, we choose a set of functions $\varphi_m(t)$ that are *orthonormal* in the sense that they have the property:

$$\int_0^T dt\varphi_q(t)\varphi_r(t) = \delta_{qr} (= 1 \text{ if } q = r, \text{ else} = 0). \tag{A1}$$

Then $u^{(n)}(t)$ may be represented as a weighted sum of these basis functions:

$$u^{(n)}(t) = \sum_q u_q^{(n)}\varphi_q(t) \tag{A2}$$

where the weighting coefficients $u_m^{(n)}$ may be evaluated from the data by,

$$u_m^{(n)} = \int_0^T dt\varphi_m(t)u^{(n)}(t). \tag{A3}$$

This claim can be verified if we substitute (Eq. A2) into (Eq. A3) and then use (Eq. A1) to evaluate the integral. Here our choice of the $\varphi_m(t)$ will be the conventional normalized sinusoids:

$$\varphi_m(t) = \begin{cases} \sqrt{2/T}\sin 2\pi((m+1)/2)(t/T) \text{ for } m \text{ odd} \\ \sqrt{2/T}\cos \pi m(t/T) \text{ for } m \text{ even} \end{cases} \tag{A4}$$

It is a straightforward exercise to show that these functions have the property required by (Eq. A1).

Now let us see what follows from $T >> t^*$. Divide the full time-span T into K sub-intervals by defining the division times:

$$t_k = (k/K)T \tag{A5}$$

and define the integrals over shorter sub-intervals:

$$A_{m,k}^{(n)} = \int_{t_{k-1}}^{t_k - t^*} dt\varphi_m(t)u^{(n)}(t) \tag{A6}$$

$$B_{m,k}^{(n)} = \int_{t_k - t^*}^{t_k} dt\varphi_m(t)u^{(n)}(t) \tag{A7}$$

from which (Eq. A3) tells us that the Fourier coefficient $u_m^{(n)}$ is given by,

$$u_m^{(n)} = \sum_k A_{m,k}^{(n)} + \sum_k B_{m,k}^{(n)}. \tag{A8}$$

But we note that the measure of the support of the integral (Eq. A7) is smaller than that of (Eq. A6) by the ratio $t^*/((T/K) - t^*)$, and if we can pick T long enough, we can make that ratio as close to zero as we choose. So the second sum in (Eq. A8) is negligible in the limit. But now note that, because they are all separated from each other by a correlation time, the individual terms in the first sum are realizations of independent random variables. If the distribution of an individual term in the sum is constrained in any one of a number of non-pathological ways, and if there are a sufficient number of members in the sum, then the central limit theorem states that the distribution of the sum approaches a Gaussian.

In the more general case, where we have several simultaneous correlated numerical data-streams, the argument runs exactly the same way. If, for many repeated samples, at a particular frequency we compute the Fourier coefficient for each, to estimate a multivariate probability density, then from a long enough time span, by the multivariate central limit theorem that density will approach a multivariate Gaussian. Simply because the notation is easier, we elaborate the univariate case first.

Specializing, for cell response we use the spike train itself, expressed as a sequence of δ-functions, so for the r^{th} realization $u^{(r)}(t)$ of the stochastic spike-train variable $u(t)$, we have:

$$u^{(r)}(t) = \sum_{n=1}^{N_r} \delta(t - t_{(r)n}) \tag{A9}$$

where $t_{(r)n}$ is the time of the n^{th} spike of the r^{th} realization, and N_r is the total number of spikes that the cell under discussion fires in that realization.

Substituting this and also (Eq. A4) into (Eq. A3) we see that the integral may be performed at once. In the cosine case of (Eq. A4) it is,

$$u_m^{(r)} = \sqrt{2/T}\sum_{n=1}^{N_r}\cos \pi m(t_{(r)n}/T) \tag{A10}$$

Before proceeding further we look back at Eq. A8 and note that, because a cosine is bounded between +1 and −1, every term in the sums of (Eq. A8) is bounded in absolute value by $\sqrt{2/T}$ times the number of spikes in that sub-interval. As real biology will not deliver a cluster of spikes overwhelmingly more numerous than the local mean rate would estimate, the *distribution* of each term in the stochastic sum cannot be heavy-tailed, and we may trust the central limit theorem.

Thus we may estimate that the probability density function for the stochastic Fourier coefficient variable u_m is of the form,

$$p_m(u_m) = (2\pi V_m)^{-1/2}\exp\left(-(u_m-\overline{u}_m)^2/2V_m\right). \tag{A11}$$

where,

$$\overline{u}_m = \left\langle u_m\right\rangle_{p_m} \cong \frac{1}{R}\sum_{r=1}^{R}(u_m^{(r)}), \tag{A12}$$

$$V_m = \left\langle (u_m^{(r)}-\overline{u}_m)^2\right\rangle_{p_m} \cong \frac{1}{R-1}\sum_{r=1}^{R}(u_m^{(r)}-\overline{u}_m)^2. \tag{A13}$$

The right-hand-most expressions in (Eq. A12), (Eq. A13) testify that $\overline{u}_m$ and V_m can be estimated directly from the available laboratory data.

What is the information content carried by the Gaussian (Eq. A11)? The relevant integral may be performed analytically:

$$I(p_m) = -\int du_m(\ln p_m(u_m))p_m(u_m) = \frac{1}{2}\ln((2\pi e)V_m). \tag{A14}$$

For a signal with finite forgetting-time the stochastic Fourier coefficients (Eq. A10) at different frequencies are statistically independent of one another, so that the signal's full multivariate probability distribution in terms of Fourier coefficients is given by,

$$p(u_1,u_2,\ldots) = \prod_m p_m(u_m). \tag{A15}$$

It is easily shown that if a multivariate distribution is the product of underlying univariate building blocks, then its information content is the sum of the information of its components, whence

$$I(p) = \sum_{m=0}^{M-1} I(p_m) = \frac{1}{2}\sum_{m=0}^{M-1}\ln((2\pi e)V_m). \tag{A16}$$

Observing (Eq. A13) we note that this can be evaluated from available laboratory data.

Generalization of the information rate calculation to the case of multiple neurons is conceptually straightforward but notationally messy due to additional subscripts. The *r*th realization's spike train from the *q*th neuron (out of a total of *Q* neurons) may be defined as a function of time $u_{(q)}^{(r)}(t)$ just as in (Eq. A9) above, and from our orthonormal set of sines and cosines we may find the Fourier coefficient $u_{(q)m}^{(r)}$. This number is a realization drawn from an ensemble whose multivariate probability density function we may call:

$$p_m(u_{(1)m},u_{(2)m},..,u_{(Q)m}). \tag{A17}$$

This density defines a vector center of gravity $\overline{u}_m$ whose *Q* components are of the form:

$$\overline{u}_{(q)m} = \left\langle u_{(q)m}\right\rangle_{p_m} \cong \frac{1}{R}\sum_{r=1}^{R}u_{(q)m}^{(r)}, \tag{A18}$$

and similarly it defines a covariance matrix V_m whose (*q*,*s*)th matrix element is given by,

$$\begin{aligned} V_{(q,s)m} &= \left\langle (u_{(q)m}-\overline{u}_{(q)m})(u_{(s)m}-\overline{u}_{(s)m})\right\rangle_{p_m} \\ &\cong \frac{1}{R-1}\sum_{r=1}^{R}(u_{(q)m}^{r}-\overline{u}_{(q)m}^{r})(u_{(s)m}^{r}-\overline{u}_{(s)m}^{r}). \end{aligned} \tag{A19}$$

This covariance matrix has a matrix inverse A_m:

$$A_m = V_m^{-1}. \tag{A20}$$

Clearly (Eq. A18) and (Eq. A19) are the multivariate generalizations of (Eq. A12) and (Eq. A13) above. The central limit theorem's multivariate Gaussian generalization of (Eq. A11) is,

$$p_m(u_{(1)m},..,u_{(Q)m}) = ((2\pi)^Q\det V_m)^{(-1/2)}\exp\left(-\frac{1}{2}\sum_{q,s}(u_{(q)m}-\overline{u}_{(q)m})A_{(q,s)m}(u_{(s)m}-\overline{u}_{(s)m})\right). \tag{A21}$$

This expression becomes less intimidating in new coordinates $Z_{(q)}$ with new origin located at the center of gravity and orthogonally turned to diagonalize the covariance matrix (Eq. A19). We need not actually undertake this task. Call the eigenvalues of the covariance matrix

$$\lambda_{(1)m},..,\lambda_{(Q)m}. \tag{A22}$$

Under the contemplated diagonalizing transformation, the double sum in the exponent collapses to a single sum of squared terms, and in the new coordinates p_m becomes,

$$\hat{p}_m(Z_1,..,Z_Q) = \prod_{q=1}^{Q}(2\pi\lambda_{(q)m})^{-1/2}\exp\left(-Z_q^2/2\lambda_{(q)m}\right), \tag{A23}$$

a form that is familiar from (Eq. A15) above. Its corresponding information is the sum of those of the individual terms of the product and is

$$I(p_m) = \frac{1}{2}\sum_{q=1}^{Q}\ln((2\pi e)\lambda_{(q)m}). \tag{A24}$$

Shannon (1949, chapter 4), in a formally rather analogous context, has noted that much care is needed in the evaluation of expressions similar to (Eq. A24) from laboratory data. The problem arises here if the eigenvalues approach zero (and their logarithms tend to $-\infty$) before the sum is completed. However, the information in signal-plus-noise in the *m*th coefficient, expressed by (Eq. A24) is

not of comparable interest to the information from signal alone. With some caution, this signal-alone information contribution may be obtained by subtracting from (Eq. A24) a similar expression for noise alone, taken from additional laboratory data in which the *same* stimulus was presented repeatedly. If we use 'μ' to annotate the eigenvalues of the covariance matrix which emerges from these runs, then the information difference of interest, following from (Eq. A24) is

$$I_m(\text{signal alone}) = \frac{1}{2}\sum_{q=1}^{Q}\left\{\ln((2\pi e)\lambda_{(q)m}) - \ln((2\pi e)\mu_{(q)m})\right\} = \frac{1}{2}\sum_{q=1}^{Q}\ln\left(\frac{\lambda_{(q)m}}{\mu_{(q)m}}\right). \quad \text{(A25)}$$

Equation A25 expresses the multi-cell information contributed by the *m*th frequency component. To obtain the total multi-cell information, it is to be summed over increasing *m* until further contributions become inappreciable.

An entirely analogous procedure applies to obtain the information of signal alone for an individual cell. Call the variance of the *m*th frequency component of the unique runs V_{mu}, and that of the repeat runs V_{mr}. Each will yield a total information rate expressed by (Eq. A16) above, and their difference, the information rate from signal alone, consequently will be:

$$I\left(\text{cell, signal alone}\right) = \frac{1}{2}\sum_{m=0}^{M-1}\ln\left(\frac{V_{mu}}{V_{mr}}\right). \quad \text{(A26)}$$

In the data analysis in the main text, the single-cell sums (Eq. A16), for both uniques and repeats, approached a common, linearly advancing value which they achieved near 160 Hz, which is the stimulus frame-rate. Consequently, the summation over frequency of signal only information was cut off at that frequency, both for single cells (see Eq. A26) and for combinations of cells.

In both the simulations and the experiments, each run was of $T = 8$ s duration. In consequence the orthonormalized sines and cosines of (Eq. A4) advanced by steps of 1/8 Hz.

EFFECT OF THE NUMBER OF RESPONSE SPIKES

With reference to small-sample bias, a further word is appropriate here regarding our methodology. If the number of runs is modest, the total number of spikes in response to the repeated stimulus may show a significant statistical fluctuation away from the total number of spikes in response to the unique runs. In this case, the asymptotic high-frequency entropy values, as seen in our **Figure 1**, will not quite coincide, and consequently the accumulated mutual information will show an artifactual small linear drift with increasing frequency. This introduces a bit of uncertainty in the cut-off frequency and in the total mutual information. This asymptotic drift may be turned into a more objective way to evaluate the total mutual information. In cases where the problem arises, we divide our repeat runs into two subsets: the half with the most spikes and the half with the least. Accumulating both mutual information estimates at high frequency, we linearly extrapolate both asymptotic linear drifts back to zero frequency, where they intersect at the proper value of mutual information.

ACKNOWLEDGMENTS

This work was supported by NIH grants *EY16224, EY16371, NIGM71558 and Core Grant EY12867*. We thank Drs. J. Victor, Y. Xiao and A. Casti for their help with this project.

REFERENCES

Bair, W., Zohary, E., and Newsome, W. T. (2001). Correlated firing in macaque visual area MT: time scales and relationship to behavior. *J. Neurosci.* 21, 1676–1697.

Bialek, W., Rieke, F., de Ruyter van Steveninck, R. R., and Warland, D. (1991). Reading a neural code. *Science* 252, 1854–1857.

Borst, A., and Theunissen, F. (1999). Information theory and neural coding. *Nat. Neurosci.*, 2, 947–957.

Brainard, D. H. (1989). Calibration of a computer controlled color monitor. *Color Res. Appl.* 14, 23–34.

Brenner, N., Strong, S. P., Koberle, R., Bialek, W., and de Ruyter van Steveninck, R. R. (2000). Synergy in a neural code. *Neural Comput.* 12, 1531–1552.

Brown, E. N., Kass, R. E., and Mitra, P. P. (2004). Multiple neural spike train data analysis: state-of-the-art and future challenges. *Nat. Neurosci.* 7, 456–461.

DiCaprio, R. A. (2004). Information transfer rate of nonspiking afferent neurons in the crab. *J. Neurophysiol.* 92, 302–310.

Fiset, P., Paus, T., Daloz, T., Plourde, G., Meure, P., Bonhomme, V., Haij-Ali, N., Backman, S. B., and Evans, A. (1999). Brain mechanisms of propofol-induced loss of conciousness in humans: a positron emission tomography study. *J. Neurosci.* 19, 5506–5513.

Gawne, T. J., and Richmond, B. J. (1993). How independent are the messages carried by adjacent inferior temporal cortical neurons? *J. Neurosci.* 13, 2758–2771.

Ince, R. A. A., Petersen, R. S., Swan, D. C., and Panzeri, S. (2009). Python for information theoretic analysis of neural data. *Front. Neuroinformatics* 3:4. doi: 10.3389/neuro.11.004.2009.

Kaplan, E. (2007). "The M, K, and P streams in the primate visual system: what do they do for vision?" Chapter 1.16, in *The Senses* eds R. Masland and T. D. Albright (San Diego: Elsevier), 369–382.

Knight, B. W. (1972). Dynamics of encoding in a population of neurons. *J. Gen. Physiol.* 59, 734–766.

Montani, F., Kohn, A., Smith, M. A., and Schultz, S. R. (2007). The role of correlations in direction and contrast coding in the primary visual cortex. *J. Neurosci.* 27, 2338–2348.

Optican, L. M., and Richmond, B. J. (1987). Temporal encoding of two-dimensional patterns by single units in primate inferior temporal cortex. III. information theoretic analysis. *J. Neurophysiol.* 57, 162–178.

Pillow, J. W., Paninski, L., Uzzell, V. J., Simoncelli, E. P., and Chichilnisky, E. J. (2005). Prediction and decoding of retinal ganglion cell responses with a probabilistic spiking model. *J. Neurosci.* 25, 11003–11013.

Pillow, J. W., Shlens, J., Paninski, L., Sher, A., Litke, A. M., Chichilnisky, E. J., and Simoncelli, E. P. (2008). Spatio-temporal correlations and visual signalling in a complete neuronal population. *Nature* 454, 995–999.

Pillow, J. W., and Simoncelli, E. P. (2006). Dimensionality reduction in neural models: an information-theoretic generalization of spike-triggered average and covariance analysis. *J. Vis.* 6, 414–428.

Quiroga, R. Q., and Panzeri, S. (2009). Extracting information from neuronal populations: information theory and decoding approaches. *Nat. Rev. Neurosci.* 10, 173–185.

Reinagel, P., and Reid, R. C. (2000). Temporal coding of visual information in the thalamus. *J. Neurosci.* 20, 5392–5400.

Richmond, B. J., and Optican, L. M. (1987). Temporal encoding of two-dimensional patterns by single units in primate inferior temporal cortex. II. quantification of response waveform. *J. Neurophysiol.* 57, 147–161.

Richmond, B. J., Optican, L. M., Podell, M., and Spitzer, H. (1987). Temporal encoding of two-dimensional patterns by single units in primate inferior temporal cortex. I. Response characteristics. *J. Neurophysiol.* 57, 132–146.

Rieke, F., Warland, D., Steveninck, R. D., and Bialek, W. (1997). *Spikes: Exploring the Neural Code.* Cambridge, MA: MIT Press.

Schneidman, E., Bialek, W., and Berry, M. J. (2003). Synergy, redundancy, and independence in population codes. *J. Neurosci.* 23, 11539–11553.

Shannon, C., and Weaver, W. (1949). *A Mathematical Theory of Communication.* Chicago, IL: University of Illinois Press.

Shannon, C. E. (1949). Communication in the presence of noise. *Proc. IEEE* 37, 10–21.

Shoham, S., Fellows, M. R., and Normann, R. A. (2003). Robust, automatic spike sorting using mixtures of multivariate t-distributions. *J. Neurosci. Methods* 127, 111–122.

Strong, S. P., Koberle, R., de Ruyter van Steveninck, R. R., and Bialek, W. (1998). Entropy and information in neural spike trains. *Phys. Rev. Lett.* 80, 197–200.

Uglesich, R., Casti, A., Hayot, F., and Kaplan, E. (2009). Stimulus size dependence of information transfer from retina to thalamus. *Front. Syst. Neurosci.* 3:10. doi: 10.3389/neuro.06.010.2009.

van Hateren, J. H. (1997). Processing of natural time series of intensities by the visual system of the blowfly. *Vis. Res.* 37, 3407–3416.

Wandell, B. A. (1995). *Foundations of Vision*. Sunderland, MA: Sinauer Associates.

Zohary, E., Shadlen, M. N., and Newsome, W. T. (1994). Correlated neuronal discharge rate and its implications for psychophysical performance. *Nature* 370, 140–143.

Conflict of Interest Statement: The authors declare that the research was conducted in the absence of any commercial or financial relationships that could be construed as a potential conflict of interest.

Received: 03 December 2009; paper pending published: 31 December 2009; accepted: 29 March 2010; published online: 26 April 2010.

Citation: Yu Y, Crumiller M, Knight B and Kaplan E (2010) Estimating the amount of information carried by a neuronal population. Front. Comput. Neurosci. ***4****:10. doi: 10.3389/fncom.2010.00010*

2.2 Estimating the amount of information conveyed by a population of neurons.

Crumiller M, Knight B, Yu Y, Kaplan E.

Front Neurosci. 2011 Jul 15;5:90

frontiers in
NEUROSCIENCE

FOCUSED REVIEW
published: 15 July 2011
doi: 10.3389/fnins.2011.00090

Estimating the amount of information conveyed by a population of neurons

Marshall Crumiller[1], Bruce Knight[2], Yunguo Yu[3] and Ehud Kaplan[1]*

[1] *The Fishberg Department of Neuroscience and Friedman Brain Institute, The Mount Sinai School of Medicine, New York, NY, USA*
[2] *The Laboratory of Biophysics, The Rockefeller University, New York, NY, USA*
[3] *Department of Neuroscience, Weill Medical College, New York, NY, USA*

Recent technological advances have made the simultaneous recording of the activity of many neurons common. However, estimating the amount of information conveyed by the discharge of a neural population remains a significant challenge. Here we describe our recently published analysis method that assists in such estimates. We describe the key concepts and assumptions on which the method is based, illustrate its use with data from both simulated and real neurons recorded from the lateral geniculate nucleus of a monkey, and show how it can be used to calculate redundancy and synergy among neuronal groups.

Keywords: information, neural population, redundancy, frequency analysis

Edited by:
Jakob H. Macke, University College London, UK

Reviewed by:
Stefano Panzeri, Italian Institute of Technology, Italy
Jakob H. Macke, University College London, UK

****Correspondence:***

***Ehud Kaplan** studied psychology at the Hebrew University in Jerusalem, Israel, and neurophysiology at Syracuse University, NY. From 1973 to 1995 he was at The Biophysics lab at The Rockefeller University, NY. In 1995 he moved to the Mount Sinai School of Medicine, NY, where he is a professor of neuroscience and the director of the Center for Excellence in Computational and Systems Neuroscience at the Friedman Brain Institute. He uses electrophysiological, imaging and computational approaches to study quantitatively how neural signals are processed in the brain.*
ehud.kaplan@mssm.edu

1 INTRODUCTION

The brain processes information by the coordinated activity of many neurons, and it is therefore natural to ask: *How much information does a given set of neurons transmit?* In the past, several methods that estimated information rates from the firing pattern (Optican and Richmond, 1987; Richmond and Optican, 1987; Richmond et al., 1987; Bialek et al., 1991; Rieke et al., 1997; Strong et al., 1998; Brenner et al., 2000) or membrane potential (Borst and Theunissen, 1999; DiCaprio, 2004) of single neurons have been used. The information contained in spike trains was estimated by calculating the **entropy** associated with the various temporal patterns of spike discharge, using Shannon's formula (Shannon, 1949; Shannon and Weaver, 1949; Victor, 2006). For a thorough review of existing approaches, see Quiroga and Panzeri (2009).

Such calculations become impractical when we are dealing with a substantial number of neurons, and since all brain functions involve many interacting neurons, it is important to provide similar information estimates for a neuronal population. Simply adding up the information delivered by individual neurons in the population is not a valid procedure because of these interactions (see, for example, Zohary et al., 1994; Bair et al., 2001; Latham and Nirenberg, 2005; Pillow et al., 2008). Methods adequate for single neuron data, such as the *Reconstruction Method* (Bialek et al., 1991) or the *Direct Method* (Strong et al., 1998), become impractical for a substantial population of neurons because of the "curse of dimensionality": the huge multi-dimensional space inhabited by many diverse spike trains can only be sampled rather sparsely by most real-life neurophysiological experiments.

Calculating the information carried by a population of many neurons thus has remained a significant challenge (Brown et al., 2004; Quiroga and Panzeri, 2009), while the need for such estimates has become increasingly urgent: the technology of recording simultaneously from many neurons has become affordable and wide-spread, and data from such recordings are becoming common.

A quantitative measure of the information transmitted by a neural population should make it possible to investigate **synergy** (population codes; for example, Gat and Tishby, 1999; Brenner et al.,

2000; Latham and Nirenberg, 2005) and **redundancy** (less than additive combination of information) among interacting neurons, and thus provide new insights into the computational principles employed by the brain. Here we describe a method that estimates the amount of information transmitted by a population of spiking neurons, and demonstrate its use with both simulated data and data recorded from the *lateral geniculate nucleus* (LGN) of an anesthetized macaque monkey. To make the method accessible to a broader audience of interested neuroscientists, we minimize here the explicit use of mathematics. Interested readers can find details in the appendix of our original paper (Yu et al., 2010), where the details of the experimental procedures used to obtain the laboratory recordings can also be found.

2 ESTIMATION OF THE RATE AT WHICH A NEURAL ENSEMBLE DELIVERS INFORMATION

2.1 INFORMATION

In everyday usage, the word "information" refers to the amount of novelty transmitted in a message – data that enable us to choose among alternatives. In its quantitative, technical meaning, the information in a message refers to the reduction in uncertainty associated with a presupposed probability distribution of possible events. In this sense, information is a function of both the contents of the message and of an *a priori* assumption concerning the relative likelihood of possible events. Consider, for example, a message sent as ASCII characters, which is received as a string of 0's and 1's. This bitstream of 0's and 1's contains several levels of information that we might decompose. On a per-character basis, every group of eight bits corresponds to a single ASCII character. Given that each bit is either a 0 or a 1, we have 2^8, or 256, total possible characters for every eight bits. Each additional bit of information reduces the remaining uncertainty of the sequence by half. Conversely, we might say that each bit doubles the number of potential choices: the number of possible sequences is 2^N, where N is the number of bits.

Does each bit carry the same amount of information? Usually not. For example, all 36 alphanumeric characters in English begin with one of only five unique 4-bit sequences: 0011, 0100, 0101, 0110, and 0111. Note that the first bit of every character is a 0. Since this 0 occurs with 100% probability, it carries zero information with respect to the alphabet. In a similar vein, the character *e* occurs almost 172 times as often as the letter *z* (Lewand, 2000), and so it is wasteful to use the same number of bits for both: an efficient encoding scheme would require fewer bits for common characters than for rare ones. To encode otherwise introduces redundancy into the system – informally defined as the number of "wasted" bits used in transmitting the message. Because an *e* will appear in English with higher probability than a *z*, our uncertainty is reduced to a lesser extent when it occurs. Our total uncertainty, therefore, is a function of the probability of occurrence of the characters. It is this uncertainty, dubbed *entropy*, that Claude Shannon quantified in his seminal paper *A Mathematical Theory of Communication* (1948).

In a similar manner, a neuron in the nervous system encodes information about a stimulus via a sequence of action potentials. How might we calculate the entropy from such a sequence? As just discussed, at the heart of Shannon's entropy lies the probability distribution – a description of the likelihood of different messages. With this in mind, to calculate entropy we must do two things: (1) define what a neuronal "message" is, and (2) calculate the probability distribution of the various messages. Several methods have been proposed for accomplishing these tasks, yet dealing with more than a few neurons recorded simultaneously has remained beyond reach.

2.2 FEATURES OF THE FORMULATION

The methodology of information theory may be addressed not only to the example of messages in ASCII code, but also to situations that are more general in several different respects (Cover and Thomas, 2006). In a rather remarkable way, a useful theory emerges which has several unexpected features.

Suppose we had a very large collection of signals of a specified duration, each occurring numerous times. From that ensemble we could derive a list of the probability of occurrence of each distinct signal. The first step of information theory is to observe that any such list of probabilities gives rise to an essentially unique number – its entropy – which states, in bits, *the potential capability of an average member of that ensemble to convey a message*. Entropy is the central concept and central building-block of information theory and is constructed from the list of probabilities by the formula

$$H = -\sum_r p_r \log_2 p_r \qquad (1)$$

where p_r indicates the probability of a specific signal r.

Equation 1 has the following property: if we regard two separate signals as two consecutive "chapters" of a longer signal, then the entropy of a set of these longer signals is the sum of the

Entropy
In information theory, entropy is a measure of the uncertainty associated with a random variable. It quantifies the disorder, or unpredictability, of a collection of signals. Entropy is the expected value of the information contained in a message, and is measured in bits. The concept was introduced in this context by C. Shannon's 1948 paper "A Mathematical Theory of Communication."

Synergy/Redundancy
If all the neurons in a population were independent, their group information would equal the sum over the information each of them carries. If their group information is less than that sum, we have redundancy: some of the information delivered by some neurons is also delivered by others. If their group information has more than that sum, we have synergy, providing information that depends on the coordinated firing of some neurons, and cannot be extracted by examining individual neurons.

entropies calculated for its two consecutive chapters. The distribution p of all n signals is maximized when p is the uniform distribution (that is, all signals are equally likely, with probability $1/n$). When this occurs, the formula reduces to $\log_2 n$.

Equation 1 is the only way to satisfy two requirements: (1) in the case of equal probabilities, as above it reduces to a simple logarithm, and (2) as in the "chapter" example above, the sum of the entropies of two signals is equal to the entropy of the signals taken together.

2.2.1 Noise and signal entropies

Experimental data typically contain noise: the accuracy and precision of any measurement are limited by noise in both the production of the stimulus signal, the transduction of the signal through the inherently noisy nervous system, and the recording of the output signal through the measurement devices. In the complete absence of noise, any differential response of the nervous system would indicate its ability to discriminate different stimuli. With noise, however, our system's ability to discriminate between stimuli is greatly reduced: the signal is muddied, and the reduction in uncertainty accompanying any measured output signal – the information in the signal – is itself diminished. Variations in the measured output signal still exist, but we can no longer reliably ascribe such variations to changes in the input. Some of the variability in the signal, therefore, contains not *signal entropy* (which would allow us to discriminate stimuli), but *noise entropy* – entropy that is due entirely to noise.

To properly calculate the actual signal information of the system, we must remove from the entropy calculation the contribution of noise. By analogy with the calculation of the total entropy (denoted by H_T), the noise entropy (H_N) is calculated from observing the variability of responses to repeated presentations of a (typical) stimulus, with a formula similar to equation 1; The distribution of these responses provides the probabilities that the entropy formula requires. The (noiseless) information available in our signal (often called **Mutual Information**) is thus

$$I = H_T - H_N \tag{2}$$

Mutual Information
Mutual information between stimulus and response quantifies (in bits) the reduction in stimulus uncertainty gained from analyzing the response. It is calculated by subtracting from the total entropy the noise entropy, which is estimated from the variability of responses to repeated presentations of a stimulus.

This equation describes the process of measuring and removing the amount of variability in the signal that is due to noise. Details of the derivation of this equation can be found in Rieke et al. (1997, see Section 3.1.3) and in Cover and Thomas (2006, chap. 7). We note that the need to estimate the noise entropy together with the total entropy over a long experiment requires the use of repeated presentations of a chosen stimulus (referred to as *repeats*), which are interleaved with presentations of non-repeating stimuli (referred to as *uniques*).

2.2.2 Continuous signals

So far we have dealt with signals composed of sequential, well-defined markers. Information theory generalizes to signals that are continuous in time and to parallel multiples of such signals.

A natural way to approach such an extension is to study a sequence of approximations, in each of which a continuous signal in time is discretized into progressively shorter time-steps. At each successive level of approximation, the situation may be represented (as discussed above) as a sequence of discrete symbols. In doing so, however, difficulties arise, some with a surprising resolution.

2.2.2.1 The timestep problem. The probability of a continuous variable is characterized by its probability density function. When this density function is divided into very small intervals, the probability associated with each interval approaches zero; as these divisions are further refined, the total entropy and noise entropy diverge to infinity. However, these two entropies diverge together, and the offending divergence is thus canceled by taking the difference of the two entropies, and the resulting signal information (equation 2) approaches a well-defined limiting value. In this sense, the signal information is more fundamental than is either of the two entropies from which it is calculated.

2.2.2.2 The finite-sampling problem. There is a second problem that arises from dividing time into brief intervals. As we saw in the early discussion, the number of alternative code-word possibilities increases exponentially with the number of intervals. Straightforward evaluation of their probabilities for use in equation 1 demands many repeated presentations of each stimulus, and eventually becomes experimentally unfeasible. In consequence, the deep theoretical structure of this problem has received a great deal of attention, and insightful methods have been advanced for extrapolation from more modest and feasible data sets (for example, Panzeri et al., 2007). When one considers a response composed of several parallel signals, the difficulty is severely compounded, since the number of possible messages increases greatly. These extrapolation procedures (which continue to be refined) have so far successfully addressed the challenge of eight simultaneously recorded neurons.

In the following section, we advance an alternative approach that avoids the difficult step of dividing continuous time into brief discrete segments. If the specific probability density function is known *analytically*, one may proceed as above to evaluate its entropy directly, following equation 1. For example, the entropy of a Gaussian with variance σ^2 is

$$H_G(\sigma^2) = \frac{1}{2}\log_2(2\pi e\sigma^2)\,\text{bits} \qquad (3)$$

Our method exploits the *a priori* knowledge of the statistical distribution of the data to overcome the finite-sampling problem, and thus has allowed us to compute the entropy of 1024 parallel simulated signals on a desktop computer in a matter of minutes.

Shannon has observed (Shannon, 1948; Shannon and Weaver, 1949, chap. 3) that, in the continuous-time limit, the underlying random variables of the signal information may be expressed in numerous ways. In fact, *any* smooth transformation of variables leads to a new expression for signal information. Shannon then made the remarkable observation (Shannon and Weaver, 1949, chap. 4) that such transformations leave the bit-value of the signal information (but not the values of its two component entropies) unchanged. Following Shannon, the electronic communication community has used this observation to express the bit-rate of a time-varying continuous signal in terms of required frequency bandwidth. We observe here that similar treatment is applicable to spike trains.

2.2.3 Frequency representation (Fourier Analysis) and spike trains

Under diverse circumstances, a signal defined at every moment of time and over a fixed span of time can be approximated indefinitely well by a constant plus a sum of weighted sines and cosines that oscillate with frequencies that are integer multiples of a single fundamental frequency. Such a representation as a weighted sum of sines and cosines is technically a *Fourier series* representation, and its list of weighting coefficients (technically Fourier coefficients) fully characterizes the signal (Bendat and Piersol, 2010).

The weighting coefficients of each sinusoid may be calculated for a large ensemble of signals, and may thus be characterized by a probability distribution. From this distribution one can calculate, using equation 1, the associated entropy. A signal representing a spike train may be expressed as a series of delta functions (smooth "spikes" of infinitesimal width, infinite height, and area 1), with each spike representing an action potential fired by the neuron at that moment in time. The Fourier coefficients of this resulting smooth function of time may be directly evaluated (**Figure 1**, top). This procedure may be applied to the laboratory data of the experiment discussed above, where spike trains driven by *unique* and *repeat* stimuli were interleaved. From the responses to each of the two kinds of stimuli we can estimate a multivariate probability distribution for the Fourier coefficients and, by Shannon's observation above, evaluate the signal information. Several further features simplify this approach.

2.2.4 Features of the frequency representation

Our signal technically constitutes a time-stationary random process with finite memory, and from this it can be shown that Fourier components at different frequencies are uncorrelated. Thus, the multi-frequency probability distribution can be parceled into independent distributions at the separate frequencies.

We discussed above an ambiguous width in the representation of spikes as tall, narrow pedestals with unit area. In fact, one might have represented the spikes with tall, narrow positive functions of *any* shape. On closer inspection the Fourier coefficients separate into two natural frequency sets. At low frequencies, the coefficients essentially depend only on the pattern of the spikes and not on their shapes. Once the period of the sine wave becomes briefer than most spike separation times, the Fourier coefficients become dependent only on the spike shape, and not on their firing pattern. In this regime the probability distribution is the same for the repeat stimuli and for the non-repeat set. Fourier coefficients at these higher frequencies do not contribute to the signal information. The remaining influences of spike shape may be removed by taking the narrow unit-area spikes toward the limit of zero width, which assigns well-defined limiting values to the Fourier coefficients, and leaves the features above intact.

This approach greatly simplifies the calculation of Fourier coefficients from laboratory data: each Fourier coefficient is simply the sum, over all spike times, of the values of the relevant sinusoid at those times.

A further great simplification takes place: that sum of values may be broken up across time as a sum of sub-sums that are, in the ensemble, statistically independent of one another, because the signal has finite memory. Here the central limit theorem applies, and we conclude that the coefficient's distribution is Gaussian, which we have verified for both simulated and laboratory data (See Yu et al., 2010, Figure 5). The entropy of a Gaussian depends only upon its variance (equation 3), and a modest sample from a distribution

Fourier Analysis
We are interested here in a neuron's rate of transmitting information, rather than in the development of the neuronal signal over time. Since Fourier analysis decomposes a set of neuronal outputs into a sum of sine and cosine coefficients at various frequencies, it provides insight into the underlying processes that gave rise to the signal.

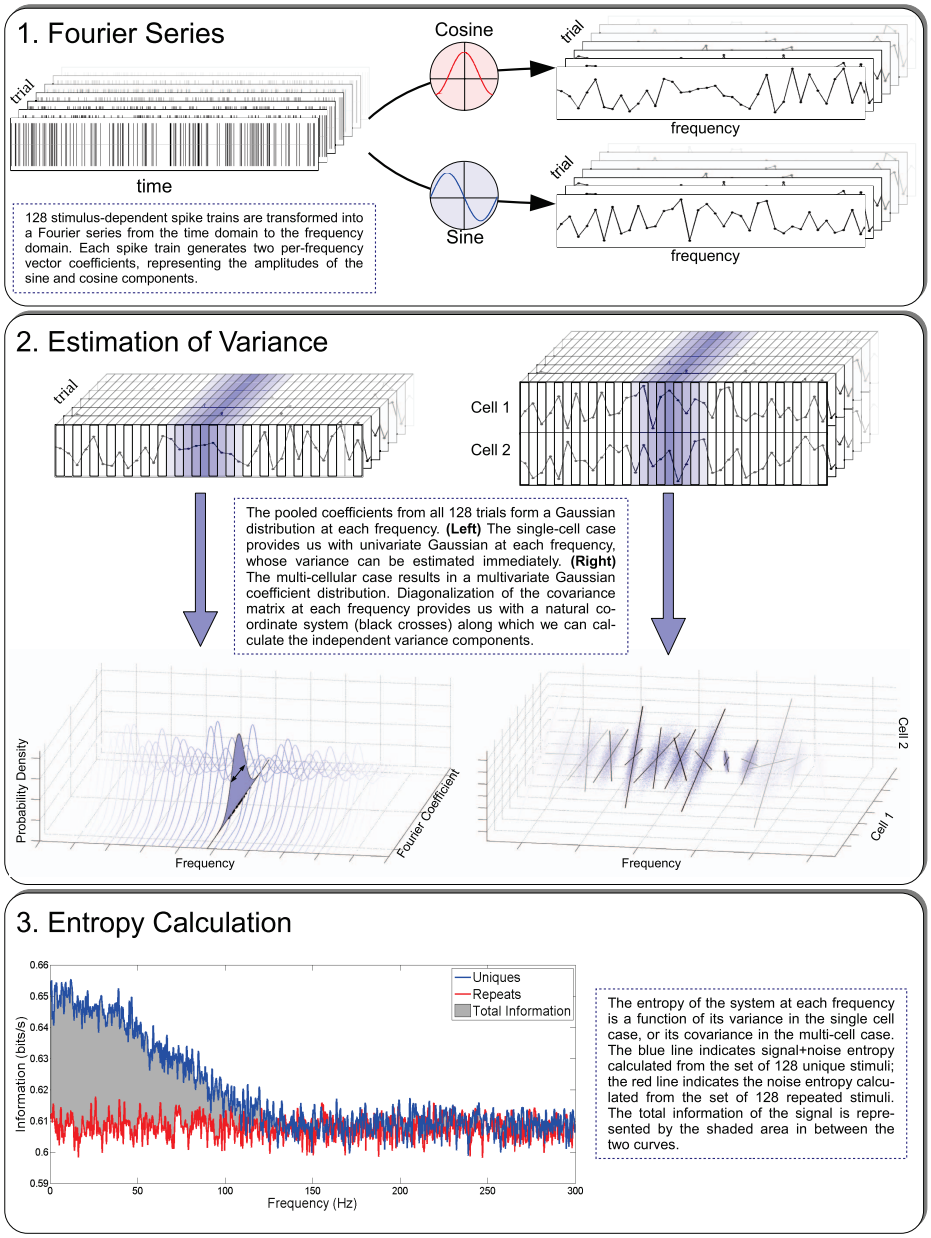

FIGURE 1 | The three steps that are required for calculating the information carried by a neural population: Fourier representation of each spike train; variance estimation, and entropy-information calculation.

known to be Gaussian is sufficient to reasonably determine its variance (**Figure 1**, middle left). Since any empirical sample is finite, the variance estimation is still slightly biased, but the bias is small compared to the bias encountered in more direct approaches that attempt to fully characterize a distribution of unknown form from a limited sample. Thus we may evaluate the signal information by summing the Gaussian entropies of equation 3 over the range of frequencies for which the entropies for responses to the two different types of stimuli (unique and repeated) are unequal.

2.3 INFORMATION IN MULTIPLE-NEURON SPIKE TRAINS

In the previous section we described how the entropy of a single neuron may be calculated from the variances of its Fourier coefficients over a range of frequencies. In the more general situation, in which several neurons are recorded simultaneously, a common input may lead to features in common in those neurons' outputs. This would imply that the response of a given neuron was, in part, predictable from the responses of others, and consequently the amount of information

delivered by the group would be less than the sum of what was calculated for the individual neurons. The way this situation can be addressed quantitatively may be illustrated by the case of two neurons, as presented in **Figure 2**.

We choose a Fourier coefficient at one particular frequency, and for each of a sequence of trials we plot its value for cell A horizontally and its value for cell B vertically. In the left frame we consider the case where the cells are firing independently. The points are thus drawn from a two-dimensional distribution that is the product of the horizontal distribution and the vertical distribution that are both Gaussian. The two-dimensional distribution is thus the product of two univariate Gaussians. We have chosen for the vertical cell B a Gaussian with a smaller variance than that of cell A. The entropy of the distribution is the sum of the two entropies, each obtained from its variance as in equation 3.

The right frame of **Figure 2** shows what happens when the firings of the two cells are correlated, as in response to some common input. It is evident in the figure that a positive Fourier coefficient for one cell predisposes the Fourier coefficient of the other cell to be positive, and similarly for negatives.

But here, again, there is a simple calculation for the distribution's entropy. The single-cell argument above, that the central limit theorem applied and that therefore the distribution must be Gaussian, generalizes to the present case. By the same argument the multivariate distribution of the Fourier coefficients across cells is governed by the multivariate central limit theorem, and so must be a multivariate Gaussian distribution. A multivariate Gaussian distribution has the special property that by rotation one can always find a new set of coordinates, in which the distribution becomes the product of univariate Gaussians, and one can then proceed as before. Technically, a multivariate Gaussian is characterized by a covariance matrix whose principal component vectors define the special choice of the new coordinates. For the case of two cells this is shown by the red axes in the right frame of **Figure 2**. Performing this at many frequencies (**Figure 1**, middle right) on both Repeat and Unique trial sets allows the direct calculation of the signal entropy (**Figure 1**, bottom).

2.4 ESTIMATING REDUNDANCY AND SYNERGY

We have seen above how the simple summation of information from individual cells can easily overestimate the actual amount of information conveyed by the group. This overestimation arises from the fact that the information content of the cells' outputs overlaps, and is thus redundant. In some systems, the converse may be true: the communal output of cells might exceed the sum total information of the individuals, and we have synergy. The circumstances in a complex system from which redundancy or synergy may arise have been the subject of much interest and theoretical discussion (Gawne and Richmond, 1993; Gat and Tishby, 1999; Panzeri et al., 1999; Brenner et al., 2000; Panzeri and Schultz, 2001; Petersen et al., 2001; Bezzi et al., 2002; Pola et al., 2003; Schneidman et al., 2003; Latham and Nirenberg, 2005; Montani et al., 2007).To quantify redundancy (we refer here to redundancy, but the discussion applies to synergy as well), we must quantify the amount of entropy overlap in a group and compare this amount to the total

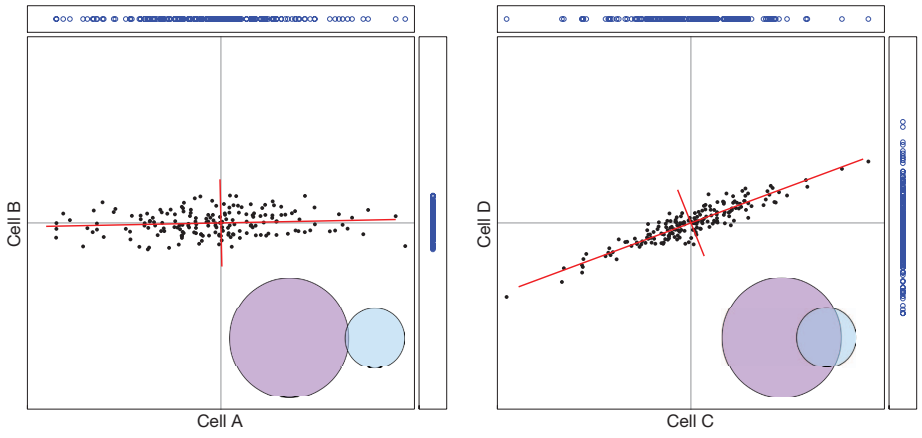

FIGURE 2 | *Left:* the two cells (A and B) fire independently; a two-dimensional distribution is the product of two one-dimensional distributions. *Right:* the two cells (C and D) are *correlated* in this bi-variate Gaussian distribution; when new coordinates (red axes) are chosen, the distribution becomes a product of two one-dimensional Gaussian distributions.

information being transmitted. Using our 2-cell example, we represent each neuron's information output by the two circles in the bottom right of each panel (**Figure 2**). In this way we can visualize the amount of information redundantly conveyed by both neurons: it is the overlapping area. Quantifying these two values with the Fourier method is straightforward – the overlap is equal to the difference between the sum total and the group entropy. Calculation of redundancy with any number of cells proceeds exactly in the same manner. When each cell conveys unique information there is no overlap between the information from the various cells, and redundancy is zero.

In the case of synergy, the information conveyed by the group is *greater* than the sum total of information; cells work synergistically to convey more information than the algebraic sum of the contributions of each one alone. Here the notion of overlap does not apply. However, one may regard the extra information as "negative overlap," still defined by the difference between sum total entropy and group entropy, and proceed in the same manner as above.

2.4.1 Examples

2.4.1.1 Information from individual neurons. **Figure 3** shows, in its left frame, simulated results from eight model neurons. These were of the currently much-used Poisson type: each produced an inhomogeneous Poisson point process at a time-dependent rate that was directly proportional to the fluctuating luminance levels used as a visual stimulus in the laboratory; as a result, the model Poisson neurons and the real laboratory neurons were driven by experiments with equal number of trials and, therefore, the number of samples from the two sets was identical. The mean rates of these 8 neurons were set at the mean rates of 8 the actual neurons we recorded in our monkey LGN. The lower lines show the cumulative information, with advancing frequency, of those individual simulated neurons. The upper line in red shows the sum of those eight cumulative information plots. The dashed blue line below it shows the cumulative information calculated for the merged group of 8. The difference between the two curves is a measure of the redundancy of the information that those neurons carry individually.

The right frame of **Figure 3** shows the corresponding calculation for real neurons recorded in our laboratory from the monkey LGN. We see several new features. The individual neurons, not surprisingly, show a low-frequency cutoff, and as expected, the details of that cutoff are somewhat different for different neurons. When we compare the cumulative information of the merged group to the summed information of the individuals, we see that redundancy at lower frequencies crosses over to synergy at higher frequencies. This recurring observation, which is absent in the simulated neurons, merits further study.

2.4.1.2 Merging information from smaller groups of neurons. In **Figure 4** we examine the effect of merging groups of neurons into a single, larger group. For both the simulated neurons and

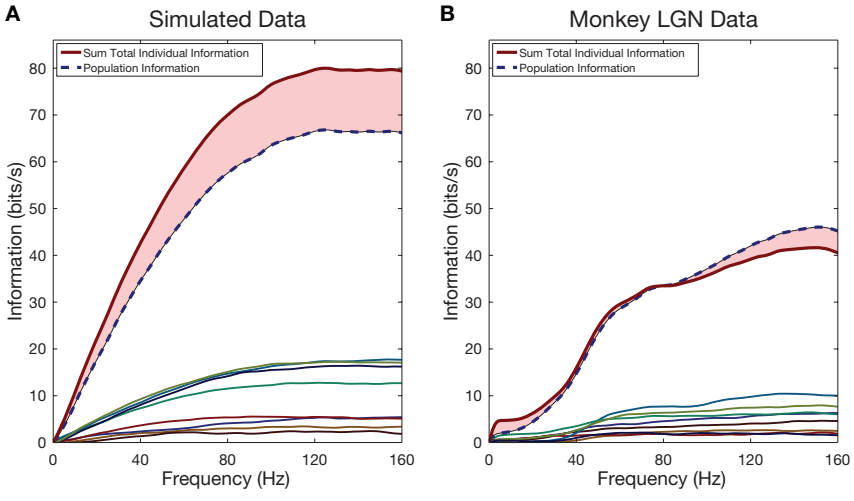

FIGURE 3 | Cumulative information rates as a function of frequency for single cells and for a neural population. Colored lines near the bottom indicate the cumulative information for each of the eight simulated cells **(A)** and eight LGN cells **(B)**. In simulated cells, the sum total information of all individual cells exceeds the information conveyed by the group together, indicating redundancy. In the monkey LGN cells, the sum total exceeds the group information until approximately half the stimulus frequency, after which synergy dominates.

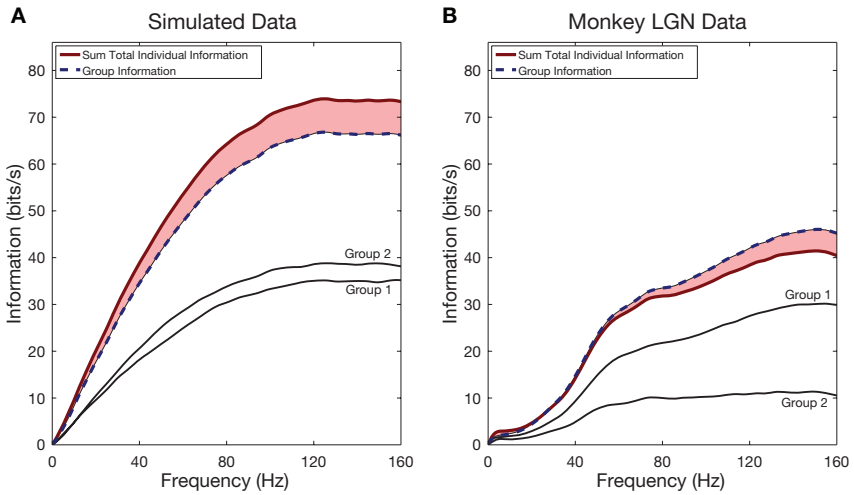

FIGURE 4 | Redundancy and Synergy among groups of neurons in a population. Information rates from simulated Poisson spike trains **(A)**, created to match the firing rates of monkey LGN neurons **(B)**. In both panels the eight cells were split into two groups, matched approximately for firing rates. The total group information is shown in a dashed blue line, and the summed information from two groups is shown in a solid red line. For the LGN cells, but not for the simulated cells, the curves cross around 30 Hz: below 30 Hz we see redundancy, while above it we see synergy.

the LGN neurons we divided the neurons into two groups: we ranked the neurons in order of increasing mean firing rate, and placed the even and odd numbered neurons in separate groups. From **Figure 3** for simulated neurons we recall that this merger removed redundant information, so the information of the two groups should already be reduced from the total single neuron information, which is confirmed in the left frame. Similarly for the laboratory data (right frame) the gap is reduced from what the previous figure showed. Again, for the two groups of LGN cells we see that as frequency increases there is a transition from redundancy to synergy.

3 DISCUSSION

We have described a new method (Yu et al., 2010) for the estimation of the amount of information delivered by the discharges of a neuronal population. The method fills a gap in the armamentarium of the neuroscientist who is interested in the information processing aspects of the brain, and is timely in view of the abundance of multi-neuron recordings appearing in the literature. We now mention a few caveats, and comment on other recent approaches.

3.1 CAVEATS AND CHALLENGES

3.1.1 Differences between responses to unique and repeat stimuli

The methodology presented here confronts the "curse of dimensionality" head-on. In our application, every 8-s spike train is represented as a point in a space of $2 \times 8 \times 160 = 2{,}560$ dimensions: sine and cosine Fourier coefficients at evenly spaced frequencies from 1/8 to 160 Hz. The challenge becomes tractable when we note that the central limit theorem tells us a great deal about how these points must be distributed in that large space, and, in particular, that correlations across dimensions are confined to two-dimensional sub-spaces defined by a sine–cosine pair at each frequency. The needed computations may be performed one pair at a time, and the central limit theorem further tells us that the final result may be derived from a simple analytic expression.

However, the laboratory data consist of only *finite* samples, while the theory addresses an ensemble of indefinite size. For example, the third panel in **Figure 1** illustrates how an atypical sample may lead to a challenge in data analysis. In that figure we see that total entropy and noise entropy converge at high frequencies, which furnishes a cutoff for the sum in equation 26 of Yu et al. (2010). This convergence is predicted by the theory. But in the laboratory, the noise entropy is estimated from responses to repetitions of one sampled "repeat" stimulus, and if that sample is atypical, the computed noise entropy may converge to a slightly different value than the corresponding total entropy. Knowing the origin of the problem, one can apply a small common sense adjustment to remove it. But currently there is no overall theory to point the way that such small-sample adjustments should be made. We look forward to future developments

that would help bring this approach to a more mature usefulness.

3.1.2 Do we need repeated stimuli?

Our method requires repeated presentations of a stimulus in order to calculate the noise entropy. This requirement is shared by other methods, such as the *Direct Method* of Strong et al. (1998). It would be beneficial to have a method that did not require repeated presentations of a stimulus, and which offered some other way of estimating the noise entropy. This might require different approaches to the estimation of complexity, entropy, and information. Steps in that directions have begun to appear in the past few years with the emergence of methods that sidestep the requirement for repeated stimuli. For example, entropy can be estimated with the Lempel and Ziv (1976) complexity measure, as was done recently by Szczepanski et al. (2003), Amigó et al. (2004), and Szczepanski et al. (2011). The complexity and entropy of spike trains can also be estimated by deducing the (hidden) computational structure of a system that could generate the observed spike train (Shalizi et al., 2002; Haslinger et al., 2010).

3.1.3 Non-sensory systems

Most of the information-theory applications to neuroscience have been to data from sensory neurons, where a well-defined stimulus is used, often repeatedly. However, studies of other parts of the brain, such as the hippocampus, the pre-frontal cortex, or the nucleus accumbens, which often involve recordings without any specific experimenter-controlled stimulus, could also benefit from estimates of how much information is carried by the recorded neurons. The methods used by (Amigó et al., 2004) are a step in this direction, but additional methods to provide such estimates would be highly desirable.

3.1.4 Robustness against errors in spike sorting

In our experience, the method is reasonably robust against errors in spike sorting, such as missed spikes, mis-assigned spikes, etc. However, its robustness has limits: if many spikes are erroneously assigned to more than one neuron, this is bound to affect the redundancy/synergy calculation.

3.1.5 Computational efficiency

The information calculations illustrated here may be performed on a desktop computer in a few seconds. Computing time scales roughly with the number of spikes fired by the neuronal population, and our approach can easily handle hundreds of neurons.

3.1.6 Available software

The software used in the analysis discussed in this review is freely available at http://camelot.mssm.edu/~kaplane/Fourier_information.zip

3.2 OTHER APPROACHES

To calculate Shannon information, one needs to know the distribution of the underlying variables. This can be rather challenging with experimental data, which are finite and usually provide only biased estimates of the underlying distribution (Panzeri et al., 2007). On the other hand, if one has a credible model of the process that is being investigated, the model's parameters can be optimized to bring the model's output close to the experimental data. The model now can provide robust and accurate estimates of the distribution, and that distribution can be sampled to yield entropy estimates, using equation 1.

Model-based approaches to spike encoding seek to define an optimal set of parameters for a given model from which the observed spike trains are most likely to have been generated. Such models are useful in that providing a stimulus-response paradigm allows for testable criteria concerning the nature of the encoding process, including statistical measures of accuracy and confidence, and also lends itself well to the application of Shannon Information. Paninski et al. (2007) suggested three criteria for the development of such models: the model must be powerful enough to properly describe the data, it must be both computationally tractable and simple enough to understand, and finally it must fit well with current physiological and anatomical knowledge of the system being studied. The maximum entropy principle, put forth by Jaynes (1957), states that given a set of constraints, the current state of knowledge is best described by the probability distribution with the greatest entropy.

The application of the maximum entropy principle to model-based approaches representing neural systems has garnered much attention among neuroscientists seeking to describe spike encoding. Some recent models (Schneidman et al., 2006; Shlens et al., 2006; Nirenberg and Victor, 2007) have explored the ability to account for the firing patterns of groups of neurons using only parameters that describe single neurons and the interactions between pairs of neurons, since the nature and consequences of the interactions among neurons in the population are at the heart of the issue of population codes and synergy. Whether applications of this type of model will be valid for much larger populations of cells, as found in the nervous system, remains a subject of future exploration (Roudi et al., 2009).

These decoding methods utilize the principle of maximum entropy in determining maximum parameter likelihoods. Likelihood-based models, such as the *Generalized Linear Model*, are tractable due to the concavity of their log-likelihood functions; absence of local maxima in the likelihood function allows for standard numerical ascent techniques in determining optimal parameter choices (Paninski et al., 2007).

The current literature on alternative methods for estimating information is large and growing. These methods, more fully described in Victor (2006) and Dimitrov et al. (2011), directly cast spike-train data, from one or several neurons, into a form that fits into equation 1. Such methods operate either directly on the spike trains, represented as point processes, or on continuous functions of time derived from such processes. For example, a time-span of neuronal output may be divided into a sequence of intervals in such a manner that neuronal output statistics may be gathered and processed so as to produce a measure of entropy, as in the *Direct Method* of Strong et al. (1998). As mentioned above, the major challenge to these approaches is the problem of small-sample bias. This contrasts with our Fourier method, which is based on estimating the variance of Gaussians, which is a relatively unbiased statistic (see Figure 5 of Yu et al., 2010). A recent additional method (Pola et al., 2005; Montemurro et al., 2007; Panzeri et al., 2007; Magri et al., 2009; Ince et al., 2010) cleverly approximates the problem in such a manner as to allow the information calculation to be split, not into the *Total* and *Noise* entropies, but rather into pieces that involve both the exact and the approximate problems, giving rise to further cancelation of the small-sample bias. However, with such bias corrections it was only possible to estimate signal information from laboratory data of correlated spikes recorded from only a handful of neurons.

ACKNOWLEDGMENTS

This research was supported by NIH grants EY016371, EY12867, GM71558, and core grant EY01867. We thank Youping Xiao for his help with this project.

REFERENCES

Amigó, J. M., Szczepanski, J., Wajnryb, E., and Sanchez-Vives, M. V. (2004). Estimating the entropy rate of spike trains via lempel-ziv complexity. *Neural Comput.* 16, 717–736.

Bair, W., Zohary, E., and Newsome, W. T. (2001). Correlated firing in macaque visual area MT: time scales and relationship to behavior. *J. Neurosci.* 21, 1676–1697.

Bendat, J. S., and Piersol, A. G. (2010). *Random Data: Analysis and Measurement Procedures.* Hoboken, NJ: John Wiley and Sons, Inc.

Bezzi, M., Diamond, M. E., and Treves, A. (2002). Redundancy and synergy arising from pairwise correlations in neuronal ensembles. *J. Comput. Neurosci.* 12, 165–174.

Bialek, W., Rieke, F., de Ruyter van Steveninck, R. R., and Warland, D. (1991). Reading a neural code. *Science* 252, 1854–1857.

Borst, A., and Theunissen, F. (1999). Information theory and neural coding. *Nat. Neurosci.* 2, 947–957.

Brenner, N., Strong, S. P., Koberle, R., Bialek, W., and de Ruyter van Steveninck, R. R. (2000). Synergy in a neural code. *Neural Comput.* 12, 1531–1552.

Brown, E. N., Kass, R. E., and Mitra, P. P. (2004). Multiple neural spike train data analysis: state-of-the-art and future challenges. *Nat. Neurosci.* 7, 456–461.

Cover, T., and Thomas, J. (2006). *Elements of Information Theory,* 2nd Edn. Hoboken, NJ: Wiley Interscience.

DiCaprio, R. A. (2004). Information transfer rate of nonspiking afferent neurons in the crab. *J. Neurophysiol.* 92, 302–310.

Dimitrov, A. G., Lazar, A. A., and Victor, J. D. (2011). Information theory in neuroscience. *J. Comput. Neurosci.* 30, 1–5.

Gat, I., and Tishby, N. (1999). "Synergy and redundancy among brain cells of behaving monkeys," in *Advances in Neural Processing Systems*, Vol. 11, eds M. Kearns, S. Solla, and D. Cohn (Cambridge, MA: MIT press), 465–471.

Gawne, T. J., and Richmond, B. J. (1993). How independent are the messages carried by adjacent inferior temporal cortical neurons? *J. Neurosci.* 13, 2758–2771.

Haslinger, R., Klinkner, K. L., and Shalizi, C. R. (2010). The computational structure of spike trains. *Neural Comput.* 22, 121–157.

Ince, R. A. A., Senatore, R., Arabzadeh, E., Montani, F., Diamond, M. E., and Panzeri, S. (2010). Information-theoretic methods for studying population codes. *Neural Netw.* 23, 713–727.

Jaynes, E. (1957). Information theory and statistical mechanics. *Phys. Rev.* 106, 620–630.

Latham, P. E., and Nirenberg, S. (2005). Synergy, redundancy, and independence in population codes, revisited. *J. Neurosci.* 25, 5195–5206.

Lempel, A., and Ziv, J. (1976). On the complexity of finite sequences. *IEEE Trans. Inf. Theory* 22, 75–88.

Lewand, R. (2000). *Cryptological Mathematics*, Washington, DC: The Mathematical Association of America.

Magri, C., Whittingstall, K., Singh, V., Logothetis, N. K., and Panzeri, S. (2009). A toolbox for the fast information analysis of multiple-site lfp, eeg and spike train recordings. *BMC Neurosci.* 10, 81. doi: 10.1186/1471-2202-10-81

Montani, F., Kohn, A., Smith, M. A., and Schultz, S. R. (2007). The role of correlations in direction and contrast coding in the primary visual cortex. *J. Neurosci.* 27, 2338–2348.

Montemurro, M. A., Senatore, R., and Panzeri, S. (2007). Tight data-robust bounds to mutual information combining shuffling and model selection techniques. *Neural Comput.* 19, 2913–2957.

Nirenberg, S. H., and Victor, J. D. (2007). Analyzing the activity of large populations of neurons: how tractable is the problem? *Curr. Opin. Neurobiol.* 17, 397–400.

Optican, L. M., and Richmond, B. J. (1987). Temporal encoding of two-dimensional patterns by single units in primate inferior temporal cortex. III. information theoretic analysis. *J. Neurophysiol.* 57, 162–178.

Paninski, L., Pillow, J., and Lewi, J. (2007). Statistical models for neural encoding, decoding, and optimal stimulus design. *Prog. Brain Res.* 165, 493–507.

Panzeri, S., and Schultz, S. R. (2001). A unified approach to the study of temporal, correlational, and rate coding. *Neural Comput.* 13, 1311–1349.

Panzeri, S., Schultz, S. R., Treves, A., and Rolls, E. T. (1999). Correlations and the encoding of information in the nervous system. *Proc. Biol. Sci.* 266, 1001–1012.

Panzeri, S., Senatore, R., Montemurro, M. A., and Petersen, R. S. (2007). Correcting for the sampling bias problem in spike train information measures. *J. Neurophysiol.* 98, 1064–1072.

Petersen, R. S., Panzeri, S., and Diamond, M. E. (2001). Population coding of stimulus location in rat somatosensory cortex. *Neuron* 32, 503–514.

Pillow, J. W., Shlens, J., Paninski, L., Sher, A., Litke, A. M., Chichilnisky, E. J., and Simoncelli, E. P. (2008). Spatio-temporal correlations and visual signalling in a complete neuronal population. *Nature* 454, 995–999.

Pola, G., Petersen, R. S., Thiele, A., Young, M. P., and Panzeri, S. (2005). Data-robust tight lower bounds to the information carried by spike times of a neuronal population. *Neural Comput.* 17, 1962–2005.

Pola, G., Thiele, A., Hoffmann, K. P., and Panzeri, S. (2003). An exact method to quantify the information transmitted

by different mechanisms of correlational coding. *Network* 14, 35–60.

Quiroga, R. Q., and Panzeri, S. (2009). Extracting information from neuronal populations: information theory and decoding approaches. *Nat. Rev. Neurosci.* 10, 173–185.

Richmond, B. J., and Optican, L. M. (1987). Temporal encoding of two-dimensional patterns by single units in primate inferior temporal cortex. II. quantification of response waveform. *J. Neurophysiol.* 57, 147–161.

Richmond, B. J., Optican, L. M., Podell, M., and Spitzer, H. (1987). Temporal encoding of two-dimensional patterns by single units in primate inferior temporal cortex. I. response characteristics. *J. Neurophysiol.* 57, 132–146.

Rieke, F., Warland, D., Steveninck, R. d., and Bialek, W. (1997). *Spikes: Exploring the Neural Code*. Cambridge, MA: MIT Press.

Roudi, Y., Nirenberg, S., and Latham, P. E. (2009). Pairwise maximum entropy models for studying large biological systems: when they can work and when they can't. *PLoS Comput. Biol.* 5, e1000380. doi: 10.1371/journal.pcbi.1000380

Schneidman, E., Berry, M. J., Segev, R., and Bialek, W. (2006). Weak pairwise correlations imply strongly correlated network states in a neural population. *Nature* 440, 1007–1012.

Schneidman, E., Bialek, W., and Berry, M. J. (2003). Synergy, redundancy, and independence in population codes. *J. Neurosci.* 23, 11539–11553.

Shalizi, C. R., Shalizi, K. L., and Crutchfield, J. P. (2002). *An Algorithm for Pattern Discovery in Time Series*. Technical Report, Santa Fe Institute, 1–26. Available at http://arxiv.org/abs/cs.LG/0210025

Shannon, C. (1948). A mathematical theory of communication. *Bell Syst. Technical J.* 27, 379–423, 623–656.

Shannon, C., and Weaver, W. (1949). *The Mathematical Theory of Communication*. Chicago, IL: University of Illinois Press.

Shannon, C. E. (1949). Communication in the presence of noise. *Proc. IEEE* 37, 10–21.

Shlens, J., Field, G. D., Gauthier, J. L., Grivich, M. I., Petrusca, D., Sher, A., Litke, A. M., and Chichilnisky, E. J. (2006). The structure of multi-neuron firing patterns in primate retina. *J. Neurosci.* 26, 8254–8266.

Strong, S. P., Koberle, R., de Ruyter van Steveninck, R. R., and Bialek, W. (1998). Entropy and information in neural spike trains. *Phys. Rev. Lett.* 80, 197–200.

Szczepanski, J., Amigó, J. M., Wajnryb, E., and Sanchez-Vives, M. V. (2003). Application of lempel-ziv complexity to the analysis of neural discharges. *Network* 14, 335–350.

Szczepanski, J., Arnold, M., Wajnryb, E., Amigó, J. M., and Sanchez-Vives, M. V. (2011). Mutual information and redundancy in spontaneous communication between cortical neurons. *Biol. Cybern.* 104, 161–174.

Victor, J. D. (2006). Approaches to information-theoretic analysis of neural activity. *Biol. Theory* 1, 302–316.

Yu, Y., Crumiller, M., Knight, B., and Kaplan, E. (2010). Estimating the amount of information carried by a neuronal population. *Front. Comput. Neurosci.* 4:10. doi: 10.3389/fncom.2010.00010

Zohary, E., Shadlen, M. N., and Newsome, W. T. (1994). Correlated neuronal discharge rate and its implications for psychophysical performance. *Nature* 370, 140–143.

Conflict of Interest Statement: The authors declare that the research was conducted in the absence of any commercial or financial relationships that could be construed as a potential conflict of interest.

*Received: 17 January 2011; accepted: 28 June 2011; published online: 15 July 2011. Citation: Crumiller M, Knight B, Yu Y and Kaplan E (2011) Estimating the amount of information conveyed by a population of neurons. Front. Neurosci. **5**:90. doi: 10.3389/fnins.2011.00090*

2.3 The Measurement of Information Transmitted by a Neural Population: Promises and Challenges.

Crumiller M, Knight B, Kaplan E.

Entropy. 2013. 15, no. 9: 3507-3527.

Entropy **2013**, *15*, 3507-3527; doi:10.3390/e15093507

OPEN ACCESS

entropy

ISSN 1099-4300

www.mdpi.com/journal/entropy

Article

The Measurement of Information Transmitted by a Neural Population: Promises and Challenges

Marshall Crumiller [1], Bruce Knight [2] and Ehud Kaplan [1,*]

[1] The Fishberg Department of Neuroscience and The Friedman Brain Institute, The Icahn School of Medicine at Mount Sinai, New York, NY 10029, USA; E-Mail: mcrumiller@gmail.com

[2] Laboratory of Biophysics, The Rockefeller University, New York, NY 10065, USA; E-Mail: bruce.knight@rockefeller.edu

* Author to whom correspondence should be addressed; E-Mail: ehud.kaplan@mssm.edu; Tel.: +1-212-241-9607.

Received: 10 May 2013; in revised form: 19 August 2013 / Accepted: 27 August 2013 / Published: 3 September 2013

Abstract: All brain functions require the coordinated activity of many neurons, and therefore there is considerable interest in estimating the amount of information that the discharge of a neural population transmits to its targets. In the past, such estimates had presented a significant challenge for populations of more than a few neurons, but we have recently described a novel method for providing such estimates for populations of essentially arbitrary size. Here, we explore the influence of some important aspects of the neuronal population discharge on such estimates. In particular, we investigate the roles of mean firing rate and of the degree and nature of correlations among neurons. The results provide constraints on the applicability of our new method and should help neuroscientists determine whether such an application is appropriate for their data.

Keywords: information; neural population; spike trains; dynamics

1. Introduction

1.1. Methods for Estimating Information Content in Single Spike Trains

In the past twenty years, rapid advancements in multi-unit recording technology have created a need for analyses applicable to many neurons. While all brain functions require the coordinated activity of

many neurons, neuroscience thus far has been focused primarily on the activity of single neurons [1]. These continuing advancements in both recording and imaging technologies allow the scientist to monitor an increasingly large number of neurons, and it has become desirable to estimate quantitatively the amount of information that a neural population delivers to its targets. However, the application of Shannon's information theory [2] to neuronal discharge from more than one neuron has encountered great difficulties. At the root of the problem is the need to estimate the entropy of the discharge of many neurons from laboratory data, an estimate that is thwarted by the combinatorial explosion of the possible activity patterns. This explosion, which is severe, even for a handful of neurons, prevents the direct application of Shannon's approach, in which entropy is defined as:

$$H = -\sum_i p_i \log(p_i) \tag{1}$$

where each p_i is the probability of a particular pattern of spike-events. The reason for this failure is that laboratory data sample the space of possible activity patterns rather sparsely, and this sparsity undermines our confidence in the knowledge of the underlying distribution, a knowledge that is critical for the determination of the probabilities in Equation (1). This difficulty is referred to in the literature as the *small sample bias*, and several *ad hoc* counter-measures have been proposed, although those have been limited to a small handful of neurons [3–5].

The primary purpose of this paper is to test the robustness of our recently developed Fourier-based method [6,7] that in common, reasonable circumstances bypasses the small sample bias when applied to simulated or real data. We first describe a general linear modeling simulation [8,9] that we used to generate simulated data, and, then, present a series of tests, each of which is designed to pit the method against a specific set of parameters; we present the tests sequentially along with their results.

1.2. The Fourier Method

In general, and particularly for signals as complex as those found in the brain, far fewer data points are required to describe a probability distribution whose shape is known *a priori*, as in the case of a Gaussian distribution, than for distributions of arbitrary shape. Well-established methods, such as the *Direct Method* [10], require large data sets, because those arbitrary distributions must be well-described before information can be estimated. The Fourier Method exploits the fact that the entropy of a Gaussian-distributed process can be analytically calculated from its variance:

$$H(x) = \frac{1}{2}\log\left(2\pi e\sigma^2\right). \tag{2}$$

Our method further exploits the fact that stochastic variables that lose correlation with their past history yield Fourier coefficients that follow a Gaussian distribution [6], allowing us to directly apply this analytic measure of entropy.

1.2.1. Representing Neural Signals in the Frequency Domain

Visual neuroscientists are concerned with the mapping of visual scenes to patterns of neural activity. Since the primary mechanism by which many neurons communicate information is the action potential,

a neural activity pattern can be described as a list of spike times, t_n, which we call a *spike train*, and is commonly expressed as a sequence of δ-functions:

$$u(t) = \sum_{n=1}^{N} \delta(t - t_n) \tag{3}$$

where t_n is the time of the n^{th} spike. We may now represent this signal as the weighted sum of a set of conventional orthonormal basis functions consisting of cosines and sines:

$$u(t) = \frac{1}{2}a_0 + \sum_{m=1}^{\infty} a_m \cos\frac{2\pi m}{T}t + b_m \sin\frac{2\pi m}{T}t \tag{4}$$

with the weighting coefficients evaluated directly from the data by:

$$\begin{aligned} a_m &= \frac{2}{T}\int_0^T u(t)\cos\frac{2\pi m}{T}t\,dt \quad \text{and} \\ b_m &= \frac{2}{T}\int_0^T u(t)\sin\frac{2\pi m}{T}t\,dt \end{aligned} \tag{5}$$

When the statistics of a neuron are stationary, as required for this method, the variance of the mean rate across trials is small, and therefore, spike trains of sufficiently long duration carry very little information in the mean value of the signal. The initial term, a_0, can thus be discarded. Additionally, when the input signal, $u(t)$, is represented by a series of δ functions at times t_n, $u(t)$ is zero for all $t \neq \{t_n\}$, and the weighting coefficients in Equation (5) can be directly expressed in terms of the spike times, *e.g.*:

$$a_m = \frac{2}{T}\sum_{n=1}^{N} \cos\left(\frac{2\pi m}{T}t_n\right) \tag{6}$$

Through this process, we convert a spike train to a series of cosine and sine coefficient pairs that advance in frequency in increments of $1/T$. While a full description of the original signal requires that we measure these coefficients to infinite frequencies, in practice, we can determine a natural cutoff frequency above which no further information is carried. The determination of this cutoff is described in Section 1.2.4. .

1.2.2. The Fast Fourier Transform

An alternative representation, in which spike trains are discretized into bins of length δt, such that a one represents a spike and a zero represents the absence of a spike, allows for the application of the Fast Fourier Transform, which in modern computer systems, is highly optimized and provides significant speed improvements over implementations of the classical Fourier system described above.

1.2.3. Entropy in the Neural Signal

If we generate multiple realizations (trials) of the neural signal in response to a particular class of stimuli, we build, at each frequency bandwidth, ω, distributions of cosine and sine coefficients, $P_{\cos}(\omega)$ and $P_{\sin}(\omega)$. As is discussed in [6], these distributions are Gaussian, and their respective variances,

$\sigma^2_{\cos}(\omega)$ and $\sigma^2_{\sin}(\omega)$, are used as in Equation (2) to evaluate the entropy of each distribution; the entropies of the cosine and sine coefficients together sum to form the entropy of the process at a given frequency bandwidth, with the entropy of the complete signal being the sum of the entropies contained in all bandwidths:

$$H = \sum_{\omega} H(P_{\cos}(\omega)) + H(P_{\sin}(\omega)). \tag{7}$$

The entropies, $H(P_{\cos})$ and $H(P_{\sin})$, are calculated from the Gaussian-distributed Fourier coefficients across trials, using Equation (1):

$$H = \sum_{\omega} (\frac{1}{2}\log_2 e\sigma^2_{\cos}(\omega)) + (\frac{1}{2}\log_2 e\sigma^2_{\sin}(\omega)) \tag{8}$$

Figure 1A shows histograms of several cosine component distributions from data taken from the lateral geniculate nucleus (LGN) of *Macaca fascicularis* using 128 trials. Q-Qplots at three select frequencies (indicated by red, green and blue) are displayed in the inset; the linearity of these plots demonstrates that typical electrophysiological data do indeed follow a Gaussian distribution. The robustness of this Gaussian assumption is further tested in Section 3.3.1. .

Figure 1. Fourier coefficient variance and covariance. (**A**) Fourier cosine coefficients from the monkey lateral geniculate nucleus (LGN) are collected and form Gaussian distributions at each frequency, represented by histograms. The inset shows Q-Q plots of the three highlighted distributions; the linearity of the sample points indicates Gaussianity. The variance of each of these distributions is used to calculate the entropy at each frequency. (**B**) Simulated data to illustrate the multivariate case. The variance along the principal axes (black) is determined by the covariance matrix of the coefficients and informs us of the information conveyed by the population.

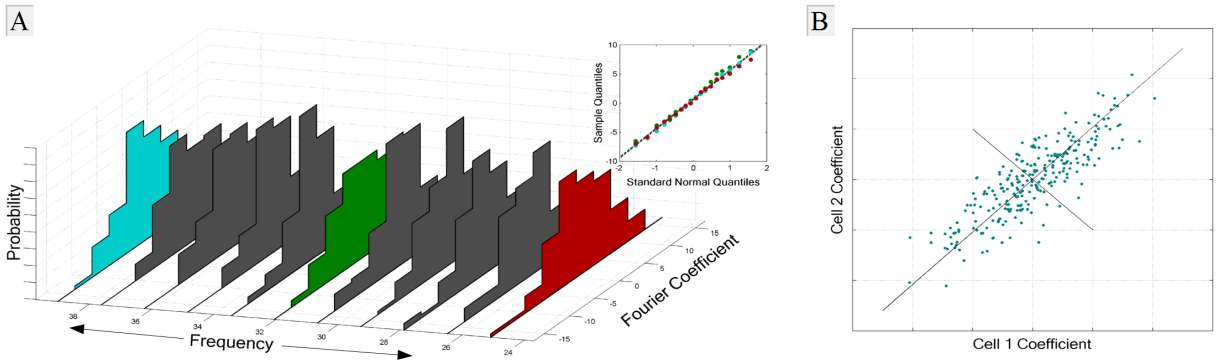

The process of extending the Fourier entropy calculation to multiple neurons becomes intuitive from inspection of the two-neuron example in Figure 1B, which shows a two-dimensional plot of the cosine coefficients of each neuron at a chosen frequency, with one (simulated) data sample per trial. Each neuron's coefficients form a one-dimensional Gaussian distribution, whose variance provides us with an estimate of that neuron's entropy alone at that particular frequency (Equation (2)). When the coefficients

for the two neurons are plotted against each other, correlations between neurons induce correlations in their respective coefficients. In this case, the output from one neuron informs us to some degree of the output of the other, the result being a reduction in entropy associated with their joint distribution. This reduction is taken into account when the coefficients are expressed along their more compact Principal Component axes, shown in black; in this new coordinate system, information conveyed about the structure of the correlations between the neurons, rather than information about the stimulus, is discarded, and the joint distribution entropy, which we call the *group entropy*, $H(G)$, is revealed [11]. The entropy of this multivariate Gaussian distribution is readily calculated by replacing the variance, σ^2, in the single-neuron case with the covariance matrix of the multiple neurons' coefficients and is the sum of the entropies along these principal axes. We call the difference between the group entropy and the sum total of the individual neurons' entropies the *redundancy*, which we express as a proportion of the total entropy, summed over all frequencies:

$$R = 1 - \frac{H(G)}{H(C)} \tag{9}$$

where:

$$H(C) = \sum_{c \in C} H(c) \tag{10}$$

where $H(G)$ is the group entropy rate that conveys the signal entropy, taking correlations into account, and $H(C)$ is the sum of the individual entropy contributions of each neuron, which ignores correlations. In the special case in which $H(G) > H(C)$, R becomes negative, and we have *synergy*; a population code. This method generalizes to a large number of neurons and is described in detail in our previous publications [6,7].

1.2.4. Noise and Signal Entropies

Fluctuations in spike times due to noise produce additional entropy, the magnitude of which is limited only by the precision at which spike times are measured. This entropy due to noise, H_N, must be subtracted from the total entropy, H_T, in order to measure the information in the signal:

$$I = H_T - H_N. \tag{11}$$

Experimentally, one may measure the imprecision of a system by observing the variability of its responses to repeated, identical inputs. Our simulations and experiments apply this technique through the use of a repeat-unique paradigm. In such a paradigm, the total entropy is calculated from a rich variety of unique signals to which the neuron responds noisily, while the entropy due to this noise alone is calculated from responses to identical, repeated patterns of input. Thus, the variation in the response of a neuron to a repeated stimulus provides a measure of its noise. Example stimuli are shown in Figure 2B, first with the repeated stimuli, all identical, plotted in red, and, then, followed by unique stimuli, plotted in blue. The responses of a neuron (simulated or real) to unique and repeat trials are represented with a raster plot, with each row representing a separate trial and hash-marks indicating spike times (Figure 2C).

Figure 2. Simulated neuronal response to the repeat-unique stimulation paradigm. (**A**) General linear modeling (GLM) flow diagram, adapted with permission from Macmillan Publishers Ltd: *Nature* [12], ©2008. (**B**) A subset of the trials of a typical stimulus are displayed. Repeat stimuli (red) are all identical, whereas unique stimuli (blue) are each different from all others. (**C**) Raster plot of the responses of a simulated neuron to repeat and unique stimuli. Each row of the raster corresponds to a single trial, seen on the left. Responses to 128 trials are displayed in the raster; because repeat stimuli are all identical, the neuron produces similar spike trains (red spikes), evidenced by the appearance of vertical stripes. The response of the neuron to unique stimuli is different with each trial, and therefore, no stripes appear. (**D**, **top**) The entropy rate calculated in response to the repeated stimuli (red) is subtracted from the entropy rate calculated in response to the unique stimuli (blue); the difference between the entropies (shaded area) is the signal information rate. The integral of this entropy difference over frequency is dimensional information times frequency or equivalently bits per second. (**D**, **bottom**) The information rate is plotted as a cumulative sum across frequencies; the plot levels off with a near-zero slope at frequencies above which signal information is zero.

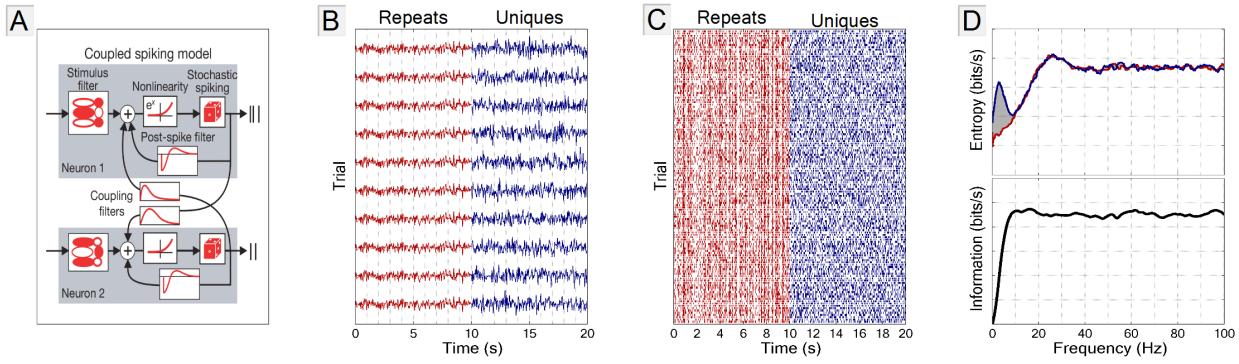

1.3. Overview

In simulation, we are not subjected to the limitations of experiment. Consequently, the accuracy of our calculation increases with the amount and quality of available data, over which we have direct control. Here, we explore the performance of the Fourier Method when applied to various kinds of neuronal populations and discharge patterns. In particular, we wish to establish the constraints imposed on the method by some important aspects of the neuronal discharge, such as the mean rate and variability of the discharge, as well as the degree and nature of the interactions (correlations) among the neurons in the population.

We begin with simple information profiles of neurons with a wide range of firing rates in response to a stimulus of increasing frequency. We then address the basic question of data quantity—what is the minimum recording length required to generate valid information estimates, and how does this requirement depend on the firing rates of the neurons? Following this, a series of potentially confounding experimental factors are introduced: firing rate non-stationarity, spike-to-neuron assignment errors and biased estimates of noise entropy. We conclude with a study

of the effects of scaling the method to multiple neurons and demonstrate its strength in dealing with very large populations of cells.

2. Methods

2.1. The GLM Simulation

To explore the performance of our method, it is appropriate to use simulated data sets, where we have control over the relevant parameters. Among many possible simulation frameworks, we chose the general linear modeling (GLM) approach described by [8,9], which was effectively used by these authors to model populations of primate retinal ganglion cells [12]. This framework allows us to control important features of the dynamics of individual neurons, as well as to control the strength and dynamics of the interactions among the simulated neurons in the population. A detailed description of the model can be found in [8,9,12] and is illustrated in Figure 2A [12]. An input stimulus is first passed through the stimulus filter, designed to mimic ON retinal ganglion cells that maximally respond to increases in light intensity. A nonlinearity is applied to the filtered output, and a stochastic spiking model produces stimulus-dependent spikes. Following a spike, a post-spike filter is applied to the input, generating a refractory period. If multiple neurons are simulated, additional post-spike coupling filters are applied, which allow neurons to influence each other. The coupling filters can be unique for each pair of neurons, allowing for a variety of connection types and strengths within a single network.

2.2. Stimulus

Figure 2A includes a stimulus filter designed to selectively emphasize stimuli of a particular spatial pattern, and while the GLM simulation is capable of handling a variety of complex, spatially-rich stimuli, we first chose to drive each neuron with a one-dimensional stimulus, in order to reduce the number of input parameters. The stimulus filter carries a time-component, as well, allowing one to mimic some of the properties of neurons found in the brain. Our choice of one-dimensional stimulus and a spatial filter effectively models a full-field stimulus driving a retinal ganglion cell whose maximal response arises from a sharp increase in stimulus intensity. The stimulus provided to our simulated neurons consists of Gaussian-distributed random intensity values, each lasting for a brief interval, whose mean value determines the mean firing rate of the cell. An offset is applied to simulate neurons of any desired mean firing rate. The interval during which each stimulus value is shown determines the stimulus sampling rate, which is a parameter in our simulation. Figure 2B shows the inputs of ten sample trials of Gaussian inputs presented at 25 Hz.

2.3. Frequency vs. *Information Plots*

Typical plots of entropy and information as a function of temporal frequency are displayed in Figure 2D. The difference between the entropy calculated from the unique runs (blue) and repeated runs (red) is the signal information (shaded gray area). The bottom panel in Figure 2D displays a

cumulative plot of signal information, which levels off at frequencies above which no signal information is transmitted.

2.4. Measurement of Error and Confidence

Many of the simulations that follow require a measure of the relative quality of the information estimation. Given that the sources of our data here are (simulated) neurons, a calculation of error requires a comparison between a measured and a "true" information rate. Our calculations provide estimates with units of bits per second, and in situations where the estimation may be improved by simply increasing the quantity of data, we can declare our *true information rate* to be that rate estimated from a large quantity of data. Our error is thus defined to be the absolute value of the difference between the measured rate and the true rate, divided by the true rate and represented as a percentage. Thus, our error is bounded by zero below and is unbounded above. We calculate this confidence interval by generating multiple instances of the true rate and determining the standard deviation of such results.

Figure 3 displays the intrinsic variability of neurons with various firing rates responding to a $25\,\mathrm{Hz}$ stimulus, as described in Section 2.2. Panel A displays the spread of information for neurons of three different firing rates, with mean values plotted as solid lines. The resulting spread is used to define the 95% confidence interval (1.96 standard deviations), which is shown in Panel B for a more densely sampled choice of firing rates, and fit with a function of the form, ax^b. Notably, the reliability of the information estimate increases with the firing rate.

Figure 3. Intrinsic variability of neural responses. (**A**) Twenty instances of cumulative information rates from three single neurons, with firing rates of 21, 7 and 2 spikes/s. (**B**) Standard deviations of information rates from twenty neurons, three of which are derived from the neurons in the left panel, fitted with the function, ($y = 1.29x^{-0.497}$). The fitted curve is used to describe the 95% confidence interval of the information estimation.

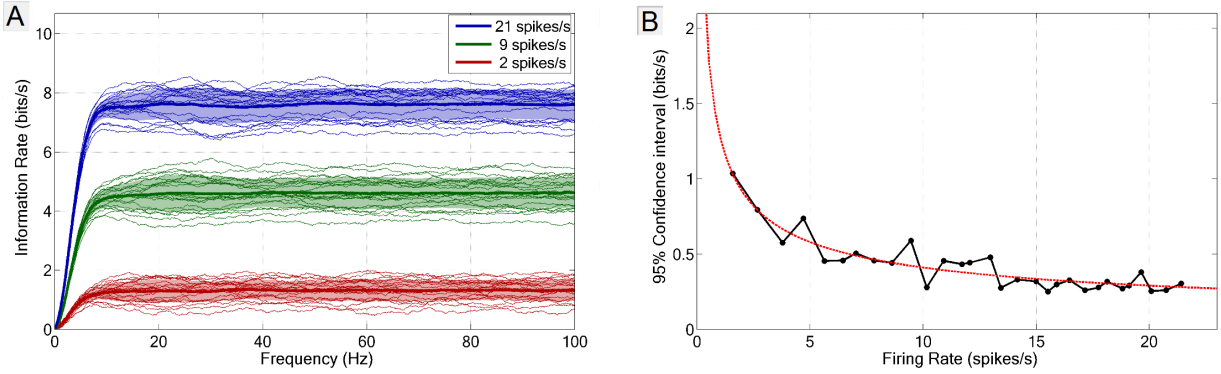

3. Results

3.1. Comparison with the Direct Method

We begin with a brief comparison of our method with a well-known standard of information estimation: the Direct Method [10]. The Direct Method is named for its simplistic approach: spike

trains are discretized into binary vectors of length $\Delta\tau$ and subdivided into words of window length L, with the resulting distribution of words subjected to Shannon's formula in Equation (1); the entropy of the words of window length T and bin width $\Delta\tau$ is thus:

$$H(T;\Delta\tau) = -\sum_i p_i \log_2(p_i). \tag{12}$$

Calculation of the true information rate requires that we calculate this sum to the limit as $L \to \infty$ and $\Delta\tau \to 0$. The small sample bias precludes estimation of even modest word length L, and therefore, an extrapolation towards the infinite data limit is required [10].

Figure 4A compares the Direct Method with the Fourier Method. We applied both methods to the discharge of 25 simulated neurons with firing rates ranging from 5 spikes/s to 30 spikes/s, ensuring a range of information rates. For this comparison, we provided 4,096 trials of 30 s each in order to ensure that the Direct Method was not limited by the sample size; this corresponds to approximately 68 hours of recording for each choice of firing rate and sensitivity. The results show that the two methods produce similar results. Figure 4B demonstrates the increase in information rate errors as the number of trials decreases, with the inverse of the number of trials shown on the abscissa. While the rate error resulting from use of the Direct Method increases drastically as the number of trials decreases, the Fourier Method remains robust even in the face of a small sample size. Approximately one tenth of the quantity of data required by the Direct Method is needed for the Fourier method to achieve a comparably reliable estimate. Because of the far smaller response to noise in the Fourier method, the vertical scatter in Figure 4A can be regarded as an indication of the accuracy limitations in the Direct Method.

Figure 4. Comparison with the Direct Method. (**A**) Spike trains from 25 simulated neurons of varying firing rates and input sensitivities were subjected to both the Fourier and Direct methods of information measurement, using 4,096 trials of 30 s each to ensure enough data. (**B**) Rate errors expressed as a function of the inverse of the number of trials. The rate errors produced by the Fourier method remain small compared to those produced by the Direct Method as the number of trials decreases.

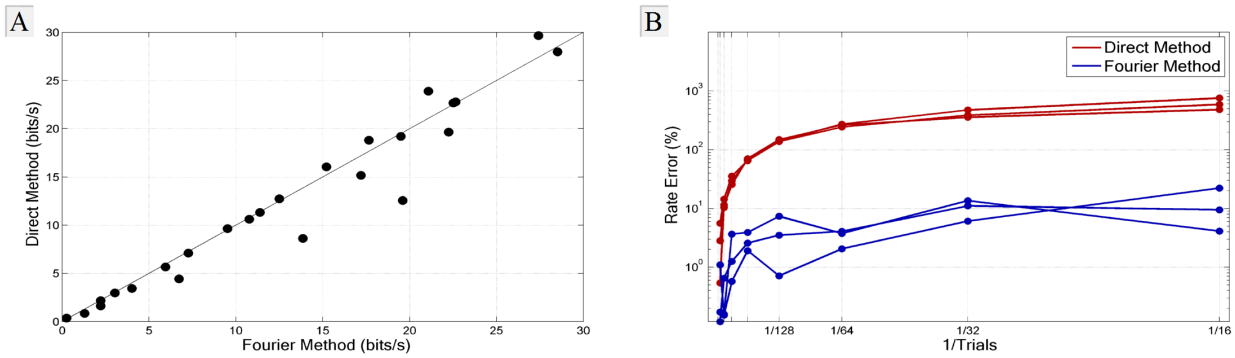

3.2. Experimental Requirements

A data set extracted from an experiment is but a small sample of the total neural activity, acquired during a limited time period. An important question arises, therefore: how much data does one need

to properly estimate information rates? Statistical inference relies on the ability of a limited sample to represent features of a population; the sample must therefore be a faithful representative of the population and be sufficiently informative for the scientist to extract the relevant features. How much data do we need to measure information in the discharge of a neuronal population?

The range of properties of individual neurons encountered in the brain is large, even among neurons confined to individual nuclei. In our simulation, we chose a set of model parameters that covers a typical range of neuronal properties encountered in the laboratory. We address the issue of experimental requirements—how much data one needs to measure information—by an iterative process of the reduction of sample size until the error renders the method unusable. We have explored three independent parameters (Figure 5) in this investigation: mean firing rate, trial length and number of trials, all of which contribute to the total number of spikes recorded. For each input firing rate, we generated a reference measurement using 2,048 trials, each of them $10\,\mathrm{s}$ in length, which we deemed sufficient as a basis for comparison. While the information rate of a neuron is not simply tied to its mean firing rate, our wish to gain valid statistical measures requires that we have enough spikes to accurately characterize the distribution of Fourier coefficients at any relevant frequency.

Figure 5. Experimental requirements for information calculation. In this simulation, trial length and number of trials were altered independently. Information rates were calculated and compared to a reference information rate, with the difference expressed as a percentage deviation from the true (reference) rate. (**A**) Rate errors are displayed as a function of both the number of trials and trial length, with red indicating parameter choices that produced high rate errors. Slices represent the choice of input firing rate into the model. (**B**) Rate error plotted as a function of the total spike count, which is itself dependent on trial length, number of trials and firing rate. Rate errors in the right panel were fitted with a function of the form, $E = ax^b$.

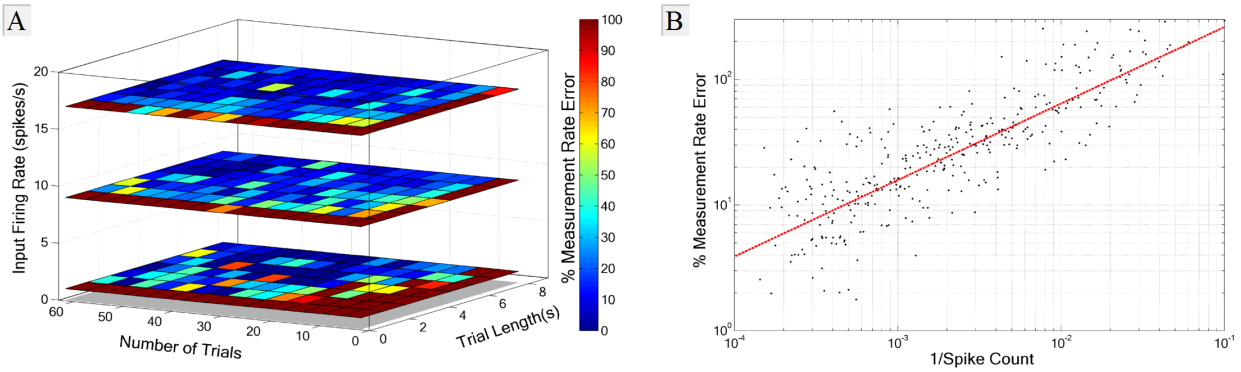

The results of the simulation can be seen in Figure 5. The error is represented as a percentage deviation of the reference simulation from the 95% confidence interval of the information rate measurement. The independent contributions of trial number and trial length can be seen along the columns and rows of Figure 5A. Not surprisingly, rate errors increase significantly as the amount of data is reduced. Slices indicate the three input firing rates of one, nine and 17 spikes/s, and each data point represents the mean rate error of five runs with identical input. As firing rate increases, the restrictions on trial length and

number of trials decrease. Figure 5B shows the error in information rate purely as a function of the inverse of the number of spikes. The total spike count itself, while not entirely indicative of the ability of the method to accurately estimate information, provides a good rough estimate for the amount of data required to produce low-error estimates. The dotted red line was fitted to the data by the function, $y = 1063x^{0.609}$; the 5% error level occurs at approximately 6,636 spikes; for a typical cortical neuron that fires at five spikes/s, an experimentalist would thus require approximately 22 minutes of data.

3.3. Recording Pitfalls

Recording stability is often imperfect in the laboratory: varying levels of anesthesia, electrode drift, attentional effects and interference all affect the recording. These effects can manifest themselves in several ways, including:

- Firing non-stationarity
- Spike-to-neuron assignment errors during spike sorting
- Biased estimation of noise entropy

To assess the impact of these pitfalls, we have created the three simulations described below.

3.3.1. Firing Rate Non-Stationarity

Electrophysiological experiments are often performed on animals under anesthesia, during which brain activity assumes a state of slow-wave oscillatory behavior, commonly associated with sleep. In unanesthetized animals, the high-conductance neuronal states found in thalamocortical and cortical systems during wakefulness give rise to increased neuronal activation, accompanied by increased sensitivity to stimuli, more variable spiking patterns, greater desynchronization [13] and a shortened membrane time constant, a consequence of which is higher temporal precision [14]. The phasic activity observed during anesthesia and the transitions between wakefulness and sleep due to fluctuations in the metabolism of anesthetics can both contribute to changes in the firing rates of neurons that are not necessarily stimulus-induced. In addition, many neurons in the brain have been found to exhibit discharge patterns indicative of high and low firing states. These *Up* and *Down* states can result from either intrinsic properties of the membrane or from network-related activity and have been observed most prominently in cortical pyramidal cells and striatal spiny neurons, with stable *Down* states consisting of periods of low activity, and either stable or meta-stable *Up* states, where the neuron enters a heightened state of activity (see [15] for a review of the subject). Similarly, neurons of the lateral geniculate nucleus are known to display tonic and burst firing patterns [16] that may play a role in the transmission of visual information [17]. Regardless of the mechanism, it is important to determine the effect of such instability on the calculation of information.

A primary concern is that a neuron exhibiting multiple modes of activity might violate the requirements of the Central Limit Theorem and produce non-Gaussian Fourier coefficient distributions. We address this potential concern by simulating *Up* and *Down* states in neurons, with two variable parameters: the difference between firing rates in the two states (reversal amplitude) and the average rate of fluctuation between the two states (reversal rate). All neurons in this simulation had a mean firing

rate of 15 spikes/s; two sample neurons can be seen in Figure 6A with different reversal amplitudes and rates. To test the possibility that the normality assumption of Fourier coefficients is violated in neurons exhibiting multiple modes of firing, we subjected the coefficient distributions at each frequency used in the information calculation to the Shapiro-Wilk test for non-normality ($N = 4,000$ distributions; $\alpha = 0.05$) and display the results as a percentage of the number of distributions that did not violate the Gaussian property at the 5% significance level.

Figure 6. Effects of firing rate instability. Neurons with bimodal firing statistics were simulated, switching between *Up* and *Down* states throughout each trial. The firing rate difference between *Up* and *Down* states is represented as a proportion of the mean firing rate and the average duration of each state by its reciprocal in Hz. (**A**) Firing rates of two sample neurons are plotted in red, each with a mean firing of 10 spikes/s. The top neuron oscillates between five and 15 spikes/s (reversal amplitude = 0.5), with a mean fluctuation rate of $0.5\,\mathrm{Hz}$. The bottom neuron oscillates between zero and 20 spikes/s (reversal amplitude = 1.0), with a mean fluctuation rate of 3 Hz. (**B**) Heat map illustrating the effect of state fluctuation on information rates. All neurons had mean firing rates of 15 spikes/s; information decreased with reversal amplitude, with the effects of the decrease being partially mitigated by increases in reversal rate. (**C**) The fraction of of Fourier coefficients distributions that were Gaussian plotted against reversal amplitude and reversal rate. Fourier coefficient distributions at each frequency were subjected to the Shapiro-Wilk test for non-normality at the 5% significance level (dashed red line).

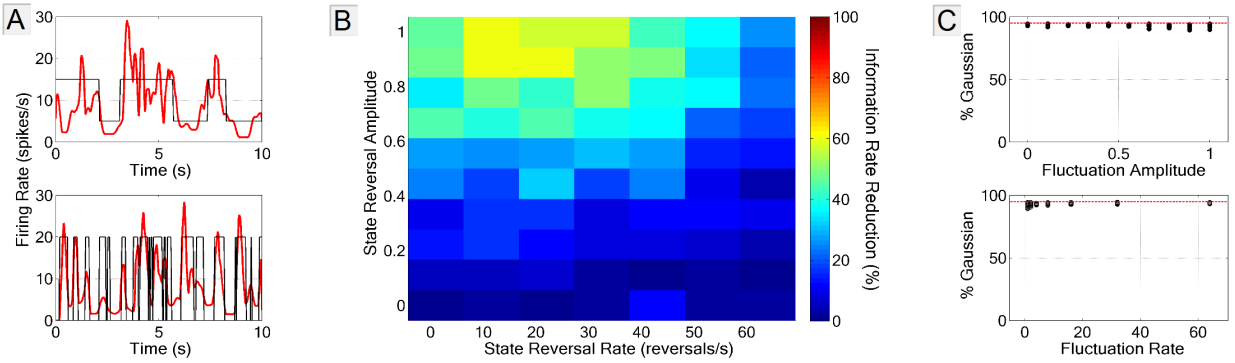

Figure 6B shows the dependence of the information estimation on both the state reversal rate and the reversal amplitude. Reversal amplitude had a largely negative effect on information rates, whereas reversal rate had the opposite effect. This mitigating effect results from a trend toward homogeneity of the firing rate as the reversal rate increases. Note that values are not reported as rate errors, but as information rate reductions; this is because the observed decreases in information are due not to failure of the method, but because properties of the simulated neuron itself affect the information rates. Indeed, Figure 6C shows that the distributions remained Gaussian, even in the case of prominent changes in a neuron's firing state and pattern. Clearly, the non-stationarity of firing patterns did not violate the Gaussian requirement, and our method is applicable under such circumstances. We do, however, stress the importance of testing for Gaussianity. While the data provided in our experimental paradigm generate

signals with necessarily short autocorrelation times, other experiments may result in violation of the Gaussianity assumption.

3.3.2. Spike-Neuron Misassignment

Electrophysiologists are familiar with the challenging process of spike sorting that is routinely encountered in the context of multi-electrode recordings, in which the activity of many neurons is recorded. Voltage recordings from such experiments provide estimations of the number of neurons and the timing of spikes associated with each neuron. While the probabilistic methods that are utilized in spike sorting often result in reliable assignments of spikes to their respective neurons, they still rely on incomplete knowledge of the environment; the misassignment, over-assignment or under-assignment of spikes to neurons is sometimes unavoidable. In sub-optimal recordings, spike sorting is limited by the signal-to-noise ratio, and unidentified action potentials muddle the knowledge of the true time course of a neuron's activity. To study the impact of spike misassignment on information rate, we ran a simulation in which a percentage of spikes from each neuron were distributed equally and at random to the other neurons (Figure 7A). Rate errors were represented as the percent deviation from the true rate, in which no spikes were misassigned; a value of 0% thus indicates no misassignment and a value of 100% means that every spike from each neuron is evenly assigned to the other neurons. In this simulation, neurons were driven by separate, uncorrelated stimuli to remove correlations between neurons induced by the stimulus. We progressively increased the group size to determine whether the problem of misidentified spikes is exacerbated by a greater number of neurons. Twenty four group sizes and nine misassignment percentages were chosen, both along a logarithmic scale, and information rate errors calculated for these 24×9 conditions and linearly interpolated along both dimensions.

Figure 7. Effect of spike-neuron misassignment on information rate. (**A**) The spike neuron misassignment procedure follows three steps: (1) spike rasters for individual neurons are generated; (2) a percentage of spikes from each neuron, highlighted in red, are selected at random; (3) the selected spikes are evenly distributed to the other neurons. (**B**) Average rate errors are expressed as a function of both the number of neurons and of the misassignment percentage. Sampled points are displayed as black dots, and the values are interpolated to create a smooth heat map. (**C**) Average rate errors, averaged across group sizes, with the special case of two neurons excluded.

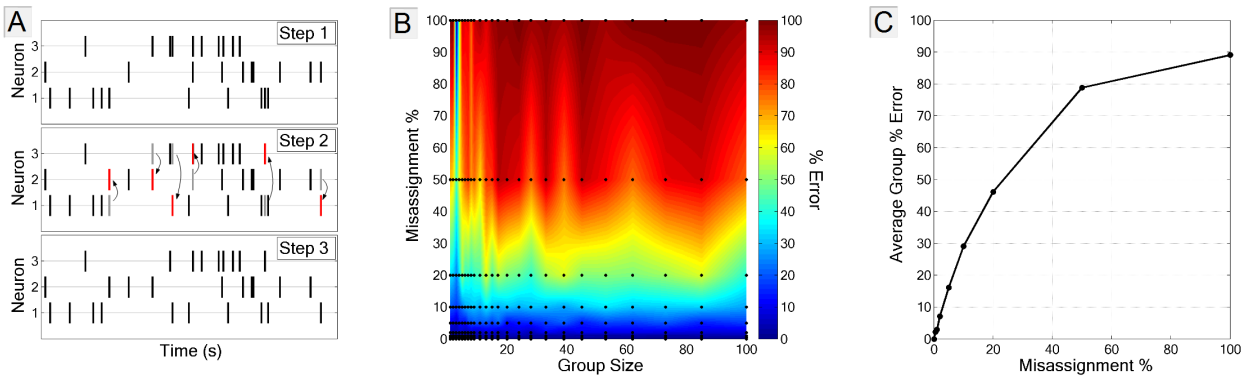

Figure 7B demonstrates the impact of spike misassignment on information rate. The 24×9 conditions in which the impact of spike misassignment was calculated can be seen in Figure 7C, and the sampled values are indicated by the black dots; these data were interpolated to produce the smooth heat map. As expected, complete misassignment results in a nearly complete destruction of signal information, with the exception of the two-cell case, in which a full 100% misassignment of spikes is equivalent to swapping the two neurons and can be observed by the vertical blue line centered at group size $= 2$. Group size plays little role in calculating the impact of misassignment, and the values averaged across group sizes, with the two-neuron cases excluded, are shown in Figure 7C. A misassignment of as little as 10% of spikes can degrade information calculations by up to 30%, underlining the importance of careful and proper spike sorting.

It is important to note that the neurons used in this simulation have identical tuning properties, and therefore, the stimulus patterns about which the neurons are reporting will be correlated to some extent. The result is that these neurons will report on similar features of the stimulus and, therefore, will be redundant. Consequently, a complete misassignment of spikes to neurons still yields a low information rate, and therefore, the rate error approaches, but does not quite reach, complete error.

3.3.3. Biased Estimate of Noise Entropy

For a proper measure of signal information, it is crucial to estimate accurately the noise entropy of the system. Because signal information is the difference between the unique and repeat entropies, any situation in which the noise (repeat) entropy is miscalculated will lead to an invalid estimate of signal information. It is therefore important that the repeated stimulus be a faithful representative of the unique stimulus ensemble. An atypical repeat stimulus can be detected from the resulting spike trains and the bias corrected to the extent possible, but it is clearly in the interest of the experimenter to reduce the level of *post-hoc* statistical adjustments to a minimum.

A simple, but crude, indication of a statistically atypical repeat stimulus is the difference in the number of spikes produced in response to the unique and repeat stimulus sets. An atypical repeat stimulus may generate a neuronal response that contains fewer or more spikes than those produced on average by the unique stimuli. The resulting effect on the cumulative information plot is easily recognizable: as one proceeds toward high frequency, information accumulates at a constant rate, with a steady increase or decrease in the cumulative plot at frequencies past the signal frequency cutoff. The cosine and sine terms of a Fourier coefficient together define a vector on the unit circle of the complex plane. At sufficiently high frequencies, at which no two consecutive impulses are correlated, the phase becomes a uniformly distributed random variable, and the complex Fourier coefficient is the result of a two-dimensional random walk of unit-length steps, corresponding to each spike, in random directions. The two-dimensional variance of these coefficients across trials at these high frequencies therefore depends only on the number of spikes. Ideally, a collection of coefficients at such frequencies from repeats should have the same variance as coefficients from uniques, yet differences in the number of spikes create an inequality in these variances. The two entropies, which depend on these variances, are consequently unequal, and a resulting negative or positive information content accumulates. A simple and effective method of resolving the spike-count discrepancy error is the random deletion of spikes, until the repeat and unique sets contain an equal number of spikes (Figure 8A). The extent to which this

affects the information calculation is dependent on the number of spikes deleted, but in most cases, the result is a minimal change at the relevant frequencies. The concern is the accumulation of information at frequencies beyond the signal cutoff frequency, which, in the case where responses to repeats and uniques have unequal spike counts, is determined entirely by the arbitrary frequency at which one stops the calculation.

Figure 8. Spike Deletion Procedure. (**A**) Deletion of randomly selected spikes (shown in red) from the spike train with more spikes abolishes high-frequency information miscalculation. (**B**, **top**) Information accumulates (cool colors) at high frequencies in the case where the number of unique spikes exceeds the number of repeat spikes, and declines (warm colors) when the repeat set is larger. (**bottom**) After the spike deletion procedure, information accumulation trends are abolished. (**C**) The percentage of information reduced as a function of the percentage of spikes deleted in both the repeat and unique sets.

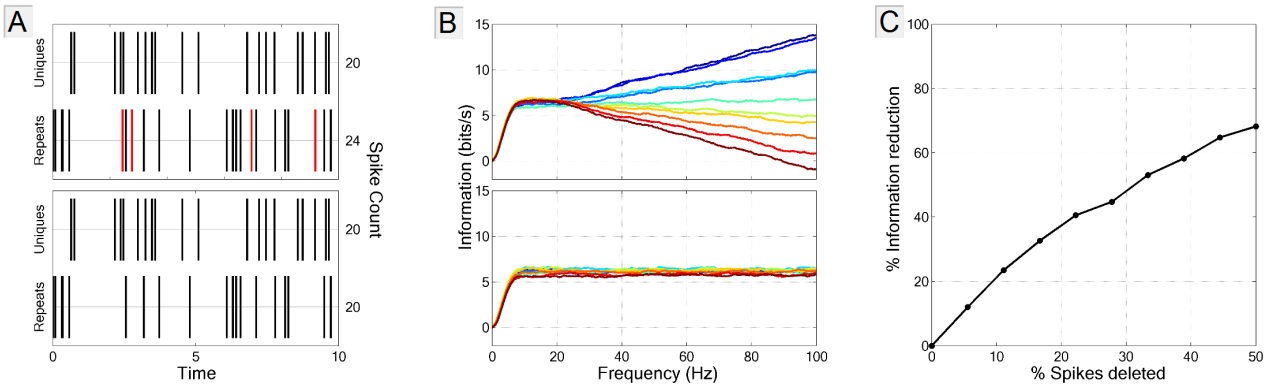

Figure 8B shows results from ten sample simulated neurons, whose firing rates in response to the unique stimuli were systematically adjusted from 14–16 spikes/s and paired with a repeat stimulus rate of 15 spikes/s. When the repeat spike count exceeds the unique spike count, a negative trend occurs (warm-color curves), with positive trends (cool-color curves) occurring when responses to the uniques exceed those elicited by the repeats. Application of the spike deletion procedure effectively abolishes the information accumulation problem (Figure 8B). The resulting information rates form a distribution around the true information rates with a standard deviation of 0.2 bits/s, which corresponds to a spread of approximately 3%.

To gauge the extent to which information is affected by spike deletion, we ran a simulation (Figure 8C) that illustrates the relationship between the number of spikes and the percentage reduction in information. Note, however, that the right panel of Figure 8 does not indicate spike-count discrepancies, but rather, percentage deletion from both uniques and repeats in tandem; in the case where discrepancies between unique and repeat spike counts exist in the laboratory, the number of spikes deleted will be roughly half of those deleted in our simulation, because such a discrepancy necessitates deletion from only one of the two (unique or repeat) sets. To get a sense of the number of spikes that must be deleted on average, we turned to a recent recording of neurons in the lateral geniculate nucleus of *Macaca fascicularis*. The spikes from these LGN cells were sorted using in-house software, and neurons with firing rates less than 0.5 spikes/s were discarded. Of the 25 resulting neurons, the average spike count discrepancy

between unique and repeat sets was 1.9% with a standard deviation of $\pm 1.4\%$; these values correspond to 0.95% $\pm$ 0.7% of the total spikes that must be deleted to equalize the two spike counts. Following the trends in Figure 8C, one would expect an information reduction of approximately 1%.

3.4. Multi-Neuron Information and Redundancy

3.4.1. Signal and Intrinsic Correlations

The role of correlations between neurons has been of great interest with respect to population coding. The millisecond [18] and even sub-millisecond [19] precision at which the brain operates in response to external stimuli, in addition to the complexity of features encoded by the brain, necessitates an ensemble of many neurons in the processing of information [20,21]. Historically, the study of multineuronal coding has been limited to methods employing measures of correlation between pairs of neurons. While there is little doubt that the "signal correlations" [22] induced by stimulus alone do not sufficiently account for the levels of correlation found in the brain [23,24] and that the levels of correlation between neurons dynamically adjust in a stimulus-specific manner [25–29], the importance of these correlations in the transmission of information has been debated [30–33]. More recent measures utilizing information-theoretic approaches [34–36] rely on assumptions imposed by a decoder model, in which the amount of information conveyed through pairwise correlations is estimated from the loss or gain of information after correlation assumptions are relaxed (see [36] for further discussion). The lack of tools capable of measuring information carried in neuronal correlations has hindered efforts to measure coding at the population level, despite evidence that encoding procedures require the concerted effort of many neurons [37–40].

To measure the effects of stimulus correlation on information redundancy, we independently altered the stimulus and the coupling strength between neurons. We first progressively increased the correlation between the stimuli provided to each neuron separately. Adjusting the stimulus correlation was accomplished by generating two uncorrelated stimuli and a third reference stimulus; each neuron was presented with a weighted average between one of the two uncorrelated stimuli and the reference stimulus; the weights thus determined the strength of the correlation with the stimuli driving the two neurons. The resulting stimuli, by virtue of being the sum of two Gaussian distributions with standard deviations, whose sum is less than unity, must be multiplied by an adjustment factor to restore the standard deviation back to a value of one, which in the GLM simulation, is analogous to stimulus contrast. We then increased the coupling strength between neurons, which was determined by a scaling factor applied to the post-spike coupling filter of the GLM simulation (Figure 2A). For this simulation, we used mutually excitatory coupling measures, compensating for the firing rate increases that occur due to the additional excitational input, and measured the effects of these parameters on information rates and redundancy. While the GLM model places no upper limit on the strength of the coupling kernel, we restricted its influence to a reasonable range and report the maximum coupling strength with one and the minimum strength of zero, indicating that the two neurons are uncoupled.

Figure 9A shows the changes in information rates and redundancy as a function of stimulus correlation. The upper panels show typical cumulative information plots when stimuli are nearly completely decorrelated ($r = -0.0019$) and when completely correlated ($r = 1$; the neurons are driven

by identical stimuli), with the shaded gray area corresponding to the redundant information. Firing rates did not appreciably change across parameter choices (maximum deviation: 2.8%). As one would predict, increases in redundancy accompany increases in stimulus correlation; neuronal noise prevents complete redundancy. The solid and dotted black lines in Figure 9B show redundancy expressed as a proportion of total information conveyed by the two neurons and demonstrates the effects that increases in stimulus correlation and neuronal coupling strength have on redundancy. Figure 9C shows the reduction in group information that accompanies neuronal coupling.

Figure 9. Signal- and coupling-induced correlations. (**A**) Effects of signal correlation on redundancy. Responses of two uncoupled neurons to stimuli of increasing correlation are compared. Cumulative information plots of the two extreme cases of low and high stimulus correlation are displayed on top. For low correlation ($r \approx 0$), group information (red curve) and the sum of information from all the individual cells (blue curve) are nearly identical, due to the lack of correlation in the neural responses; high correlation ($r = 1$) in the stimulus induces correlation in the neural responses, and the amount of redundant information (shaded gray area) increases. (**Bottom**) The relationship between stimulus correlation and both group (red) and summed individual total information (blue). (**B**) Redundancy calculated as a function of stimulus correlation (solid black line) and coupling strength (dotted black line). (**C**) Effects of neuronal coupling on redundancy. In the upper left panel, neuronal coupling is weak (coupling strength = 0), and the neurons transmit the same (independent) information. In the upper right panel, the coupling is strong (coupling strength = 1), resulting in redundant information (grey area between the group information, shown in red, and total information, shown in blue).

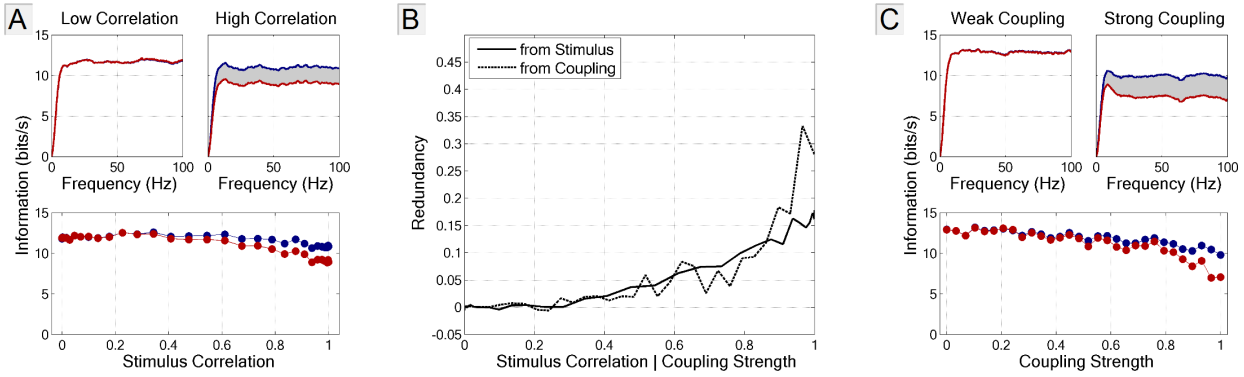

3.4.2. Application to Large Populations

An important benefit of using the Fourier Method to display neuronal signals in the frequency domain is that the temporal distribution of spiking activity, which is difficult to describe (and becomes prohibitively so as the number of neurons is increased), is transformed into a collection of simple Gaussian distributions, for which the calculation of entropy is straightforward. While the length of the description of spike patterns in the time domain increases as an exponential of the number of neurons ($O\left(2^N\right)$ for an N-neuron bit pattern), in the frequency domain, the corresponding calculation is

constrained by the speed of diagonalization of the Fourier component covariance matrix; algorithms for this computation, such as the Cholesky decomposition method, have order $O(N^3)$ (see, for example, [41]). As a result, the information rates and levels of redundancy for populations of neurons numbering in the hundreds can be calculated on an ordinary desktop computer in a matter of minutes.

An example provided in Figure 10A demonstrates the increase in redundancy as the number of uncoupled neurons responding to the same stimulus progressively increases. Despite the lack of synaptic influence within the network, correlations induced by the stimulus alone are of sufficient magnitude to drastically increase the amount of redundant information (shaded gray area) as the number of neurons increases. The contribution of each successive neuron added to the group decreases, as a fraction of its signal information is inferable from other neurons. It becomes immediately apparent that extrapolation of pairwise redundancy to larger populations can result in egregious misrepresentations of the true signal information rate.

Figure 10B provides information calculation times for groups of up to 500 neurons, calculating up to 100 Hz for 128 trials each. Clearly, the method can easily handle larger neural populations than can be recorded with current technologies. This figure demonstrates the capability of the Fourier information method to scale with large populations of neurons and shows how the influence of both signal and intrinsic correlations affect levels of information and redundancy.

Figure 10. Information in large neural populations. (**A**) Group size *versus* sum total and group information using the GLM model. The sum total information, which does not take into account correlations between cells, increases linearly with the number of cells (blue), whereas the group information rate (red) climbs sub-linearly, due to the progressive increase in redundant information (shaded gray area). (**B**) Processing times on a desktop computer for group sizes of up to 500 neurons. Calculations were performed on an Intel® Core™ i7-3770K running at 3.9 GHz with 32 GB RAM.

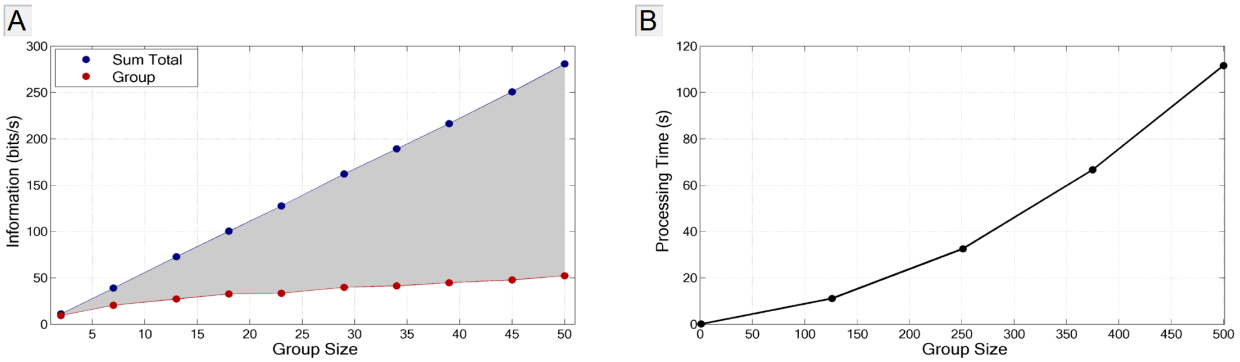

4. Summary and Conclusions

We used the GLM framework to simulate single neurons and populations of neurons and explored the influence that various aspects of the discharge and of the interactions between neurons have on our estimate of the amount of information transmitted by the population discharge.

We found that our method is applicable over a wide range of mean firing rates and is robust against both the non-stationarity of the firing rate and errors in the assignment of spikes to neurons in the recorded population. We also described ways to correct for potential inaccuracies in the estimation of information rates from a neural population. Finally, we showed that our method scales to population sizes that exceed the capabilities of current technology and that information in such large groups can be calculated quickly and efficiently.

Acknowledgements

This work was supported by NIH grants EY-1622, NIGMS-1P50GM071558 and NIMH-R21MH093868. We thank Alex Casti for helpful comments on the manuscript.

Conflicts of Interest

The authors declare no conflict of interest.

References

1. Nicolelis, M.A.L.; Ribeiro, S. Multielectrode recordings: The next steps. *Curr. Opin. Neurobiol.* **2002**, *12*, 602–606.
2. Shannon, C. A mathematical theory of communication. *Bell Syst. Tech. J.* **1948**, *27*, 379–423, 623–656. Reprinted with corrections. Available online: http://cm.bell-labs.com/cm/ms/what/shannonday/shannon1948.pdf (accessed on 8 May 2013).
3. Panzeri, S.; Senatore, R.; Montemurro, M.A.; Petersen, R.S. Correcting for the sampling bias problem in spike train information measures. *J. Neurophysiol.* **2007**, *98*, 1064–1072.
4. Quiroga, R.Q.; Panzeri, S. Extracting information from neuronal populations: Information theory and decoding approaches. *Nat. Rev. Neurosci.* **2009**, *10*, 173–185.
5. Ince, R.A.A.; Senatore, R.; Arabzadeh, E.; Montani, F.; Diamond, M.E.; Panzeri, S. Information-theoretic methods for studying population codes. *Neural Netw.* **2010**, *23*, 713–727.
6. Yu, Y.; Crumiller, M.; Knight, B.; Kaplan, E. Estimating the amount of information carried by a neuronal population. *Front. Comput. Neurosci.* **2010**, *4*, doi: 10.3389/fncom.2010.00010 .
7. Crumiller, M.; Knight, B.; Yu, Y.; Kaplan, E. Estimating the amount of information conveyed by a population of neurons. *Front. Neurosci.* **2011**, *5*, doi:10.3389/fnins.2011.00090.
8. Pillow, J.W.; Paninski, L.; Uzzell, V.J.; Simoncelli, E.P.; Chichilnisky, E.J. Prediction and decoding of retinal ganglion cell responses with a probabilistic spiking model. *J. Neurosci.* **2005**, *25*, 11003–11013.
9. Paninski, L.; Pillow, J.; Lewi, J. Statistical models for neural encoding, decoding, and optimal stimulus design. *Prog. Brain Res.* **2007**, *165*, 493–507.
10. Strong, S.P; Koberle, R.; de Ruyter van Steveninck, R. R.; Bialek, W. Entropy and information in neural spike trains. *Phys. Rev. Lett.* **1998**, *80*, 197–200.
11. Linkser, R. Self-organization in a perceptual network. *Computer* **1988**, *21*, 105–117.

12. Pillow, J.W.; Shlens, J.; Paninski, L.; Sher, A.; Litke, A.M.; Chichilnisky, E.J.; Simoncelli, E.P. Spatio-temporal correlations and visual signalling in a complete neuronal population. *Nature* **2008**, *454*, 995–999.
13. Destexhe, A.; Rudolph, M.; Paré, D. The high-conductance state of neocortical neurons *in vivo*. *Nat. Rev. Neurosci.* **2003**, *4*, 739–751.
14. Destexhe, A.; Paré, D. Impact of network activity on the integrative properties of neocortical pyramidal neurons *in vivo*. *J. Neurophysiol.* **1999**, *81*, 1531–1547.
15. Wilson, C. Up and down states. *Scholarpedia J.* **2008**, *3*, doi:10.4249/scholarpedia.1410.
16. Sherman, S.M. Tonic and burst firing: Dual modes of thalamocortical relay. *Trends Neurosci.* **2001**, *24*, 122–126.
17. Reinagel, P.; Godwin, D.; Sherman, S.M.; Koch, C. Encoding of visual information by LGN bursts. *J. Neurophysiol.* **1999**, *81*, 2558–2569.
18. De Charms, R.C.; Merzenich, M.M. Primary cortical representation of sounds by the coordination of action-potential timing. *Nature* **1996**, *381*, 610–613.
19. Carr, C.E. Processing of temporal information in the brain. *Annu. Rev. Neurosci.* **1993**, *16*, 223–243.
20. Braitenberg, V. Cell assemblies in the cerebral cortex. *Lecture Notes Biomath.* **1978**, *21*, 171–188.
21. Sakurai, Y. Population coding by cell assemblies–what it really is in the brain. *Neurosci. Res.* **1996**, *26*, 1–16.
22. Gawne, T.J.; Richmond, B.J. How independent are the messages carried by adjacent inferior temporal cortical neurons? *J. Neurosci.* **1993**, *13*, 2758–2771.
23. Meister, M.; Lagnado, L.; Baylor, D.A. Concerted signaling by retinal ganglion cells. *Science* **1995**, *270*, 1207–1210.
24. Oram, M.W.; Hatsopoulos, N.G.; Richmond, B.J.; Donoghue, J.P. Excess synchrony in motor cortical neurons provides redundant direction information with that from coarse temporal measures. *J. Neurophysiol.* **2001**, *86*, 1700–1716.
25. Eckhorn, R.; Bauer, R.; Jordan, W.; Brosch, M.; Kruse, W.; Munk, M.; Reitboeck, H.J. Coherent oscillations: A mechanism of feature linking in the visual cortex? *Biol. Cybern.* **1988**, *60*, 121–130.
26. Gray, C.M.; König, P.; Engel, A.K.; Singer, W. Oscillatory responses in cat visual cortex exhibit inter-columnar synchronization which reflects global stimulus properties. *Nature* **1989**, *338*, 334–337.
27. Vaadia, E.; Haalman, I.; Abeles, M.; Bergman, H.; Prut, Y.; Slovin, H.; Aertsen, A. Dynamics of neuronal interactions in monkey cortex in relation to behavioural events. *Nature* **1995**, *373*, 515–518.
28. Steinmetz, P.N.; Roy, A.; Fitzgerald, P.J.; Hsiao, S.S.; Johnson, K.O.; Niebur, E. Attention modulates synchronized neuronal firing in primate somatosensory cortex. *Nature* **2000**, *404*, 187–190.
29. Wang, Y.; Iliescu, B.F.; Ma, J.; Josić, K.; Dragoi, V. Adaptive changes in neuronal synchronization in macaque V4. *J. Neurosci.* **2011**, *31*, 13204–13213.
30. Nirenberg, S.; Carcieri, S.M.; Jacobs, A.L.; Latham, P.E. Retinal ganglion cells act largely as independent encoders. *Nature* **2001**, *411*, 698–701.

31. Levine, M.W.; Castaldo, K.; Kasapoglu, M.B. Firing coincidences between neighboring retinal ganglion cells: Inside information or epiphenomenon? *Biosystems* **2002**, *67*, 139–146.
32. Averbeck, B.B.; Lee, D. Neural noise and movement-related codes in the macaque supplementary motor area. *J. Neurosci.* **2003**, *23*, 7630–7641.
33. Golledge, H.D.R.; Panzeri, S.; Zheng, F.; Pola, G.; Scannell, J.W.; Giannikopoulos, D.V.; Mason, R.J.; Tovée, M.J.; Young, M.P. Correlations, feature-binding and population coding in primary visual cortex. *Neuroreport* **2003**, *14*, 1045–1050.
34. Brenner, N.; Strong, S.P.; Koberle, R.; Bialek, W.; de Ruyter van Steveninck, R.R. Synergy in a neural code. *Neural Comput.* **2000**, *12*, 1531–1552.
35. Abbott, L.F.; Dayan, P. The effect of correlated variability on the accuracy of a population code. *Neural Comput.* **1999**, *11*, 91–101.
36. Latham, P.E.; Nirenberg, S. Synergy, redundancy, and independence in population codes, revisited. *J. Neurosci.* **2005**, *25*, 5195–5206.
37. Abeles, M.; Bergman, H.; Margalit, E.; Vaadia, E. Spatiotemporal firing patterns in the frontal cortex of behaving monkeys. *J. Neurophysiol.* **1993**, *70*, 1629–1638.
38. Maldonado, P.E.; Gerstein, G.L. Neuronal assembly dynamics in the rat auditory cortex during reorganization induced by intracortical microstimulation. *Exp. Brain Res.* **1996**, *112*, 431–441.
39. Nicolelis, M.A.; Lin, R.C.; Chapin, J.K. Neonatal whisker removal reduces the discrimination of tactile stimuli by thalamic ensembles in adult rats. *J. Neurophysiol.* **1997**, *78*, 1691–1706.
40. Ikegaya, Y.; Aaron, A.; Cossart, R.; Aronov, D.; Lampl, I.; Ferster, D.; Yuste, R. Synfire chains and cortical songs: Temporal modules of cortical activity. *Science* **2004**, *304*, 559–564.
41. Watkins, D.S. *Fundamental of Matrix Computations*, 1st ed.; Wiley: New York, NY, USA 1991; p. 84.

3 Application to the Visual System

Our primary motivation thus far has been to develop a useful tool for dealing with measurements recorded from many neurons in the brain. As we have emphasized, the brain is composed of many neurons working in tandem, and electrophysiologists have hastened to make use of the burgeoning multi-channel technology that allows for a more precise monitoring of brain activity at the cellular level. The three published papers prior to this chapter have described a method that makes use of such signals in a practical manner, allowing for the estimation of information in much larger populations of neurons than was previously possible. In this chapter, we provide a few examples of how the application of the Fourier method may be useful in answering questions concerning the nature of information processing in real brains. We begin with a brief description of the process by which neurophysiological signals are acquired and prepared for analysis, and then proceed with real data recorded from the Lateral Geniculate Nucleus and V1 of the macaque.

3.1 Materials and Methods

3.1.1 Surgery & Setup

The data used in this chapter were acquired from four recordings in three separate monkeys, using the techniques described in Yu et al. (2010) and Crumiller et al. (2011). All surgical procedures were performed in accordance with the National Institute of Health and guidelines and approved by the Icahn School of Medicine at Mount Sinai Institutional Animal Care and Use Committee. Adult macaque monkeys (*macaca fascicularis*) were anesthetized with an IM injection of ketamine hydrochloride (Ketaset, $10\,\mathrm{mg/kg}$), followed by propofol (Diprivan) and local anesthetic (xylocain) as needed during surgery. Anesthesia was maintained with sufentanil ($0.05\,\mu\mathrm{g/kg-hr}$), which was given intravenously (IV) throughout the experiment. Cannulae were inserted into the femoral veins for IV infusion, the right femoral artery for the monitoring of blood pressure, the bladder for urine relief and measurement, and the trachea for respiration. Phenylephrine hydrochloride (10%) and atropine sulfate (1%) were applied to the eyes, and the corneas covered with gas-permeable contact lenses to prevent drying.

Blood pressure, electrocardiogram, and body temperature were measured and kept within physiological range. An infusion of vecuronium bromide ($.02 - .06\,\mathrm{mg/kg-hr}$) induced paralysis, and the animal was artificially respired; the respiration rate and stroke volume were adjusted to produce an end-expiratory value of 3.4-4% $\mathrm{CO_2}$ at the exit of the trachea cannula. A continuous IV flow of Ringer's solution with 5% dextrose was maintained to keep the animal hydrated throughout the experiment. The eyes were refracted and focused with correcting lenses at a distance of $57\,\mathrm{cm}$.

3.1.2 Stimuli & Data Acquisition

Stimuli were presented monocularly on a video monitor (luminance: $10 - 50\,\mathrm{cd/m^2}$) and driven by software developed using the Psychtoolbox in MATLAB (Brainard, 1989; Pelli, 1997; Kleiner et al., 2007). Electrophysiological recordings were made using electrodes developed by *Neuronexus*: a 32-channel electrode beta PTRODE for the LGN, and an 8-shank, 64-channel Buzsaki-type 64-64A electrode for V1. The output of each electrode was amplified, band-pass filtered, and sampled at 20 or $40\,\mathrm{kHz}$ and stored in a *Plexon* MAP computer for further analysis.

3.1.3 Spike Sorting: Msort

Spike sorting, the process of identifying action potentials and the neurons from which they are derived, is fraught with difficulties (Brown et al., 2004; Buzsáki, 2004; Lewicki, 1998). The large, spatio-temporal recordings that result from multi-channel recordings generate time- and location-dependent voltage traces influenced by the firing of many neurons. The large amount of digitized voltage data generated from a high sampling frequency, multi-channel setup, compounded with both cortical and electrical noise, poses a difficult problem for the neurophysiologist. Some of the recordings performed in our experiments span periods of hours, and the gigabytes

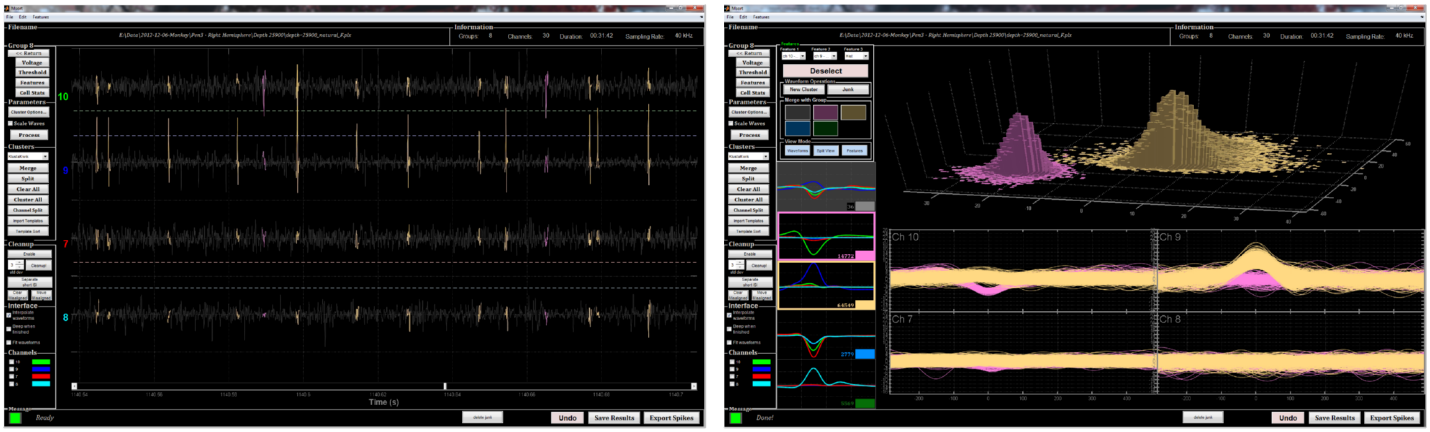

Figure 1: **Msort spike-sorting software.** In-house software developed for the use in sorting multi-channel, continuous data acquired from the Plexon data acquisition system. (Left) 4-channel voltage trace of an LGN recording; the spikes from two select neurons are highlighted in yellow and pink. (Right) 3D histogram of projection coefficients of the waveforms from the same two neurons, projected onto the first Principal Components of the two channels on which those waveforms show the highest amplitude. The histogram of the projected coefficients shows two obvious peaks, indicating that these waveforms are highly separable.

---

of data generated were found to be either computationally intractable using multi-channel sorting software or insufficiently robust using single-channel analysis procedures. To better address this issue, we have developed our own spike-sorting software, tailored specifically to lengthy multi-channel recordings. This software is known as Msort, and was developed in Matlab.

Msort is fully capable of importing raw voltage data from both Plexon and Axon Instruments, and implements filtering, waveform thresholding, arbitrary electrode configurations, both automatic and manually clustering procedures, displays cell statistics, and contains an intuitive graphical user interface that allows flexible manipulation of the data and its resulting clusters. Automatic sorting can be performed using various clustering algorithms, most notably the Gaussian-mixture algorithm developed by Ken Harris and described in Harris et al. (2000). Two sample views of the Msort screen can be seen in Figure 1. Figure 1 (left) shows a typical 4-channel voltage trace from an LGN recording, with spikes from two neurons highlighted in pink and yellow. Figure 1 (right) shows a histogram derived from the projections of the waveforms from those same two neurons onto the first Principal Components of two channels, and histogrammed along the third dimension in the top of the view; the waveforms themselves from the four channels can be seen on the bottom. Msort was used in the spike-sorting of all data acquired in the experiments described.

3.1.4 Natural Movies

The use of natural scenes in visual neurophysiological experiments has seen a resurgence in recent years. The efficient coding hypothesis proposes that the brain seeks to minimize energy usage while maximizing its ability to process information. With respect to the visual world, one would expect that our visual system is optimized to detect incoming signals that are representative of the world we see, and that the types of signals that maximize its information throughput while minimizing energy usage will have the statistics of natural scenes. Indeed, both psychophysical and electrophysiological experiments consistently demonstrate that the visual system is well-adapted to, and appears to be designed for, natural scenes. Beginning even at the level of the retina, both color information (Vasserman et al., 2013; Kellner and Wachtler, 2013) and contrast information (Mante et al., 2005; Tadmor and Tolhurst, 2000; Pamplona et al., 2013) closely match the statistics of the natural environment. The progression of the signal to the lateral geniculate nucleus involves compression and temporal decorrelation most optimized for natural scenes (Dan et al., 1996). A slew of recent studies by both psychologist

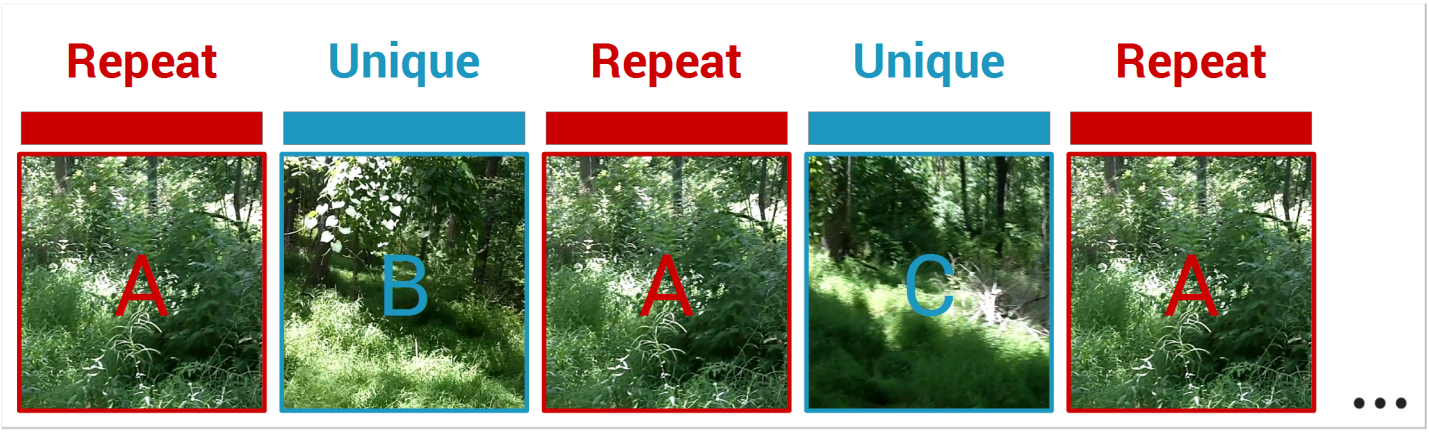

Figure 2: **Repeat-Unique Paradigm**. Repeated trials (labeled "A") are interleaved with unique trials (labeled "B" and "C"). The process of interleaving allows for a capture of unique and repeat entropy in a manner such that long-term effects of the recording, such as increases or decreases in firing rate due to levels of anesthesia, affect both entropies equally.

---

and neuroscientists alike demonstrate unequivocally stronger response by the brain to natural scene stimuli (Zhu et al., 2013; Groen et al., 2013; Zylberberg and DeWeese, 2013; Fradcourt et al., 2013; Stansbury et al., 2013; Betti et al., 2013; De Cesarei et al., 2013) regardless of the mode of assessment. Ma and Wu (2011) provides a thorough discussion of the close relationship between natural scene statistics and the parallel evolution of the visual system.

For this reason, we have chosen to use natural scene movies to maximally elicit informative responses from our recorded cells. The visual stimulation used in this section follows the repeat-unique paradigm outlined previously: a continuous movie, shot at 30 frames per second, was recorded of a walk through a wooded area in Princeton, New Jersey. The movie was subsequently subdivided into approximately eight-second sections. A single eight-second section, dubbed the "repeat" section, was interleaved with the remaining sections, which were shuffled. The resulting sequence of Repeat–Unique (Figure 2) movies allows for the estimation of noise entropy in response to the Repeats, and total entropy in response to the Uniques.

3.2 LGN responses to Natural Scenes

3.2.1 Information streams in the visual system

The extent to which the primate visual system works in a functionally hierarchical, manner (as originally proposed by Hubel and Wiesel (1962)) has become a source of contention for visual neuroscientists. The primary visual pathways in humans and monkeys consist of anatomically distinct cells and connectivity networks that lend support to the notion that the visual signal is parsed into separate information streams. Early evidence supporting this notion included the discovery of ON- and OFF center-surround retinal ganglion cells (Hartline, 1940), linearly- and nonlinearly-responding ganglion cells in the cat, and further morphological studies (Rodieck and Brening, 1983) that suggested three basic retinal ganglion cell subtypes whose morphology and connectivity suggest a functional divergence (Livingstone and Hubel, 1984b; Shipp and Zeki, 1985; Livingstone and Hubel, 1988; Ungerleider and Mishkin, 1982) along the color and luminance axes. The majority of retinal ganglion cells (80%) are midget cells (also known as P cells), which are small-bodied and densely distributed across the retina, and project to the parvocellular layers, layers 3-6, of the lateral geniculate nucleus (LGN; hence P cells) (Goodchild et al., 1996). The small diameter dendritic trees, with small receptive fields of P cells allow for greater spatial resolution, especially in the fovea, where each midget RGC receives input from a single bipolar cell driven by a single cone. In contrast, parasol cells, also known as M cells, are sparsely distributed across the retina with much larger cell bodies and therefore greater contrast sensitivity (Kaplan and Shapley, 1986; Croner and Kaplan,

1995) and larger receptive fields. These cells project to the magnocellular layers of the LGN (layers 1-2) and receive larger, diffuse input from multiple bipolar cells (Boycott and Wässle, 1991). Finally, consisting of ~9% of all retinal ganglion cells, are the bi-stratified on-center ganglion cells, which project to the small koniocellular (Hendry and Yoshioka, 1994; Dacey and Lee, 1994) cells located in-between the layers of the LGN.

These retina-LGN projections from distinct cell types maintain their segregation at the primary visual cortex (V1) (Livingstone and Hubel, 1984a,b), and are implicated in even further functional segregation past V1 to other areas of the brain via two heavily interconnected pathways called the dorsal and the ventral pathways (Ungerleider and Mishkin, 1982; Goodale and Milner, 1992), commonly referred to as the "what" and "where" pathways due to the apparent functional differences of each (DeYoe et al., 1994). The two magnocellular layers of the LGN project to layer 4Cα of V1, and are thought to compose the origin of the dorsal stream due not only to anatomical connectivity but also the superior ability of M cells to react to time-varying stimuli. The dorsal stream projects from V1 to the parietal lobe, which is known to be heavily involved in activation of gaze and attention Ohlendorf et al. (2007), oculomotor preplanning (Rizzolatti et al., 1988), saccades, and generate spatial awareness. Lesions to the posterior parietal cortex cause visually-related deficits such as simultanagnosia, optic ataxia, and akinetopsia. In addition, studies have shown (Orban et al., 1984; McKee, 1981) that cell responses in VT/MT are correlated with performance in speed-discrimination tasks. The ventral stream, in contrast, projects from the four parvocellular layers of the LGN to layer 4Cβ, through layers 4A, 3B, and 3/2a, successively, through V2 and V4 and out diffusely to the areas of the medial temporal lobe and limbic system—areas heavily involved in object recognition, memory, and emotional affect—with strong interconnections to the dorsal stream (Lamme et al., 1998; Baird et al., 2002). Despite the appealing suggestion that these two streams of visual processing subserve different functions, the evidence for the level of interconnectivity between the two has only become greater with time (Farivar, 2009), and it has been suggested (Goodale and Milner, 1992) that the two streams are not based on the visual information itself, but more so for what purpose the information itself is used.

While the morphology and anatomical connectivity of the P-parvo-ventral and M-magno-dorsal streams provide some evidence for a separation of function, the extent of overlap and ability of each to extract specific features of a visual stimulus remains to be established. In addition, all evidence for separate streams of information flow has been derived from the properties of individual cells, and a proper investigation must account for the activity of groups of neurons contributing primarily to one function or the other before a dichotomy of streams is asserted, and scientists therefore require methods capable of analyzing both quantity and type of information a group of cells preferentially process. A thorough study of information in separate visual streams is necessary in order to fill some of the gaps in the evidence concerning the relevance of specific features of a stimulus to the function of these processing streams.

A preliminary view of the LGN response in Figure 3 shows the response of neurons to natural scenes. The raster plot seen in Figure 3A shows the response of a particularly highly responsive neuron to repeats (red, left) and uniques (blue, right); the precision of the response time is manifested by vertical raster lines in the repeats that arise when the neuron responds to the same feature upon each occurrence of a repeated trial. Figure 3B shows the individual cumulative information rates of the neurons in color; the thick black lines represent the sum total information (dotted) when correlations between neurons are ignored, and the actual information conveyed by the population (solid) when correlations between neurons are taken into account. The shaded gray area shows the redundant (shared among neurons) information, and the redundancy of the population is measured as the proportion of redundant information to the sum total, which in this case is just over 0.5.

The use of information measurement can assist in the detection of specific functional groups of neurons. The Functional Clustering Algorithm (FCA) of Feldt et al. (2009) uses a parameter-free method to functionally cluster neurons whose responses have been deemed similar in a statistically significant manner. We applied a modified version of the FCA, whereby the clustering results from application of the FCA to each natural-scene trial are averaged. We first tested our method on a simulated set of twenty neurons, using the simulation methods described in Crumiller et al. (2013). All twenty neurons were stimulated with the same stimulus, yet were subdivided into four groups of five neurons each, such that neurons within a group were mutually excitatory. Our motivation was not to mimic a naturally-occuring functional cluster, but rather to generate spike trains in which the responses of neurons within a functional group are dependent not on the stimulus, but rather on the

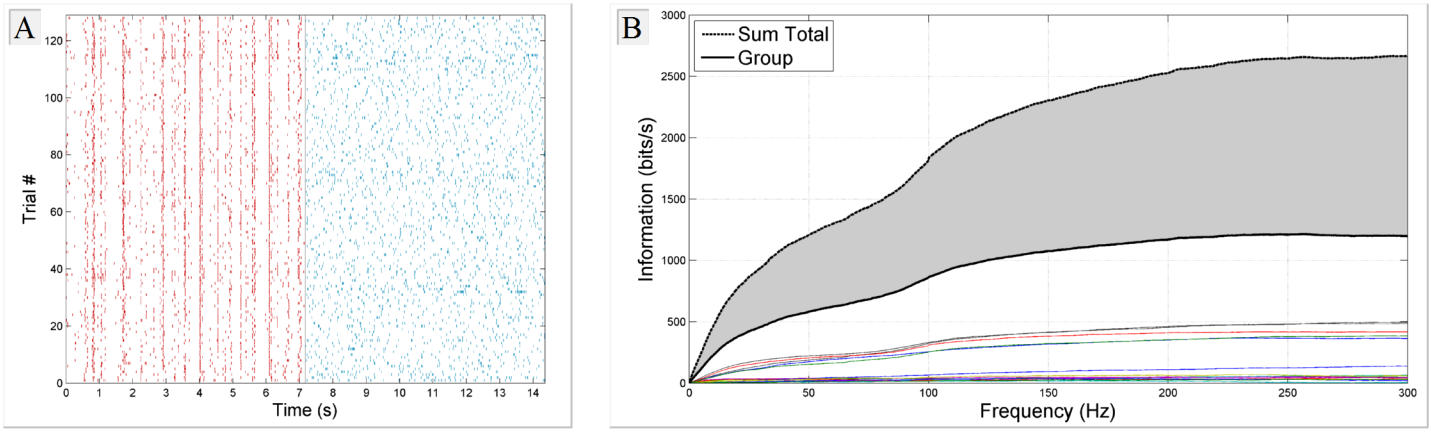

Figure 3: **LGN response to natural scenes**. (A) A raster plot of a highly responsive LGN neuron. Repeat trials are shown in red (left) and unique trials in blue (right). The vertical raster lines during the repeat trials indicate that the neuron responded similarly during each repeated presentation of the stimulus, with a high degree of temporal precision. (B) Cumulative information plots. The individual neurons (colored lines; bottom) appear to form two separate groups with respect to the amount of information conveyed about the stimulus. Their sum total (dotted black line) far exceeds the actual amount of information conveyed by the population (solid black line), indicating a high proportion of redundant information exceeding 0.5.

---

influence of the other neurons within the cluster. Furthermore, we wished to observe the ramifications of such connectedness on measures of information and redundancy within and between clusters.

Figure 4A shows the results from the simulation. The $(i, j)^{th}$ location in the *co*incidence matrix, observed in the top left, shows the proportion of trials in which each cell *i* was functionally clustered together with cell *j*. The four separate clusters are easily identified as the four red squares, indicated that the FCA method consistently detected functional groupings between mutually excitatory neurons. The coincidence values found in the coincidence matrix were used to generate a dendrogram (right), which further displays the prominent separation between the four functional groups.

To measure the level of influence that functional interconnectivity has on the measurements of information and on redundancy, we generated a probability distribution of information rates and redundancy proportions taken from 10,000 randomly-chosen groups of five cells from the twenty simulated neurons. The resulting distributions of information rates and redundancy proportions can be seen in the lower panels of A, represented by the gray histogram and shown in units of standard deviations from the mean. The within-group information and redundancy rates from all four groups are indicated by their color-coded lines on the plot. Each group's information and redundancy values exceeded 3.5 standard deviations away from the mean, indicating that the effects of functional clustering on both information and redundancy are highly statistically significant.

The apparent lack of functional clustering upon application of the averaged FCA to the LGN, seen in Figure 4B is unsurprising; all cells were recorded using an electrode spanning 800 microns, found in the same geniculate layer, and had similar receptive fields. Whether the lack of functional clustering is due to insufficient sensitivity of the method, or to a lack of functional clustering in the recorded population, remains to be determined. However, it should be noted that geniculate neurons receive independent signals pre-filtered by their respective input retinal ganglion cells, each of which are informed by potentially unique micro-circuitry formed by the earlier layers of the retina, and the similarity of these signals are governed by LGN cell type, input retinal cell type, and receptive field location. A complete picture of the anatomical situation would greatly inform our understanding of how the neural circuitry can influence the existence or non-existence of functional groupings, and the use of information theory in the manner applied to the simulated data allows us to verify that a cluster of neurons operate together in a statistically significant manner, as determined by their information rate and/or redundancy proportion.

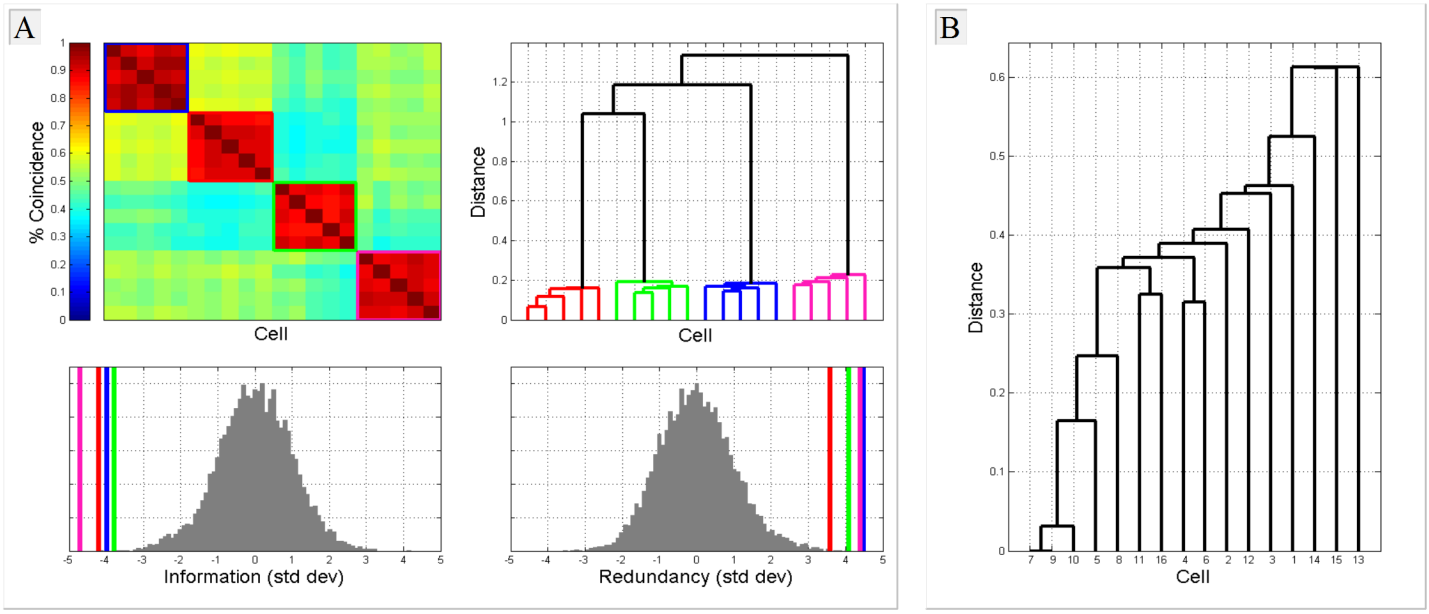

Figure 4: **Simulated and LGN functional clustering.** (A) Simulation of 20 neurons, subdivided into four functional groups of five neurons each. The results from repeated applications of the Functional Clustering Algorithm of Feldt et al. (2009) to natural-scene movie trials were averaged to produce a coincidence matrix. The $(i, j)^{th}$ position in the matrix represents the proportion of trials in which neuron *i* was positioned in the same cluster as neuron *j* by the FCA algorithm. The four distinct clusters can be easily discerned from both the coincidence matrix (left) and the dendrogram (right). (bottom) Permutation tests of random groups of five neurons were used to generate distributions of group information rates (left) and redundancy proportions (left), z-scored to produce normal distributions. The (normalized) information and redundancy of the color-coded groups as determined by the FCA are displayed as vertical lines superimposed over the between-group distributions. Each of the four groups had both information and redundancy rates exceeding 3.5 standard deviations from the mean ($p < .005$). (B) Dendrogram of averaged FCA results from the LGN. No significant clustering of functional groups was observed.

A determination of the actual *function* of a statistically significant cluster of neurons would require manipulation of the stimulus. As we see in the next section, natural scene movies continue to provide a beneficial stimulus environment for extracting information concerning the nature of a neuron's role in the deciphering of incoming visual signals.

3.3 V1

The parallel streams hypothesis proposes that information propagates through the visual system along functional streams that preferentially process different aspects of the stimulus. The ventral and dorsal streams, purported to specialize in object definition and location, respectively, should therefore extract aspects of the stimulus for which their underlying circuits are optimized. A straightforward test of this hypothesis thus involves the presentation of stimuli containing information skewed towards the preference of one stream or the other; a comparison of population information rates between neurons located in these respective visual streams should show statistically significant preferences toward one stimulus set or the other. In other words, a population of neurons in the dorsal stream should convey a greater preference, manifest as an increase in information conveyed, towards stimuli containing high temporal frequency, low spatial frequency, and decreased color information; populations in the ventral stream should out-perform those in the dorsal stream when presented with low temporal frequency, high spatial frequency, and color-rich stimuli.

Figure 5: **Processed natural scene stimuli**. A full-color movie (A) is processed using two filters: a grayscale filter (B), in which color information is removed but luminance information retained, and an isoluminant filter (C), in which luminance information is removed but color information retained.

3.3.1 Processed Natural Scenes

To create a stimulus to directly test this hypothesis, we processed our original, full-color natural scene movie (Figure 5A)) using two filters. The first filter, designed to preferentially stimulate the dorsal stream, produces a grayscale image retaining only luminance information (Figure 5B) and ignores color information. We first measured the luminance levels L_R, L_G, and L_B of the red, green, and blue guns of the stimulus monitor using an OptiCAL photometer . The luminance of each pixel at position (x, y) from the original Full Color natural movie was then calculated from these measurements, and the corresponding grayscale luminance values generated using a weighted sum of the L_R, L_G, and L_B components:

$$L_{x,y} = \left(\frac{L_R}{L_R + L_G + L_B} R_{x,y} + \frac{L_G}{L_R + L_G + L_B} G_{x,y} + \frac{L_B}{L_R + L_G + L_B} B_{x,y} \right) \quad (1)$$

where *R*, *G*, and *B* are the pixel values for the three red, green, and blue guns. The second filter, designed to preferentially stimulate the ventral stream, produces an image whereby each pixel emits the same luminance, while retaining the same color proportions of the original RGB signal (Figure 5C). This filter first chooses, for the entire duration of the stimulus, a luminance value L_{iso} to which each pixel is matched. The luminosity $L_{x,y}$ of each pixel is calculated using the monitor luminosities via Equation 1, and the scaling factor required to bring the pixel luminance to L_{iso} applied to the original full-color image to one in which each pixel has the same luminance L_{iso}:

$$I_{x,y} = \frac{L_{iso}}{L_{x,y}} \left(R_{x,y}, G_{x,y}, B_{x,y} \right)$$

The resulting 8-second trials were presented using the repeat-unique paradigm similar to that shown in Figure 2, the only difference being that each trial applied either the two filtered versions or the original full-color with equal probabilities of $1/3$, resulting in 256 trials (128 uniques/128 repeats) of each type of filtered stimulus. The random presentation of each trial avoids adaptation artifacts that might arise should one particular type of filtered stimulus always precede another. Data were acquired using the Plexon data acquisition system, and the spikes were sorted, as described above.

3.3.2 V1 responses

The neural responses to the three different stimulus classes (Full color/no filter; grayscale/luminance-only; isoluminant/color-only) can be separately observed when responses to each trial are parsed and combined. Each neuron can be represented by the proportion of its response to the three classes of stimuli. In Figure 6A (top),

we represent the neuronal response to each stimulus as a bar plot, with each color representing the proportion of spikes elicited by each stimulus class. Figure 6B (top) shows the same data plotted geometrically: the location of each dot represents the weighted spike response to each stimulus, with the three stimulus classes shown at the three corners of an equilateral triangle. The number of spikes elicited by each stimulus were generally consistent and equal, as evidenced by clustering near the center of the triangle. However, when firing rate response is replaced by the amount of information conveyed, the story is a bit different. Figure 6A (bottom) and 6B (bottom) shows the information-proportion bar plot, analogous to Figure 6A (top) and 6B (top). The information rate plots in response to each stimulus are clearly more complex: individual neurons show a marked preference for some stimulus classes over others. Clearly, simple spike-count measures are too insensitive to adequately express the types of processing occurring in primary visual cortex.

Figure 6C provides a sample measure of group redundancy of all neurons from one recording in response to the three stimulus classes. In this plot, redundancy is expressed as a function of frequency. Interesting to note is that, despite similar firing rates from all neurons for each of the three stimulus classes, the levels of redundancy for each type of stimulus are similar for high frequencies, yet display a marked redundancy signature for low frequencies, indicating that perhaps the different types of information propagating through this particular population of neurons is shared in a frequency-dependent manner. Such claims, however, require that the frequency-dependent information content of the stimulus first be properly indexed. Future studies may find the measure of redundancy in populations of neurons from different anatomical regions invaluable in determining how information in different stimulus classes are shared between neurons in a frequency-dependent manner.

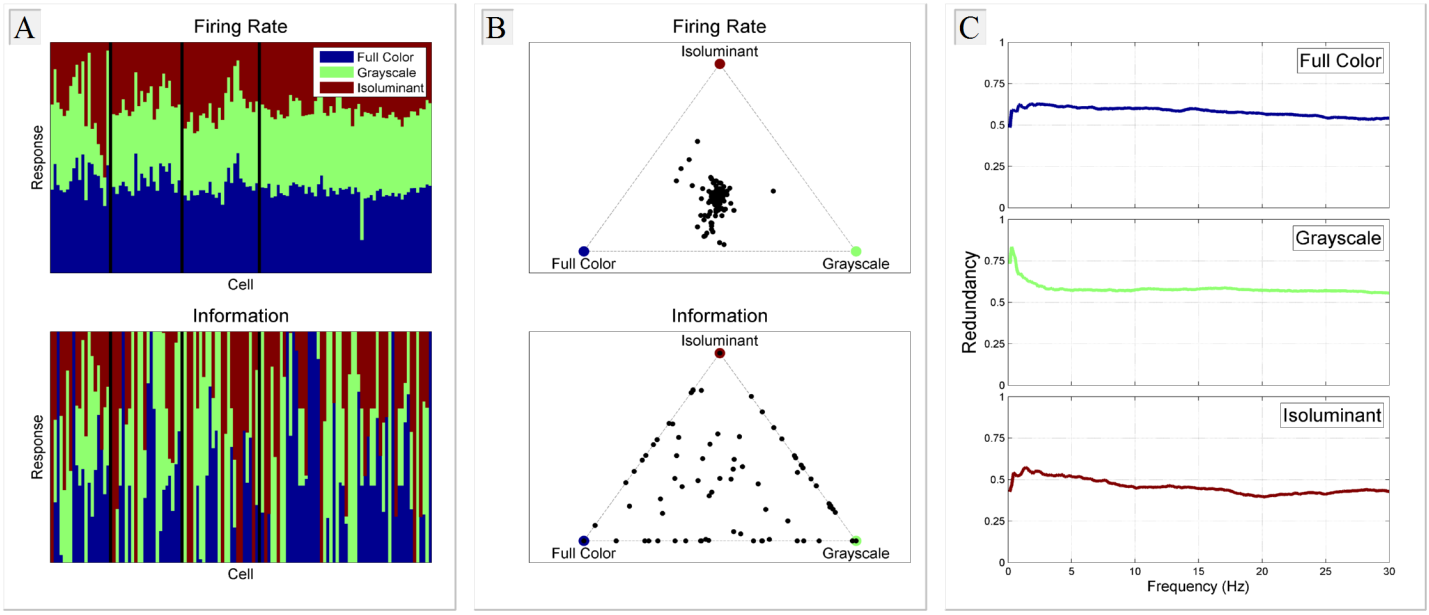

Figure 6: **V1 responses to Full color, grayscale, and isoluminant-color natural movies**. (A) Neural response to three stimulus classes as determined by spike count (top) and information (bottom). Rate responses were homogenous, with nearly equal contributions of spikes to all three stimulus types; information rates were more greatly skewed. (B) Neural responses represented geometrically. Responses represented by spike count (top) cluster near the center of gravity; responses represented as information (bottom) are more spread out, demonstrating increased neuronal specialization. (C) Group redundancy as a function of frequency for one recording. The three classes of stimuli elicit different redundancy profiles from the same population of neurons.

3.4 Single-cell Retina/LGN Information Transfer

3.4.1 The S-Potential

The function of the LGN, previously labeled as a simple relay between the retina and the visual cortex, has long been obfuscated by a multitude of inputs, recurrent connections, and feedback connections that modulate its spiking activity. Figure 7A shows a simulated spike train including spikes from both the LGN and the retina. While each LGN spike (shown in green) is driven by a retinal ganglion spike (Kaplan and Shapley, 1984), not all RGC spikes elicit an LGN response. RGC input spikes can be detected by LGN electrophysiological recordings as large sub-threshold EPSPs, which occasionally (about 40% of the time) result in a concomitant LGN relay spike (Kaplan et al., 1987; Bishop, 1953; Cleland et al., 1971; Sincich et al., 2007; Weyand, 2007). The 40% of spikes from the retina which do succeed in eliciting LGN spikes appear to contain more information than the deleted spikes, and this discrepancy increases as stimulus spot size decreases and the effect of the inhibitory surround decreases (Uglesich et al., 2009). The mechanisms by which the LGN chooses the more informative retinal spikes has been an active area of research (Carandini et al., 2005; Mante et al., 2008; Sherman, 2005; Andolina et al., 2007; Sherman and Guillery, 1998; McAlonan et al., 2006, 2008), although a distinguishing functional difference between the LGN and retinal receptive field is the extension and enhancement of the antagonistic surround in the LGN (Hubel and Wiesel, 1961; Blitz and Regehr, 2005; Dubin and Cleland, 1977). The application of the Fourier method to the retina-to-LGN transmission of information is therefore appealing, because of its ability to measure information using limited data sets.

We applied our Fourier method to single-unit recordings of the cat LGN, taken from thirteen cells recorded in eight different cats from 2005 until 2009. Recording procedures were similar to those described above for the macaque; details of the experimental preparation and recording can be found in Uglesich et al. (2009). For each cell, we recorded the spiking response of LGN neurons, and their input RGC neurons as determined by the signature S-potentials, in response to a fixed-size spot whose luminance fluctuated according to a pseudorandom distribution (van Hateren, 1997). As in the natural scenes case, $8\,\mathrm{s}$ trials were presented in a repeat-unique paradigm, in which the sequence of luminance values was the same for every repeated trial. Each cell provided multiple recordings, between which the spot size was altered to include or exclude the antagonistic surround to varying extents.

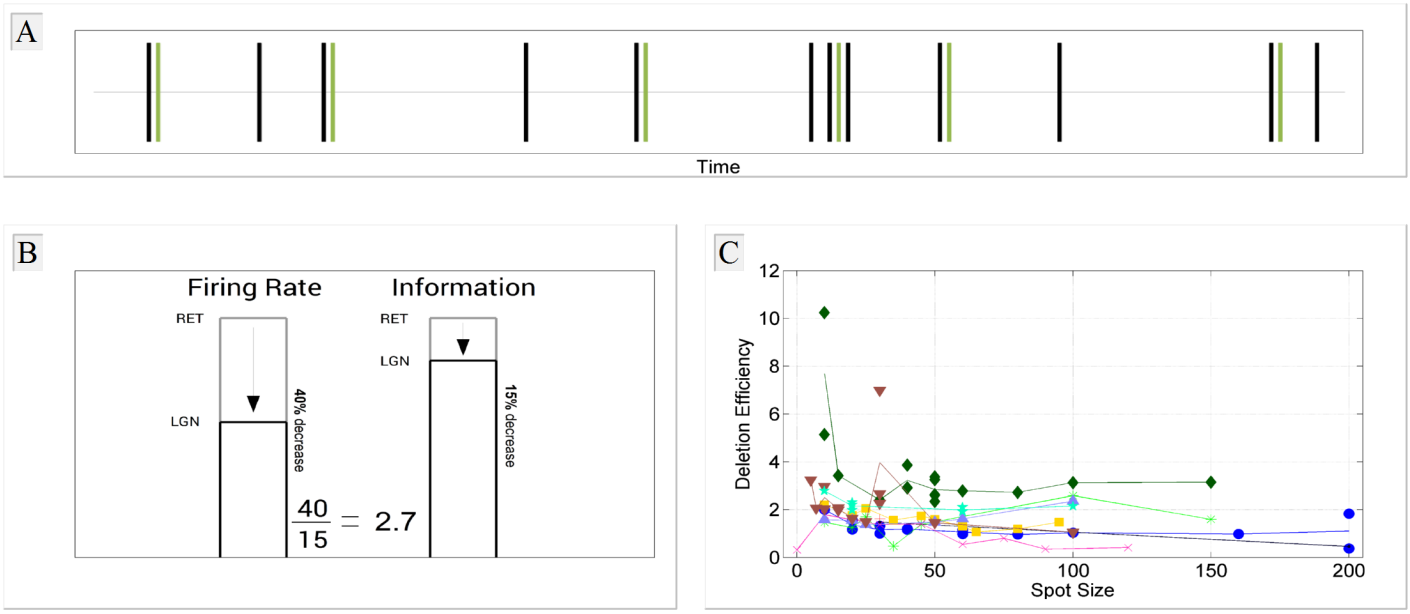

Figure 7: **Information transfer between retina and LGN**. (A) Approximately 40% of the simulated retinal input spikes (black) succeed in eliciting LGN spikes (green). Spikes from the retinal ganglion driver cell can be picked up from LGN voltage traces, appearing as an "S-potential" embedded in the initial rise of the elicited LGN spike. (B) A possible deletion efficiency between RGC and LGN spikes. The reduction in firing rate divided by a reduction in information allows us to determine whether or not spikes transmitted by the LGN to V1 contain more information. (C) Deletion efficiency as a function of spot size. As spot size increases, the deletion efficiency the LGN decreases, indicating that the inhibitory surround inputs located in the retina may play a vital role in determining how much information is conveyed by the retina.

3.4.2 Deletion Efficiency

A simple measure of deletion efficiency can be seen in Figure 7B. The LGN spike train may be thought of as a sequence of successful retinal ganglion spikes selected for throughput. We thus can compare both the firing rate of the LGN to the RGC in addition to its information content. If the proportion of spikes deleted by the LGN exceeds proportion of information loss that results from the deletion, then the deleted spikes contain less information. We can measure the efficacy of the deletion by dividing the proportion of spikes deleted to the proportion of information deleted, which we call the "deletion efficiency." In the example schematic shown in Figure 7B, a 40% reduction in spike count is accompanied by only a 15% reduction in information, resulting in a deletion efficiency of 2.7. Figure 7C shows deletion efficiency as a function of spot size, using the Fourier method to supply the information measurements. Each neuron is displayed with a unique color and symbol; different neurons provided different numbers of recordings and spot sizes, yet the emergent pattern is nonetheless in agreement with Uglesich et al. (2009): an increase in spot size is accompanied by a reduction in the efficiency of spike deletion by the LGN. Simultaneous measures of multiple neurons in the retina and LGN may provide insight into whether or not spikes are specifically chosen from each neuron in a manner, aiming, perhaps, to decorrelate input signals and reduce redundancy. A compression scheme that included the incoming signals from multiple neurons would be an expected result of the efficient coding hypothesis, and the deletion efficiency measure used here may be easily extended to measure the proportion of deletion of redundant information in a large population of retina-LGN pairs.

4 Conclusion

The work presented in this thesis addresses a longstanding problem in the field of neuroscience: how can one estimate the amount of information conveyed by the discharge of a population of neurons. The brain, composed of billions of neurons, processes information in massively parallel networks that are necessarily redundant, and as technology improves, the electrophysiologist is becoming rapidly overwhelmed with large quantities of data recorded from many neurons simultaneously. In this thesis, I have reiterated the urgent need for a large new body of research, capable of adequately processing such data, generating hypotheses, and shining light on the complex multi-neuronal activity that generates all of our perception, actions and thoughts, both conscious and subconscious. In the past, methods have existed for measuring information in groups of neurons, yet the curse of dimensionality has prevented measurements in populations larger than a small handful. The Fourier Method of estimating information exploits the fact that– under certain realistic constraints– the Fourier coefficients of uncorrelated segments of a signal are Gaussian distributed; knowledge of the underlying distribution of coefficients allows the entropy of the signal, represented in the frequency domain, to be estimated using a relatively small amount of laboratory data. As technological advancements continue to increase our ability to measure signals in the brain, tools such as the Fourier Method, capable of dealing with a large population of neurons, will become even more important.

We have outlined in detail three important facets of the method. We first introduced the motivation for developing a new measure of information, and subsequently described in detail the specific construction of the method, in both Yu et al. (2010) and Crumiller et al. (2011). The representation of neural spike trains in the frequency domain allows us not only to exploit the Gaussian distribution of Fourier coefficients, as previously discussed, but also to view the information conveyed as a function of temporal frequency. In the past, the firing rate of a neuron has heavily scrutinized, and the importance of both precise spike timing and firing rate as a function of time have propelled forth theories concerning the nature of information transfer in the brain. A view of information processing in the temporal frequency domain, as opposed to that of time, provides insight into the time scales on which a neuron communicates with its neighbors, and will doubtless yield new findings on the relationship between neural firing rate, spike time precision, and information rates.

Next, we tested the robustness of the Fourier method, as described in Crumiller et al. (2013). The somewhat boastful nature by which we espouse the virtues of the Fourier method is justified in that text. Most notably, we provided a lower bound on the quantity of data required for the Fourier method to provide reasonable estimates of information, we demonstrated that the Gaussianity assumption remains relevant in the face of strong local perturbations of the firing rate, we corroborated the results of the method with the popular *Direct Method* of Strong et al. (1998), and finally we demonstrated the computational efficiency of our method, using a modest desktop computer to calculate information rates, in minutes, of the discharge of hundreds of simultaneously firing neurons.

Our concluding chapter, Application to the Visual System, provides a brief sampling of the types of questions which may be addressed by the Fourier Method. This chapter is not intended to answer any scientific questions *per se*, but rather to lend insight into the diversity of applications for measures of information. Whether used for assistance in conjunction with functional clustering measures, such as the Functional Clustering Algorithm of Feldt et al. (2009), or to better hypothesize about the nature of stimuli preferred by a network of cells, or even to measure specifically the nature of spiking in systems of which the role is still poorly understood, as in the case of the lateral geniculate nucleus, the Fourier Method is a tool whose usefulness in answering future scientific questions should prove profitable for years to come.

5 Acknowledgements

Throughout my years spent Mount Sinai I have received a great deal of support from family, friends, colleagues, and mentors, without whom none of the work in this dissertation would have come to fruition. First and foremost, my mentor, Dr. Ehud Kaplan, has been a source of invaluable information, guidance, and kindness. He introduced me to the field of visual neuroscience before I was a graduate student, and has never failed to reinforce the notion that even those long entrenched in the field of science can retain a wonder and curiosity about the brain that drives our exploration.

I would like to thank my dissertation committee of Matthew Shapiro, Vladimir Brezina, Eric Sobie, and Hirofumi Morishita for their guidance and support over the past few years. In addition, I thank Liam Paninski for serving as my external committee member, and lending his expertise in matters of statistical and computational neuroscience, subjects entirely relevant to the content of this dissertation.

Bruce Knight, my closest collaborator and friend throughout my years at Mount Sinai, has given me a profound respect for the necessity and application of mathematics to the field of neuroscience. Bruce's ability to pick patterns out of what appear to be scribbles has constantly amazed me, and has taught me that a patient eye sees much farther than a fast one. I am truly fortunate to have crossed paths with one so brilliant and so willing to teach the treasure troves of information and techniques stored in his mind.

Youping Xiao has always been willing to set aside extensive time to help with surgical and electrophysiological techniques, imaging, and also has lent incredible insight into the many ideas that arise during our countless discussions of the literature and future plans within the lab. Alex Casti helped to introduce me to the lab, and has always been a presence as a mentor and friend during experiments and discussions. I thank Artak Khachatryan for his companionship and support during long hours both in and out of the lab. I would also like to thank all of my teachers and other colleagues who have helped me develop as a scientist during my time at Mount Sinai.

I would finally like to thank my parents, Jenny and Jonathan Crumiller, for their love and support; my sister Susan; my brother Evan; and all of the friends and loved ones I've both gained and retained through the grueling process known as graduate school, and for giving me the motivation to continue to strive in everything I do.

References

Abbott, L. (1999). Lapicque's introduction of the integrate-and-fire model neuron (1907). *Brain Research Bulletin*, 50(5):303–304.

Ahissar, E., Sosnik, R., and Haidarliu, S. (2000). Transformation from temporal to rate coding in a somatosensory thalamocortical pathway. *Nature*, 406(6793):302–306.

Andermann, M. L., Kerlin, A. M., and Reid, R. C. (2010). Chronic cellular imaging of mouse visual cortex during operant behavior and passive viewing. *Front Cell Neurosci*, 4:3.

Andolina, I. M., Jones, H. E., Wang, W., and Sillito, A. M. (2007). Corticothalamic feedback enhances stimulus response precision in the visual system. *Proc Natl Acad Sci U S A*, 104(5):1685–1690.

Attneave, F. (1954). Some informational aspects of visual perception. *Psychological review*, 61(3):183.

Averbeck, B. B. and Lee, D. (2003). Neural noise and movement-related codes in the macaque supplementary motor area. *J Neurosci*, 23(20):7630–7641.

Averbeck, B. B. and Lee, D. (2006). Effects of noise correlations on information encoding and decoding. *J Neurophysiol*, 95(6):3633–3644.

Baird, A. A., Kagan, J., Gaudette, T., Walz, K. A., Hershlag, N., and Boas, D. A. (2002). Frontal lobe activation during object permanence: Data from near-infrared spectroscopy. *NeuroImage*, 16(4):1120–1126.

Barlow, H. B. (1961). Possible principles underlying the transformation of sensory messages. *Sensory communication*, pages 217–234.

Belitski, A., Panzeri, S., Magri, C., Logothetis, N. K., and Kayser, C. (2010). Sensory information in local field potentials and spikes from visual and auditory cortices: time scales and frequency bands. *J Comput Neurosci*, 29(3):533–545.

Berry, M. J., Warland, D. K., and Meister, M. (1997). The structure and precision of retinal spike trains. *Proceedings of the National Academy of Sciences*, 94(10):5411–5416.

Betti, V., Della Penna, S., de Pasquale, F., Mantini, D., Marzetti, L., Romani, G. L., and Corbetta, M. (2013). Natural scenes viewing alters the dynamics of functional connectivity in the human brain. *Neuron*, 79(4):782–797.

Bialek, W., Rieke, F., de Ruyter van Steveninck, R. R., and Warland, D. (1991). Reading a neural code. *Science*, 252:1854–1857.

Bishop, P. O. (1953). Synaptic transmission. an analysis of the electrical activity of the lateral geniculate nucleus in the cat after optic nerve stimulation. *Proc.R.Soc. B*, 141:362–392.

Blitz, D. M. and Regehr, W. G. (2005). Timing and specificity of feed-forward inhibition within the lgn. *Neuron*, 45(6):917–928.

Bock, D. D., Lee, W.-C. A., Kerlin, A. M., Andermann, M. L., Hood, G., Wetzel, A. W., Yurgenson, S., Soucy, E. R., Kim, H. S., and Reid, R. C. (2011). Network anatomy and in vivo physiology of visual cortical neurons. *Nature*, 471(7337):177–182.

Boltzmann, L. (1872). *Weitere studien über das wärmegleichgewicht unter gasmolekülen*.

Boycott, B. B. and Wässle, H. (1991). Morphological classification of bipolar cells of the primate retina. *Eur.J.Neurosci.*, 3:1069–1088.

Brainard, D. H. (1989). Calibration of a computer controlled color monitor. *Color Res.Appl.*, 14:23–34.

Brenner, N., Strong, S. P., Koberle, R., Bialek, W., and de Ruyter van Steveninck, R. R. (2000). Synergy in a neural code. *Neural Comput*, 12(7):1531–1552.

Brown, E. N., Kass, R. E., and Mitra, P. P. (2004). Multiple neural spike train data analysis: state-of-the-art and future challenges. *Nat Neurosci*, 7(5):456–461.

Bullock, T. H. (1970). The reliability of neurons. *J.Gen.Physiol.*, 55:565–584.

Buzsáki, G. (2004). Large-scale recording of neuronal ensembles. *Nat Neurosci*, 7(5):446–451.

Buzsáki, G. and Draguhn, A. (2004). Neuronal oscillations in cortical networks. *Science*, 304(5679):1926–1929.

Carandini, M., Demb, J. B., Mante, V., Tolhurst, D. J., Dan, Y., Olshausen, B. A., Gallant, J. L., and Rust, N. C. (2005). Do we know what the early visual system does? *J Neurosci*, 25(46):10577–10597.

Carr, C. E. (1993). Processing of temporal information in the brain. *Annu Rev Neurosci*, 16:223–243.

Ch'ng, Y. H. and Reid, R. C. (2010). Cellular imaging of visual cortex reveals the spatial and functional organization of spontaneous activity. *Front Integr Neurosci*, 4.

Cleland, B. G., Dubin, M. W., and Levick, W. R. (1971). Simultaneous recording of input and output of lateral geniculate neurones. *Nat New Biol*, 231(23):191–192.

Cover, T. and Thomas, J. (2006). *Elements of information theory*. Wiley Interscience, Hoboken, NJ, second edition.

Croner, L. J. and Kaplan, E. (1995). Receptive fields of p and m ganglion cells across the primate retina. *Vision Res.*, 35:7–24.

Crumiller, M., Knight, B., and Kaplan, E. (2013). The measurement of information transmitted by a neural population: Promises and challenges. *Entropy*, 15(9):3507–3527.

Crumiller, M., Knight, B., Yu, Y., and Kaplan, E. (2011). Estimating the amount of information conveyed by a population of neurons. *Front Neurosci*, 5:90.

Dacey, D. M. and Lee, B. B. (1994). The 'blue-on' opponent pathway in primate retina originates from a distinct bistratified ganglion cell type. *Nature*, 367:731–735.

Daley, D. J. and Vere-Jones, D. (2007). *An introduction to the theory of point processes*. Springer.

Dan, Y., Atick, J. J., and Reid, R. C. (1996). Efficient coding of natural scenes in the lateral geniculate nucleus: experimental test of a computational theory. *J Neurosci*, 16(10):3351–3362.

Dayan, P. and Abbott, L. (2001). *Theoretical Neuroscience*. The MIT Press.

De Cesarei, A., Mastria, S., and Codispoti, M. (2013). Early spatial frequency processing of natural images: an erp study. *PLoS One*, 8(5):e65103.

deCharms, R. C. and Merzenich, M. M. (1996). Primary cortical representation of sounds by the coordination of action-potential timing. *Nature*, 381(6583):610–613.

Deisseroth, K. and Schnitzer, M. J. (2013). Engineering approaches to illuminating brain structure and dynamics. *Neuron*, 80(3):568–577.

DeYoe, E. A., Felleman, D. J., Van Essen, D. C., and McClendon, E. (1994). Multiple processing streams in occipitotemporal visual cortex. *Nature*, 371(6493):151–154.

DiCaprio, R. A. (2004). Information transfer rate of nonspiking afferent neurons in the crab. *J Neurophysiol*, 92(1):302–310.

Dimitrov, A. G., Lazar, A. A., and Victor, J. D. (2011). Information theory in neuroscience. *J Comput Neurosci*, 30(1):1–5.

Doi, E., Gauthier, J. L., Field, G. D., Shlens, J., Sher, A., Greschner, M., Machado, T. A., Jepson, L. H., Mathieson, K., Gunning, D. E., Litke, A. M., Paninski, L., Chichilnisky, E. J., and Simoncelli, E. P. (2012). Efficient coding of spatial information in the primate retina. *J Neurosci*, 32(46):16256–16264.

Dragoi, G. and Buzsáki, G. (2006). Temporal encoding of place sequences by hippocampal cell assemblies. *Neuron*, 50(1):145–157.

Dubin, M. W. and Cleland, B. G. (1977). Organization of visual inputs to interneurons of lateral geniculate nucleus of the cat. *J.Neurophysiol.*, 40:410–427.

Eyherabide, H. G. and Samengo, I. (2013). When and why noise correlations are important in neural decoding. *J Neurosci*, 33(45):17921–17936.

Farivar, R. (2009). Dorsal–ventral integration in object recognition. *Brain Research Reviews*, 61(2):144–153.

Feldt, S., Waddell, J., Hetrick, V. L., Berke, J. D., and Żochowski, M. (2009). Functional clustering algorithm for the analysis of dynamic network data. *Phys. Rev. E*, 79(5):056104.

Field, G. D., Gauthier, J. L., Sher, A., Greschner, M., Machado, T. A., Jepson, L. H., Shlens, J., Gunning, D. E., Mathieson, K., Dabrowski, W., Paninski, L., Litke, A. M., and Chichilnisky, E. J. (2010). Functional connectivity in the retina at the resolution of photoreceptors. *Nature*, 467(7316):673–677.

Fradcourt, B., Peyrin, C., Baciu, M., and Campagne, A. (2013). Behavioral assessment of emotional and motivational appraisal during visual processing of emotional scenes depending on spatial frequencies. *Brain Cogn*, 83(1):104–113.

Gawne, T. J. (2000). The simultaneous coding of orientation and contrast in the responses of v1 complex cells. *Experimental brain research*, 133(3):293–302.

Gawne, T. J. and Richmond, B. J. (1993). How independent are the messages carried by adjacent inferior temporal cortical neurons? *J Neurosci*, 13(7):2758–2771.

Georgopoulos, A. P., Ashe, J., Smyrnis, N., and Taira, M. (1992). The motor cortex and the coding of force. *Science*, 256:1692–1695.

Georgopoulos, A. P., Kettner, R. E., and Schwartz, A. B. (1988). Primate motor cortex and free arm movements to visual targets in three-dimensional space. II. coding of the direction of movement by a neuronal population. *J.Neurosci.*, 8:2928–2937.

Georgopoulos, A. P., Schwartz, A. B., and Kettner, R. E. (1986). Neuronal population coding of movement direction. *Science*, 233:1416–1419.

Gerstein, G. L., Bedenbaugh, P., and Aertsen, A. M. H. J. (1989). Neuronal assemblies. *IEEE Trans.Biomed.Eng.*, 36:4–14.

Gibbs, J. W. (1878). On the equilibrium of heterogeneous substances. *American Journal of Science*, (96):441–458.

Golledge, H. D. R., Panzeri, S., Zheng, F., Pola, G., Scannell, J. W., Giannikopoulos, D. V., Mason, R. J., Tovée, M. J., and Young, M. P. (2003). Correlations, feature-binding and population coding in primary visual cortex. *Neuroreport*, 14(7):1045–1050.

Goodale, M. A. and Milner, A. D. (1992). Separate visual pathways for perception and action. *Trends Neurosci.*, 15:20–25.

Goodchild, A., Ghosh, K., and Martin, P. (1996). Comparison of photoreceptor spatial density and ganglion cell morphology in the retina of human, macaque monkey, cat, and the marmoset *Callithrix jacchus*. *J. Comp. Neurol.*, 366:55–75.

Groen, I. I. A., Ghebreab, S., Prins, H., Lamme, V. A. F., and Scholte, H. S. (2013). From image statistics to scene gist: evoked neural activity reveals transition from low-level natural image structure to scene category. *J Neurosci*, 33(48):18814–18824.

Harris, K. D., Henze, D. A., Csicsvari, J., Hirase, H., and Buzsáki, G. (2000). Accuracy of tetrode spike separation as determined by simultaneous intracellular and extracellular measurements. *Journal of Neurophysiology*, 84:401–414.

Hartley, R. (1928). Transmission of information. *Bell System Technical Journal*, 7(3):535–563.

Hartline, H. K. (1940). The effects of spatial summation in the retina on the excitation of the fibers of the optic nerve. *Am.J.Physiol.*, 130:700–711.

Hebb, D. O. (1949). *The organization of behavior: A neuropsychological approach*. John Wiley & Sons.

Hendry, S. H. C. and Yoshioka, T. (1994). A neurochemically distinct third channel in the macaque dorsal lateral geniculate nucleus. *Science*, 264:575–577.

Hubel, D. H. and Wiesel, T. N. (1961). Integrative action in the cat's lateral geniculate body. *J. Physiol. (Lond.)*, 155:385–398.

Hubel, D. H. and Wiesel, T. N. (1962). Receptive fields, binocular interaction and functional architecture in the cat's visual cortex. *J.Physiol.(Lond)*, 160:106–154.

Kaplan, E., Purpura, K., and Shapley, R. M. (1987). Contrast affects the transmission of visual information through the mammalian lateral geniculate nucleus. *J.Physiol.(Lond)*, 391:267–288.

Kaplan, E. and Shapley, R. (1984). The origin of the s (slow) potential in the mammalian lateral geniculate nucleus. *Exp.Brain Res.*, 55:111–116.

Kaplan, E. and Shapley, R. M. (1986). The primate retina contains two types of ganglion cells, with high and low contrast sensitivity. *Proc Natl Acad Sci U S A*, 83(8):2755–2757.

Kellner, C. J. and Wachtler, T. (2013). A distributed code for color in natural scenes derived from center-surround filtered cone signals. *Front Psychol*, 4:661.

Kennel, M. B., Shlens, J., Abarbanel, H. D. I., and Chichilnisky, E. J. (2005). Estimating entropy rates with bayesian confidence intervals. *Neural Comput*, 17(7):1531–1576.

Kleiner, M., Brainard, D., and Pelli, D. (2007). What's new in psychtoolbox-3? *Perception*, 36. ECVP supplement.

Krüger, J. (1983). Simultaneous individual recordings from many cerebral neurons: techniques and results. In *Reviews of Physiology, Biochemistry and Pharmacology, Volume 98*, pages 177–233. Springer.

Lamme, V., Zipser, K., and Spekreijse, H. (1998). Figure-ground activity in primary visual cortex is suppressed by anesthesia. *Proc. Natl. Acad. Sci. USA*, 95:3263–3268.

Leff, H. S. and Rex, A. F. (1990). Maxwell's demon. entropy, information, computing. *Bristol: Adam Hilger, 1990, edited by Leff, Harvey S.; Rex, Andrew F.*, 1.

Levine, M. W., Castaldo, K., and Kasapoglu, M. B. (2002). Firing coincidences between neighboring retinal ganglion cells: inside information or epiphenomenon? *Biosystems*, 67(1-3):139–146.

Lewicki, M. S. (1998). A review of methods for spike sorting: the detection and classification of neural action potentials. *Network*, 9(4):R53–R78.

Livingstone, M. and Hubel, D. (1988). Segregation of form, color, movement, and depth: anatomy, physiology, and perception. *Science*, 240(4853):740–749.

Livingstone, M. S. and Hubel, D. H. (1984a). Anatomy and physiology of a color system in the primate visual cortex. *J.Neurosci.*, 4:309–356.

Livingstone, M. S. and Hubel, D. H. (1984b). Specificity of intrinsic connections in primate primary visual cortex. *J.Neurosci.*, 4:2830–2835.

London, M., Roth, A., Beeren, L., Häusser, M., and Latham, P. E. (2010). Sensitivity to perturbations in vivo implies high noise and suggests rate coding in cortex. *Nature*, 466(7302):123–127.

London, M., Schreibman, A., Hï¿œusser, M., Larkum, M. E., and Segev, I. (2002). The information efficacy of a synapse. *Nat Neurosci*, 5(4):332–340.

Ma, L.-B. and Wu, S. (2011). Efficient coding of natural images. *Sheng Li Xue Bao*, 63(5):463–471.

MacKay, D. M. and McCulloch, W. S. (1952). The limiting information capacity of a neuronal link. *The bulletin of mathematical biophysics*, 14(2):127–135.

Mante, V., Bonin, V., and Carandini, M. (2008). Functional mechanisms shaping lateral geniculate responses to artificial and natural stimuli. *Neuron*, 58(4):625–638.

Mante, V., Frazor, R. A., Bonin, V., Geisler, W. S., and Carandini, M. (2005). Independence of luminance and contrast in natural scenes and in the early visual system. *Nature Neuroscience*, 8:1690–1697.

Markram, H., Gerstner, W., and Sjöström, P. J. (2011). A history of spike-timing-dependent plasticity. *Frontiers in synaptic neuroscience*, 3.

Marsat, G. and Pollack, G. S. (2010). The structure and size of sensory bursts encode stimulus information but only size affects behavior. *J Comp Physiol A Neuroethol Sens Neural Behav Physiol*, 196(4):315–320.

Marshall, J. D. and Schnitzer, M. J. (2013). Optical strategies for sensing neuronal voltage using quantum dots and other semiconductor nanocrystals. *ACS Nano*, 7(5):4601–4609.

Masuda, N. and Aihara, K. (2002). Bridging rate coding and temporal spike coding by effect of noise. *Physical review letters*, 88(24):248101.

Maxwell, J. C. (2001). Theory of heat, 1872.

McAlonan, K., Cavanaugh, J., and Wurtz, R. H. (2006). Attentional modulation of thalamic reticular neurons. *J Neurosci*, 26(16):4444–4450.

McAlonan, K., Cavanaugh, J., and Wurtz, R. H. (2008). Guarding the gateway to cortex with attention in visual thalamus. *Nature*, 456(7220):391–394.

McKee, S. P. (1981). A local mechanism for differential velocity detection. *Vision research*, 21(4):491–500.

Mink, J. W., Blumenschine, R. J., and Adams, D. B. (1981). Ratio of central nervous system to body metabolism in vertebrates: its constancy and functional basis. *American Journal of Physiology-Regulatory, Integrative and Comparative Physiology*, 241(3):R203–R212.

Nicolelis, M. A. L. and Ribeiro, S. (2002). Multielectrode recordings: the next steps. *Curr Opin Neurobiol*, 12(5):602–606.

Nirenberg, S., Carcieri, S. M., Jacobs, A. L., and Latham, P. E. (2001). Retinal ganglion cells act largely as independent encoders. *Nature*, 411(6838):698–701.

Nirenberg, S. and Pandarinath, C. (2012). Retinal prosthetic strategy with the capacity to restore normal vision. *Proceedings of the National Academy of Sciences*, 109(37):15012–15017.

Niven, J. E. and Laughlin, S. B. (2008). Energy limitation as a selective pressure on the evolution of sensory systems. *Journal of Experimental Biology*, 211(11):1792–1804.

Nyquist, H. (1924). Certain factors affecting telegraph speed. *American Institute of Electrical Engineers, Transactions of the*, 43:412–422.

Ohlendorf, S., Kimmig, H., Glauche, V., and Haller, S. (2007). Gaze pursuit,"attention pursuit" and their effects on cortical activations. *European Journal of Neuroscience*, 26(7):2096–2108.

O'Keefe, J. and Recce, M. L. (1993). Phase relationship between hippocampal place units and the eeg theta rhythm. *Hippocampus*, 3(3):317–330.

Optican, L. M. and Richmond, B. J. (1987). Temporal encoding of two-dimensional patterns by single units in primate inferior temporal cortex. III. information theoretic analysis. *J.Neurophysiol.*, 57:162–178.

Orban, G. A., de Wolf, J., and Maes, H. (1984). Factors influencing velocity coding in the human visual system. *Vision Res.*, 24:33–39.

Pamplona, D., Triesch, J., and Rothkopf, C. A. (2013). Power spectra of the natural input to the visual system. *Vision Res*, 83:66–75.

Panzeri, S. and Schultz, S. R. (2001). A unified approach to the study of temporal, correlational, and rate coding. *Neural Comput*, 13(6):1311–1349.

Pelli, D. G. (1997). The videotoolbox software for visual psychophysics: Transforming numbers into movies. *Spatial vision*, 10:437–442.

Pillow, J. and Latham, P. (2008). Neural characterization in partially observed populations of spiking neurons. In Platt, J. C., Koller, D., Singer, Y., and Roweis, S., editors, *Advances in Neural Information Processing Systems 20*, pages 1161–1168. MIT Press, Cambridge, MA.

Pinker, S. (1999). How the mind works. *Annals of the New York Academy of Sciences*, 882(1):119–127.

Planck, M. (1945). *Treatise on thermodynamics*. Courier Dover Publications.

Pouget, A., Dayan, P., and Zemel, R. (2000). Information processing with population codes. *Nat Rev Neurosci*, 1(2):125–132.

Puchalla, J. L., Schneidman, E., Harris, R. A., and Berry, M. J. (2005). Redundancy in the population code of the retina. *Neuron*, 46(3):493–504.

Reich, D., Mechler, F., and Victor, J. (2001). Formal and attribute-specific information in primary visual cortex. *J. Neurophysiol.*, 85:305–318.

Reinagel, P. and Reid, R. C. (2000). Temporal coding of visual information in the thalamus. *J Neurosci*, 20(14):5392–5400.

Richmond, B. J. and Optican, L. M. (1987). Temporal encoding of two-dimensional patterns by single units in primate inferior temporal cortex. II. quantification of response waveform. *J.Neurophysiol.*, 57:147–161.

Rizzolatti, G., Camarda, R., Fogassi, L., Gentilucci, M., Luppino, G., and Matelli, M. (1988). Functional organization of inferior area 6 in the macaque monkey. *Experimental Brain Research*, 71(3):491–507.

Rodieck, R. W. and Brening, R. K. (1983). Retinal ganglion cells: properties, types, genera, pathways and trans-species comparisons. *Brain Behav.Evol.*, 23:121–164.

Shadlen, M. N. and Newsome, W. T. (1998). The variable discharge of cortical neurons: implications for connectivity, computation, and information coding. *The Journal of neuroscience*, 18(10):3870–3896.

Shannon, C. (1948). A mathematical theory of communication. *Bell System Technical Journal*, 27:379–423,623–656.

Shannon, C. and Weaver, W. (1949). *The Mathematical theory of communication*. Univ. of Illinois Press, Chicago, Il.

Shannon, C. E. (1945). A mathematical theory of cryptography. *Memorandum MM*, pages 45–110.

Shannon, C. E., McCarthy, J., et al. (1956). Automata studies. *Princeton: Princeton*.

Sherman, S. M. (2005). Thalamic relays and cortical functioning. *Prog Brain Res*, 149:107–126.

Sherman, S. M. and Guillery, R. W. (1998). On the actions that one nerve cell can have on another: Distinguishing 'drivers' from 'modulators'. *Proc. Natl. Acad. Sci.*, 95:7121–7126.

Shipp, S. and Zeki, S. (1985). Segregation of pathways leading from area V2 to areas V4 and V5 of macaque monkey visual cortex. *Nature*, 315:322–325.

Shirvalkar, P. R., Rapp, P. R., and Shapiro, M. L. (2010). Bidirectional changes to hippocampal theta–gamma comodulation predict memory for recent spatial episodes. *Proceedings of the National Academy of Sciences*, 107(15):7054–7059.

Sincich, L. C., Adams, D. L., Economides, J. R., and Horton, J. C. (2007). Transmission of spike trains at the retinogeniculate synapse. *J Neurosci*, 27(10):2683–2692.

Sincich, L. C., Horton, J. C., and Sharpee, T. O. (2009). Preserving information in neural transmission. *J Neurosci*, 29(19):6207–6216.

Sinha, S., Liang, L., Ho, E. T. W., Urbanek, K. E., Luo, L., Baer, T. M., and Schnitzer, M. J. (2013). High-speed laser microsurgery of alert fruit flies for fluorescence imaging of neural activity. *Proc Natl Acad Sci U S A*, 110(46):18374–18379.

Sivyer, B. and Williams, S. R. (2013). Direction selectivity is computed by active dendritic integration in retinal ganglion cells. *Nat Neurosci*.

Smith SL, Smith IT, B. T. and M, H. (2013). Dendritic spikes enhance stimulus selectivity in cortical neurons in vivo. *Nature*, 503(7474):115–120.

Softky, W. (1994). Sub-millisecond coincidence detection in active dendritic trees. *Neuroscience*, 58:13–41.

Softky, W. R. and Koch, C. (1993). The highly irregular firing of cortical cells is inconsistent with temporal integration of random EPSPs. *J.Neurosci.*, 13:334–350.

Stansbury, D. E., Naselaris, T., and Gallant, J. L. (2013). Natural scene statistics account for the representation of scene categories in human visual cortex. *Neuron*, 79(5):1025–1034.

Strong, S. P., Koberle, R., de Ruyter van Steveninck, R. R., and Bialek, W. (1998). Entropy and information in neural spike trains. *Phys Rev Lett.*, 80:197–200.

Tadmor, Y. and Tolhurst, D. J. (2000). Calculating the contrasts that retinal ganglion cells and lgn neurones encounter in natural scenes. *Vision Res*, 40(22):3145–3157.

Tan, H.-R. M., Lana, L., and Uhlhaas, P. J. (2013). High-frequency neural oscillations and visual processing deficits in schizophrenia. *Frontiers in psychology*, 4.

Tanaka, S. (1994). Numerical study of coding of the movement direction by a population in the motor cortex. *Biological cybernetics*, 71(6):503–510.

Theunissen, F. and Miller, J. P. (1995). Temporal encoding in nervous systems: a rigorous definition. *Journal of computational neuroscience*, 2(2):149–162.

Tolhurst, D. J., Movshon, J. A., and Dean, A. F. (1983). The statistical reliability of signals in single neurons in cat and monkey visual cortex. *Vision Res.*, 23:775–785.

Trimper, J. B., Stefanescu, R. A., and Manns, J. R. (2013). Recognition memory and theta-gamma interactions in the hippocampus. *Hippocampus*.

Uglesich, R., Casti, A., Hayot, F., and Kaplan, E. (2009). Stimulus size dependence of information transfer from retina to thalamus. *Front Syst Neurosci*, 3:10.

Uhlhaas, P. J. and Singer, W. (2013). High-frequency oscillations and the neurobiology of schizophrenia. *Dialogues Clin Neurosci*, 15(3):301–313.

Ungerleider, L. G. and Mishkin, M. (1982). Two cortical visual systems. In Ingle, D.J., G. M. and Mansfield, R., editors, *Analysis of Visual Behavior*, pages 549–586. MIT Press, Cambridge, MA.

Vaidya, S. P. and Johnston, D. (2013). Temporal synchrony and gamma-to-theta power conversion in the dendrites of ca1 pyramidal neurons. *Nature neuroscience*.

van Hateren, J. H. (1997). Processing of natural time series of intensities by the visual system of the blowfly. *Vision Res*, 37(23):3407–3416.

Van Rullen, R. and Thorpe, S. J. (2001). Rate coding versus temporal order coding: what the retinal ganglion cells tell the visual cortex. *Neural computation*, 13(6):1255–1283.

Vardi, R., Goldental, A., Guberman, S., Kalmanovich, A., Marmari, H., and Kanter, I. (2013). Sudden synchrony leaps accompanied by frequency multiplications in neuronal activity. *Front Neural Circuits*, 7:176.

Vasserman, G., Schneidman, E., and Segev, R. (2013). Adaptive colour contrast coding in the salamander retina efficiently matches natural scene statistics. *PLoS One*, 8(10):e79163.

Victor, J. (2005). Spike train metrics. *Current Opinion in Neurobiology*, 15:585–592.

Victor, J. and Purpura, K. (1997). Metric-space analysis of spike trains: theory, algorithms and application. *Network*, 8:127–164.

Victor, J. D. (2006). Approaches to information-theoretic analysis of neural activity. *Biological Theory*, 1(3):302–316.

Victor, J. D. and Purpura, K. P. (1996). Nature and precision of temporal coding in visual cortex: a metric-space analysis. *J Neurophysiol.*, 76:1310–1326.

Vidne, M., Ahmadian, Y., Shlens, J., Pillow, J. W., Kulkarni, J., Litke, A. M., Chichilnisky, E. J., Simoncelli, E., and Paninski, L. (2011). Modeling the impact of common noise inputs on the network activity of retinal ganglion cells. *J Comput Neurosci*.

von Neumann, J. (2000). *The Computer and the Brain: Second Edition*. Mrs. Hepsa Ely Silliman Memorial Lectures. Yale University Press; 2 Sub edition (July 11, 2000).

Welch, T. (1984). A technique for high-performance data compression. *Computer*, 17:8–19.

Weyand, T. G. (2007). Retinogeniculate transmission in wakefulness. *J Neurophysiol*.

Winograd, S. and Cowan, J. D. (1963). *Reliable computation in the presence of noise*. Number 22. MIT Press Cambridge, Mass.

Yu, Y., Crumiller, M., Knight, B., and Kaplan, E. (2010). Estimating the amount of information carried by a neuronal population. *Front Comput Neurosci*, 4:10.

Zhu, W., Drewes, J., and Gegenfurtner, K. R. (2013). Animal detection in natural images: effects of color and image database. *PLoS One*, 8(10):e75816.

Ziv, J. and A, L. (1978). Compression of individual sequences via variable-rate coding. *IEEE Transactions on Information Theory*, 24:530–536.

Ziv, J. and Lempel, A. (1978). A universal algorithm for sequential data compression. *IEEE Transactions on Information Theory*, IT-23:337–43.

Ziv, Y., Burns, L. D., Cocker, E. D., Hamel, E. O., Ghosh, K. K., Kitch, L. J., El Gamal, A., and Schnitzer, M. J. (2013). Long-term dynamics of ca1 hippocampal place codes. *Nat Neurosci*, 16(3):264–266.

Zylberberg, J. and DeWeese, M. R. (2013). Sparse coding models can exhibit decreasing sparseness while learning sparse codes for natural images. *PLoS Comput Biol*, 9(8):e1003182.